OULU 2013
C 465

ACTA UNIVERSITATIS OULUENSIS

Animesh Yadav

SPACE-TIME CONSTELLATION AND PRECODER DESIGN UNDER CHANNEL ESTIMATION ERRORS

UNIVERSITY OF OULU GRADUATE SCHOOL;
UNIVERSITY OF OULU,
FACULTY OF TECHNOLOGY,
DEPARTMENT OF COMMUNICATIONS ENGINEERING;
CENTRE FOR WIRELESS COMMUNICATIONS;
INFOTECH OULU

ACTA UNIVERSITATIS OULUENSIS
C Technica 465

ANIMESH YADAV

SPACE-TIME CONSTELLATION AND PRECODER DESIGN UNDER CHANNEL ESTIMATION ERRORS

Academic dissertation to be presented with the assent of the Doctoral Training Committee of Technology and Natural Sciences of the University of Oulu for public defence in Kuusamonsali (Auditorium YB210), Linnanmaa, on 18 October 2013, at 12 noon

UNIVERSITY OF OULU, OULU 2013

Acta Univ. Oul. C 465, 2013

Supervised by
Professor Markku Juntti
Docent Jorma Lilleberg

Reviewed by
Professor Mikael Skoglund
Professor Hamid Jafarkhani

Opponents
Professor Risto Wichman

ISBN 978-952-62-0213-6 (Paperback)
ISBN 978-952-62-0214-3 (PDF)

ISSN 0355-3213 (Printed)
ISSN 1796-2226 (Online)

Cover Design
Raimo Ahonen

JUVENES PRINT
TAMPERE 2013

Yadav, Animesh, Space-time constellation and precoder design under channel estimation errors.
University of Oulu Graduate School; University of Oulu, Faculty of Technology, Department of Communications Engineering; Centre for Wireless Communications; Infotech Oulu
Acta Univ. Oul. C 465, 2013
University of Oulu, P.O. Box 8000, FI-90014 University of Oulu, Finland

Abstract

Multiple-input multiple-output transmitted signal design for the partially coherent Rayleigh fading channels with discrete inputs under a given average transmit power constraint is consider in this thesis. The objective is to design the space-time constellations and linear precoders to adapt to the degradation caused by the imperfect channel estimation at the receiver and the transmit-receive antenna correlation. The system is partially coherent so that the multiple-input multiple-output channel coefficients are estimated at the receiver and its error covariance matrix is fed back to the transmitter.

Two constellation design criteria, one for the single and another for the multiple transmit antennae are proposed. An upper bound on the average bit error probability for the single transmit antenna and cutoff rate, i.e., a lower bound on the mutual information, for multiple transmit antennae are derived. Both criteria are functions of channel estimation error covariance matrix. The designed constellations are called as partially coherent constellation. Additionally, to use the resulting constellations together with forward error control codes requires efficient bit mapping schemes. Because these constellations lack geometrical symmetry in general, the Gray mapping is not always possible in the majority of the constellations obtained.

Moreover, different mapping schemes may lead to highly different bit error rate performances. Thus, an efficient bit mapping algorithm called the modified binary switching algorithm is proposed. It minimizes an upper bound on the average bit error probability. It is shown through computer simulations that the designed partially coherent constellation and their optimized bit mapping algorithm together with turbo codes outperform the conventional constellations.

Linear precoder design was also considered as a simpler, suboptimal alternative. The cutoff rate expression is again used as a criterion to design the linear precoder. A linear precoder is obtained by numerically maximizing the cutoff rate with respect to the precoder matrix with a given average transmit power constraint. Furthermore, the precoder matrix is decomposed using singular-value-decomposition into the input shaping, power loading, and beamforming matrices. The beamforming matrix is found to coincide with the eigenvectors of the transmit correlation matrix. The power loading and input shaping matrices are solved numerically using the difference of convex functions programming algorithm and optimization under the unitary constraint, respectively. Computer simulations show that the performance gains of the designed precoders are significant compared to the cutoff rate optimized partially coherent constellations without precoding.

Keywords: cutoff rate, difference of convex functions programming, imperfect channel state information, linear precoder, multiple-input multiple-output, sequential quadratic programming, signal design, space-time codes

Yadav, Animesh, Tila-aikakonstellaation ja esikoodauksen suunnittelu kanavanestimointivirheen läsnäollessa.
Oulun yliopiston tutkijakoulu; Oulun yliopisto, Teknillinen tiedekunta, Tietoliikennetekniikan osasto; Centre for Wireless Communications; Infotech Oulu
Acta Univ. Oul. C 465, 2013
Oulun yliopisto, PL 8000, 90014 Oulun yliopisto

Tiivistelmä

Väitöskirjassa tarkastellaan lähetyssignaalien suunnittelua osittain koherenteissa Rayleigh-häipyvissä kanavissa toimiviin monitulo-monilähtöjärjestelmiin (MIMO). Lähettimen keskimääräinen lähetysteho oletetaan rajoitetuksi ja lähetyssignaali diskreetiksi. Tavoitteena on suunnitella tila-aikakonstellaatioita ja lineaarisia esikoodereita jotka mukautuvat epätäydellisen kanavaestimoinnin aiheuttamaan suorituskyvyn heikkenemiseen sekä lähetin- ja vastaanotinantennien väliseen korrelaatioon. Tarkasteltavien järjestelmien osittainen koherenttisuus tarkoittaa sitä, että MIMO-kanavan kanavakertoimet estimoidaan vastaanottimessa, josta niiden virhekovarianssimatriisi lähetetään lähettimelle.

Työssä esitetään kaksi konstellaatiosuunnittelukriteeriä, toinen yhdelle lähetinantennille ja toinen moniantennilähettimelle. Molemmat kriteerit ovat kanavan estimaatiovirheen kovarianssimatriisin funktioita. Työssä johdetaan yläraja keskimääräiselle bittivirhetodennäköisyydelle yhden lähetinantennin tapauksessa sekä rajanopeus (*cutoff rate*), joka on alaraja keskinäisinformaatiolle, usean lähetinantennin tapauksessa. Konstellaatioiden käyttö yhdessä virheenkorjauskoodien kanssa edellyttää tehokaita menetelmiä, joilla bitit kuvataan konstellaatiopisteisiin. Koska tarvittavat konstellaatiot eivät ole tyypillisesti geometrisesti symmetrisiä, Gray-kuvaus ei ole yleensä mahdollinen.Lisäksi erilaiset kuvausmenetelmät voivat johtaa täysin erilaisiin bittivirhesuhteisiin. Tästä johtuen työssä esitetään uusi kuvausalgoritmi (*modified bit switching algorithm*), joka minimoi keskimääräisen bittivirhetodennäköisyyden ylärajan. Simulointitulokset osoittavat, että työssä kehitetyt konstellaatiot antavat paremman suorituskyvyn turbokoodatuissa järjestelmissä kuin perinteiset konstellaatiot.

Työssä tarkastellaan myös lineaarista esikoodausta yksinkertaisena, alioptimaalisena vaihtoehtona uusille konstellaatioille. Esikoodauksen suunnittelussa käytetään samaa kriteeriä kuin konstellaatioiden kehityksessä eli rajanopeutta. Lineaarinen esikooderi löydetään numeerisesti maksimoimalla rajanopeus kun rajoitusehtona on lähetysteho. Esikoodausmatriisi hajotetaan singulaariarvohajotelmaa käyttäen esisuodatus, tehoallokaatio ja keilanmuodostusmatriiseiksi, jonka havaitaan vastaavan lähetyskorrelaatiomatriisin ominaisvektoreita. Tehoallokaatiomatriisi ratkaistaan numeerisesti käyttäen *difference of convex functions* -optimointia ja esisuodatusmatriisi optimoinnilla unitaarista rajoitusehtoa käyttäen. Simulaatiotulokset osoittavat uusien esikoodereiden tarjoavan merkittävän suorituskykyedun sellaisiin rajanopeusoptimoituihin osittain koherentteihin konstellaatioihin nähden, jotka eivät käytä esikoodausta.

Asiasanat: difference of convex functions -optimointi, epätäydellinen kanavatilatieto, lineaarinen esikoodaus, monitulo-monilähtö (MIMO), rajanopeus, sarjamuotoinen kvadraattinen ohjelmointi, signaalin suunnittelu, tila-aikakoodi

Dedicated to my family

Preface

This doctoral thesis contains the results of research undertaken at the Department of Communication Engineering (DCE) and Centre for Wireless Communications (CWC), University of Oulu, Finland, during the years 2009–2013. Certainly, I would have never reached the point of finishing my dissertation without the help and support of others.

These four years have been a challenging trip, with both ups and downs. Fortunately, I was not alone on this road, but accompanied by an extended team of experts, always willing to supervise, sponsor, help, and motivate me. For this, I would like to kindly thank them.

First of all, I wish to express my deepest gratitude to my main supervisor, Professor Markku Juntti, for giving me this opportunity of becoming a doctoral student in his Communication Signal Processing (CSP) group and for all the supervision, inspring research discussions and constant support that he has provided during these years. His pursuit for the highest standards in research is a great source of inspiration for me. I am constantly surprised by his technical intuition, and I hope I have learned a bit from him in terms of the way of thinking and carrying out research. Furthermore, I would like to thank my advisor Dr. Jorma Lilleberg, who is currently with Renesas Mobile Europe, Oulu, Finland, for proposing me an interesting idea to design constellation sets for partially coherent channels. Without his ideas, advising and criticism, this thesis would not have been completed. I am grateful to the reviewers of the thesis, Professor Mikael Skoglund from the KTH Royal Institute of Technology, Stockholm, Sweden and Professor Hamid Jafarkhani from the University of California, Irvine, California, the United States. Their comments have significantly improved the clarity of the thesis.

My gratitude goes to Dr. Harri Posti and Dr. Ari Pouttu, the director of the CWC during my years here, for providing an energetic and inspiring working environment.

Most of the work presented in the thesis was conducted in the MIMO Techniques for 3G Systems and Standard Evolution (MITSE), Cooperative MIMO Techniques for Cellular System Evolution (CoMIT), Baseband and System Tech-

nologies for Wireless Evolution (BaSE) projects. I would like to thank the managers of these projects, Visa Topia and Dr. Janne Janhunen, and all my colleagues that have directly or indirectly influenced my work. The projects were funded by Finnish Funding Agency for Technology and Innovation (Tekes), Texas Instrument, Nokia, Nokia Solutions and Networks, Elektrobit, Uninord, Xilinx, and Renesas Mobile Europe, and they are acknowledged. I was also fortunate to receive personal grants for doctoral studies from the following Finnish foundations: Nokia Foundation, the Tauno Tönning Foundation, and Oulu University Scholarship Foundation. These financial support stimulated me to engage even more in my research work.

I would like to express my gratitude to professors Jari Iinatti, Matti Latva-aho, and Premanandana Rajatheva for their advice in many technical and practical matters. I am privileged to have a friendship with Professor Behnaam Aazhang, with whom I spent good time during some technical discussions and on the volleyball court.

During my doctoral studies, I have had the pleasure to be surrounded by cheerful colleagues of mine at the CWC including (in alphabetical order) Dr. Antti Tölli, Dr. Attaphongse Taparugssanagorn, Arun Sowpati, Aravind Avvru, Bidushi Barua, Bobins Agustine, Dr. Carlos Lima, Dr. Chathuranga Pradeep, Dr. Ebrahim Karami, Dr. Fatih Bayramoglu, Feng Hu, Dr. Francesco Patnisano, Ganesh Venkatraman, Harri Pennanen, Hamidreza Bagheri, Helal Chowdhury, Hirley Alves, Ikram Ashraf, Inosha Sugathapala, Dr. Juha Karjalainen, Jyotishman Veepaschit, Kamaldeep Singh, Dr. Kaveh Ghaboosi, Keeth Saliya, Dr. Le-Nam Tram, Dr. Li Wei, Matti Isohookana, Manosha Kapuruhamy, Mariella Särestöniemi, Dr. Marian Codreanu, Dr. Mehdi Bennis, Nuwan Ferdinand, Dr. Pedro Nardelli, Petri Komulainen, Dr. Pradeep Kumar, Prasanth Karunakaran, Qiang Xue, Ratheesh Kumar, Dr. Raghvendra Madanhally, Satya Joshi, Sumudu Samarakoon, Tilahun Getu, Tuomo Hänninen, Uditha, Ulrico Celentano, Dr. Vamsi Krishna, Dr. Zaheer Khan, amongst all others. During my stay at the CWC, I shared an office with Marja Kangas, Najmeh Forouzandeh Mehr, and Xiaojia Lu. I very much enjoyed our daily exchange of ideas and thoughts, and the fun moments together. I am also very grateful to the administrative staff from the CWC, more specifically Antero Kangas, Elina Komminaho, Hanna Saarela, Jari Sillanpää, Kirsi Ojutkangas, Eija Pajunen, Mari Lehmikangas, Saija Laitinen and Timo Äikäs for their patience and kindness.

I would also like to thank all my Indian friends in Oulu for all the great moments I and my family have experienced together with you. During my stay in Oulu, I have had also the privilege to make some very good family friends, including Bastian Fähnrich & family, David Olsen, Emily Vakkilainen, Iina Mattila, Judy Song, Jermey Voulu, Leena & Alpo, Mich Peedo & family, Oliver Jarde, Patrick Nesbitt & family, and Balaet Hossain & family with whom I and my family had great time in Oulu. I would also like to thank my dear friend David Mathew and his family for their support and help during the time we spent together in Oulu.

My sincerest gratitude goes to my loving parents for instilling in me the love of learning and the continuous desire for more knowledge. It was under their watchful eye that I gained so much drive and an ability to tackle challenges head on. The sacrifices you have done during my life are priceless. To my two sweet boys, Anshuman (6.5 years) and Naman (1 year), thank you for the happiness you brought into my life and for reminding me the important things in life. Last, but not least, I thank my wife, Suchita, for always being by my side, loving, supporting, and believing in me–this thesis is dedicated to you.

September 5, 2013 Animesh Yadav

List of abbreviations

2-D	two-dimensional
3G	the Third Generation
4G	the Fourth Generation
5G	the Fifth Generation
3GPP	3rd Generation Partnership Project
ABEP	average bit error probability
APEP	average pairwise error probability
ASEP	asymptotic symbol error probability
AWGN	additive white Gaussian noise
BD	Bhattacharyya distance
BEP	bit error probability
BER	bit error rate
BFGS	Broyden-Fletcher-Goldfarb-Shanno
BICM-ID	bit-interleaved coded modulation and iterative decoding
BLAST	Bell Lab's space-time
BLER	block error rate
BnB	branch-and-bound
BPSK	binary phase-shift keying
BSA	binary switching algorithm
CR	cutoff rate
CR-NZ	cutoff rate, non-zero amplitude
CR-SM	cutoff rate, self-match
CR-SM-NZ	cutoff rate, self-match with non-zero amplitude
CSI	channel state information
CSIR	channel state information at the receiver
CSIT	channel state information at the transmitter
d.c.	difference of convex
D-BLAST	diagonal-BLAST
EVD	eigenvalue decomposition
FEC	forward error control
FER	frame error rate

Gbps	gigabits per second
i.i.d.	independent and identically distributed
Kbps	kilobits per second
KLD	Kullback-Leibler divergence
LLR	log-likelihood ratio
LMMSE	linear MMSE
LP	linear program
LTE	Long Term Evolution
LTE-A	LTE-Advance
Mbps	megabits per second
MBSA	modified bit switching algorithm
MI	mutual information
MIMO	multiple-input multiple-output
ML	maximum likelihood
MMSE	minimum mean-square error
MSE	mean-square error
OSTBC	orthogonal space-time block codes
OTD	orthogonal transmit diversity
PAPR	peak-to-average power ratio
PCC	partially coherent constellation
PDF	probability density function
PEP	pairwise error probability
PSK	phase-shift keying
QAM	quadrature amplitude modulation
QP	quadratic programming
QPSK	quadrature phase-shift keying
SD	steepest descent
SER	symbol error rate
SISO	single-input single-output
SM	spatial multiplexing
SNR	signal-to-noise ratio
SQP	sequential quadratic programming
ST	space-time
STBC	space-time block code
STTC	space-time trellis code

SVD	singular value decomposition
UB	upper bound
UB-ABEP	upper bound on the ABEP
USTC	unitary space-time code
V-BLAST	vertical-BLAST
WF	waterfilling
WLAN	wireless local area network

List of symbols

$\mathcal{B}(\mathbf{S}_i\|\mathbf{S}_j)$	Bhattacharyya distance between codeword $\mathbf{S}_i$ and $\mathbf{S}_j$
$\mathcal{B}^{\star\star}_{\min}$	minimum optimal Bhattacharyya distance
$\mathcal{B}^{\star\star}_{ave}$	expected Bhattacharyya distance
$\mathcal{B}_{\min}$	minimum Bhattacharyya distance between two codewords
$\mathcal{CN}(0,1)$	complex circularly symmetric Gaussian random variable
$\mathbb{C}^{m\times n}$	set of $m \times n$ complex matrices
$\mathbf{D}_i$	diagonal matrix corresponding to Φ_i with nonnegative and equal entries
$d(\mathbf{X}_i, \mathbf{X}_j)$	Hamming distance between binary sequences representing $\mathbf{X}_i$ and $\mathbf{X}_j$
d_i	diagonal entries of matrix $\mathbf{D}_i$
$(E_b/N_0)_d$	$\mathrm{SNR_d}$ per bit
$\mathbf{F}$	linear precoder matrix
$\hat{\mathbf{H}}$	estimated channel matrix
$\mathbf{H}$	MIMO channel matrix
$\tilde{\mathbf{H}}$	channel estimation error matrix
$\mathcal{I}(\mathbf{x};\mathbf{y})$	mutual information from $\mathbf{x}$ to $\mathbf{y}$
L	number of constellation/codewords
M_R	number of receive antennae
M_T	number of transmit antennae
P_d	average total transmit power across the antennae
P_e	average error probability of the ML detector
P_t	total energy of the training sequence
P_{PAPR}	peak-to-average-power ratio threshold power
$\bar{P}_b$	average bit error probability
$\bar{P}_b^{UB}$	upper bound on the ABEP
$\Pr\{\mathbf{X}_i \to \mathbf{X}_j\}$	pairwise error probability between codewords $\mathbf{X}_i$ and $\mathbf{X}_j$
$\Pr_{p_i}$	probability w.r.t. the probability density function $p_i(\mathbf{y})$
$\mathbf{p}^i$	vertex of simplex S
p	probability density function
R	STBC code rate

R_0	cutoff rate
R_c	turbo code rate
$\mathcal{R}$	set of prisms
$\mathbf{R}_R$	receiver side correlation matrix
$\mathbf{R}_T$	transmitter side correlation matrix
$\mathbf{R}_d$	received data symbols matrix
S	$(N-1)$-dimensional simplex with $[\mathbf{p}^1, \mathbf{p}^2, \cdots, \mathbf{p}^N]$ vertices
$\mathcal{S}$	space-time or modulation signal codeword alphabet
s_{tm}	element at the tth row and mth column of the signal matrix $\mathbf{S}$
$\mathrm{SNR_d}$	SNR for data symbols
$\mathbf{S}_d$	ST codeword matrix
$\mathbf{S}_i$	ith space-time or modulation signal codeword
$\mathbf{S}_t$	orthogonal training symbol matrix
$\{\mathbf{S}_i^\star\}_{i=1}^L$	optimal set of constellation points
$\mathrm{SNR_t}$	SNR for training symbols
T	channel coherence time
T_d	data symbols transmission time
T_t	training sequence transmission time
$\mathcal{T}$	prism induces from simplex S
$\mathbf{U}_F$	beamforming matrix
$\mathbf{U}_R$	unitary matrices of the EVDs of R_R
$\mathbf{U}_T$	unitary matrices of the EVDs of R_T
$\mathbf{V}_F$	input-shaping matrix
$\mathbf{W}_t$	AWGN noise matrix during training period
$\mathbf{W}_d$	AWGN noise matrix
$[\mathbf{a}]_i$	ith element of vector $\mathbf{a}$
Λ_F	power loading matrix
Φ_i	ith matrix with orthonormal columns (i.e., $\Phi_i^H \Phi_i = \mathbf{I}_{M_T}$)
$\frac{\partial f(x)}{\partial x^*}$	complex conjugate derivative of function f w.r.t. x
$\frac{\partial f(x)}{\partial x}$	derivative of function f w.r.t. x
$\mathcal{O}(\cdot)$	big O notation
$\mathbb{R}$	set of real numbers
$\nabla_x f(x)$	gradient of function f w.r.t. x
$\otimes$	Kronecker product
π_i	ith codeword's transmission probability

$\rho(i,j)$	Bhattacharyya coefficient
ρ_R	receiver side normalized correlation coefficient of the channel
ρ_T	transmitter side normalized correlation coefficient of the channel
$\rho_{\text{cor}}(i,j)$	Bhattacharyya coefficient for the spatially correlated MIMO channels
$\rho_{\text{uncor}}(i,j)$	Bhattacharyya coefficient for the i.i.d. MIMO channels
σ_E^2	channel estimation error variance
$\tilde{\Sigma}$	correlation matrix of $\tilde{\mathbf{H}}$
$\hat{\lambda}_R^i$	ith eigenvalues of $\hat{\mathbf{R}}_R$
λ_R^i	ith eigenvalues of $\mathbf{R}_R$
λ_T^i	ith eigenvalue of $\mathbf{R}_T$
$\tilde{\lambda}_R^i$	ith eigenvalues of $\tilde{\mathbf{R}}_R$
$\mathbf{0}_n$	zero matrix of dimension $n \times n$
$\mathbf{I}_n$	identity matrix of dimension $n \times n$
$(\cdot)^H$	matrix or vector transpose operation (Hermitian)
$(\cdot)^*$	complex conjugate operation
$(\cdot)^\star$	an optimal value of a variable
$\log(\cdot)$	logarithm with base 2
$\mathbb{E}(\cdot)$	expectation operation
$\text{tr}(\cdot)$	trace operation
$\max(\cdot)$	maximization
$\min(\cdot)$	minimization
$\mathbf{X}^{-1}$	inverse of the matrix $\mathbf{X}$
$\lvert\mathbf{X}\rvert$	determinant of the matrix $\mathbf{X}$
$\lvert x\rvert$	absolute value (magnitude) of a complex scalar x
$\lvert\lvert\mathbf{x}\rvert\rvert$	Euclidian norm of vector $\mathbf{x}$
$\text{vec}(\mathbf{A})$	vector $\mathbf{a}$ which is obtained by stacking the columns of matrix $\mathbf{A}$
$\sim$	distributed according to
$\triangleq$	defined as
$\mathbb{Z}_+$	set of positive integer numbers

Contents

1 Introduction

1.1 Motivation

Wireless communication systems have evolved from basic voice communication to mobile-broadband multimedia services. Today, the key drivers for the continued technology evolution in wireless communications are emerging demands for high data rate multimedia-based services, high spectral efficiency, low power consumption, and reliable services. Due to the proliferation of wireless multimedia applications and services such as video teleconferencing, network gaming, and high quality audio/video streaming, it is apparent that a wireless cellular system such as the Third Generation (3G) or its predecessor will be unable to comply with this ever-increasing demand for broadband wireless services. The recently deployed wireless communication system, the Fourth Generation (4G), is supporting much higher data rate services compared to evolving 3G systems (up to 100 megabits per second (Mbps) in outdoor environments and up to 1 gigabits per second (Gbps) in indoor environments) [1]. However, in the near future, wireless data traffic is envisioned to increase by 1,000-fold [2]. Thus, the next generation wireless systems, the Fifth Generation (5G), is expected to support up to 1,000 times higher data volume than today's systems, with peak and cell edge rates higher than 10 Gbps and 1,000 Mbps, respectively [3].

Recent research results show that the multiple-input multiple-output (MIMO) wireless technology [4, 5] has potential to meet these demands by offering increased spectral efficiency through spatial multiplexing (SM) gain and improved link reliability due to antenna diversity gain. When perfect channel knowledge is available at the receiver, the capacity has been shown to grow linearly with the number of antennae. Most MIMO detection schemes are based on perfect channel state information (CSI) being available at the receiver. Although perfect estimates are desirable in practice, the channel estimation procedure is aided by transmitting training sequences (also referred to as pilot signals) that are known at the receiver. Since known training sequences carry no data information, they consume the useful data power and bandwidth resources. Apparently, there is a tradeoff in allocating these resources between training and data sequences. The quality of the channel estimate depends on the length and power level of the

training sequence. However, over-increasing the overhead for training reduces information capacity. Therefore, it is desirable to limit the length and power allocated to the transmitted training sequence such that the desired quality of service is still maintained.

Moreover, MIMO systems are ideal for rich scattering environments where the channel between any pair of transmit and receive antennae can be modeled as a matrix of independent and identically distributed (i.i.d.) complex Gaussian random variables. Possible occurrences of the idealized channel conditions include the class of indoor channels, such as wireless local area networks, fixed wireless networks, and wireless ad-hoc networks. However, in many practical situations, the MIMO channels can be spatially correlated due to the limited scattering environment and inter-antenna spacing. The presence of spatial correlation also degrades the performance of the system because of the limited degree of freedom in the channel [6]. The smaller the distance between the antenna elements, the larger is the spatial correlation and the loss in the channel capacity [7–9]. With the combined impact of the CSI estimation error and spatial correlation on the symbol error rate (SER) performance [10–13], outage probability and capacity has been reported to be significant [14–17].

Hence, proper signal and robust system designs are required to meet the above-mentioned challenges. It is therefore of considerable relevance to study and design *i)* the space-time (ST) modulation constellations[1], and *ii)* the linear precoder matrices to be used with the finite discrete input such as quadrature amplitude modulation (QAM) and phase-shift keying (PSK) constellations. Consequently, the wireless communication system can achieve close-to-optimal performances at low signal-to-noise ratio (SNR) and tolerate inaccuracies in the channel estimates at the receiver and presence of spatial correlation and efficiently exploit the receive antennae to improve the error rate performances.

1.2 Communication over the wireless channel

Wireless channels operate through electromagnetic radiation from the transmitter to the receiver. The transmitter maps the information bearing symbols onto the electromagnetic waves over the open atmosphere rather than using propagation medium as wires. Electromagnetic waves generally propagate according to

[1] Constellations, codebook and codes are used interchangeably throughout this thesis.

three mechanisms: reflection, diffraction and scattering. Reflections arise when the plane waves are incident upon a surface with dimensions that are very large compared to the wavelength. Diffraction occurs according to Huygen's principle when there is an obstruction between the transmitter and receiver antennae and secondary waves are generated behind the obstructing body. Scattering occurs when the plane waves are incident upon an object whose dimensions are on the order of a wavelength or less and causes the energy to be dissipated in many directions. The relative importance of these three propagation mechanisms depends on the particular propagation environment. As a result of the above three mechanisms, electromagnetic wave propagation can be roughly suffered by three nearly independent phenomena: path loss variation with distance, slow log-normal shadowing, and fast multi-path fading [18]. Generally, these impediments of a radio channel can be categorized into two types of fading: large-scale fading and small-scale fading.

Large-scale fading represents the average signal power attenuation due to motion over large areas [19]. This phenomenon is affected by prominent terrain contours (hills, forests, billboards, clumps of buildings, etc.) between the transmitter and the receiver. The receiver is often represented as being "shadowed" by such prominence. The statistics of large-scale fading provide a way of computing an estimate of path loss as a function of distance.

Small-scale fading, on the other hand, refers to the dramatic changes in signal amplitude and the phase that can be experienced as a result of small changes (as small as a half-wavelength) in the spatial separation between a receiver and a transmitter. Small-scale fading manifests itself in two mechanisms, namely, time-spreading of the signal (or signal dispersion) and time-variant behavior of the channel [20]. For mobile radio applications, the channel is time-variant because motion between the transmitter and the receiver results in a propagation path change. The rate of change of these propagation conditions account for the fading rapidity (rate of change of the fading impairments). Depending on the Doppler spread, small-scale fading can be slow or fast. The statistical time-varying nature of the envelope of a flat-fading signal is characterized by probability density functions (PDFs) such as Rayleigh, Ricean, Nakagami, etc. [20]. When the multiple reflective paths are large in number and there is no line-of-sight signal component, the envelope of the received signal is statistically described by a Rayleigh PDF. When there is a dominant non-fading signal com-

ponent present, such as a line-of-sight propagation path, the small-scale fading envelope is described by a Rician PDF [20, Chs. 3 and 4]. A generic Nakagami PDF has also been widely adopted to characterize the small-scale fading in wireless communications due to its good accuracy and versatility [21].

The fading results in attenuation, delay and sometimes even complete distortion of the transmitted signal. Moreover, fading changes with time in unpredictable ways due to user movement. Thus, in order to be able to design good wireless systems, it becomes imperative to have a good understanding of electromagnetic waves and the propagation media used in conjunction to achieve communication. Furthermore, knowledge of the wireless CSI either at the receiver or both at the receiver and at the transmitter plays a significant role in achieving reliable transmission at high data rates over wireless channels.

1.3 Wireless multiple antennae system

The pioneering works, earlier by Winter *et al.* [22] and later by Foschini [4], and Telatar [23], revealed that in a rich scattering environment, the use of multiple antenna elements on the transmitter and the receiver side forms a MIMO channel and has a potential to increase the data rates via SM (it is also regarded as a special case of ST coding) and reliability via ST coding [24, 25] given a limited amount of frequency bandwidth compared to the traditional single antenna systems.

The reason for the MIMO channel to offer greater reliability compared to a single-input single-output (SISO) channel is diversity. A signal transmitted via several antennae reaches the receiver antennae from a number of different propagation paths. Each receive antenna thereby picks up the signal transmitted by each transmit antenna. If the antennae are located sufficiently far apart from each other such that the corresponding propagation coefficients are independent, the probability that all paths are in deep fade is significantly reduced. In other words, the probability of having a useless channel is smaller, which, in turn, leads to a lower probability of error at the receiver compared to the case with only a single antenna at both the transmitter and the receiver.

Whereas the diversity benefit leading to higher robustness against channel fading is available in systems with multiple antennae at either the transmitter or the receiver (or both), the advantage of SM requires multiple antennae on

the both sides of the communication link. Essentially, the MIMO channel can then be viewed as a set of parallel and independent SISO spatial channels that can be used to send independent data. An information-theoretic discussion concerning the exploitation of both spatial multiplexing and diversity and the tradeoff between these effects is available in [26].

Consider a generic MIMO communication system with M_T and M_R transmit and receive antennae, respectively. A block diagram of such a system is shown in Figure 1. Transmit data can be jointly encoded: spatially over the transmit antennae and temporally over the time dimension. The encoding is partitioned into ST slots, where each slots represents a specific transmit antenna and a specific signalling interval. The set of schemes aimed at realizing joint encoding of multiple transmit antennae is called ST coding. Now consider a scenario where an information source generates information bits. They are encoded and fed to the multiple antenna transmitter, which parses the encoded data stream into blocks. In order for these data blocks to be transmitted over a wireless channel, the transmitter maps each block of bits to a corresponding ST channel symbol using a mapper, where a ST channel symbol represents a particular assignment of signalling waveforms to each ST slot. The set of all admissible channel symbols is usually called a ST code [27]. The signalling waveform output from the ST encoder are then amplified and fed to the transmit antennae that radiate these signals to the respective ST slots.

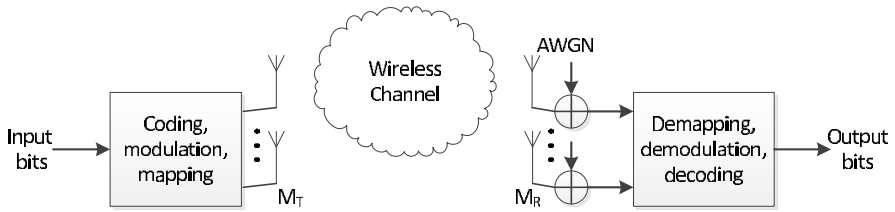

Fig. 1. Block diagram of the MIMO system.

On the receiver side, the transmission process is reversed in order to retrieve the original transmitted bits. The receiver first detects the transmitted symbols using a ST detector. These symbols are then demapped to produce one stream of data bits. This stream is then passed to the decoder, which produces a stream of bits that corresponds to the original stream of raw bits.

For the receiver to accurately detect the transmitted symbols, it needs to learn the channel. In order to do so, the receiver often requires the transmitter to send a known training sequence during some portion of the transmission interval. Since the training sequence is known at the receiver, it is used to generate the estimate of the channel coefficients. If the coherence time is sufficiently long, the receiver can feed back the acquired channel knowledge it has to the transmitter over a separate feedback channel. In this scenario, the coherence time is said to be long if the time required to acquire the channel knowledge at the communication terminals is negligible compared to the overall coherence time. Now, the transmitter has perfect CSI and it can use this information to distribute the available power to eigenmodes based on the waterfilling principle in order to maximize the mutual information[2] (MI) [29, 30]. The receiver exploits the channel information to perform efficient detection of the received signal.

While perfect channel state information at the transmitter (CSIT) and channel state information at the receiver (CSIR) allows reliable transfer at high data rates, the resources that are needed to realize this scenario are often hard to accommodate [31]. In particular, even if we assume that a separate channel is available for the receiver to feed accurate channel parameters back to the transmitter, the mobility of the transmitter and of the receiver usually limits the coherence time, and the channel may change significantly before the receiver manages to convey its channel knowledge to the transmitter. Consequently, it gives rise to the need of a more practical communication model where the receiver is assumed to be able to estimate the channel accurately but no channel information is fed back to the transmitter [31]. An interesting feature that this model shares with the previous one is that the maximum data that can be communicated over the MIMO channel is achieved through linearly structured ST coding techniques [32, 33]. A communication system where the receiver has access to an accurate channel model that facilitates the process of data recovery is usually referred to as coherent [34].

In coherent communications, the coherence time is assumed to be long enough to warrant neglecting the fraction of the transmission time required for the receiver to acquire an accurate model of the channel in comparison with the overall

[2]It is a measure of the amount of information that one random variable contains about another random variable. It is the reduction in the uncertainty of one random variable due to the knowledge of the other [28].

transmission time. In many practical situations, the variations in the channel parameters are fast and the time required for the receiver to acquire a reasonably accurate channel model may consume a significant portion of the time available for communication. This problem becomes more pronounced in systems that employ a large number of transmit antennae [26]. For these instances, the communication model is usually referred to as non-coherent [34]. Similar to the coherent channel case, the transmitter can send pilot symbols for the receiver to identify the channel parameters and perform coherent detection. However, unlike the coherent channel model, this procedure is properly accounted for in the design of the non-coherent communication system.

In addition to the communication models described in this section, there are other intersecting models in which the receiver and possibly the transmitter have access to partial channel information, i.e., some information about the channel which cannot be considered to be perfect. This can be the case when the length or energy of the training sequences is kept at a minimum (implying a noisy channel estimate) or the channel fades between subsequent channel uses are such that the current channel state is loosely correlated to the previous state (i.e., neither perfectly the same nor completely independent).

Thus, wireless communication systems can be classified into three categories in terms of the amount of channel state information available at the receiver:

– Coherent systems: perfect CSIR,
– Non-coherent systems: no CSIR,
– Partially coherent systems: estimated (hence imperfect) CSIR.

1.4 MIMO transmission design

Information theoretic results by Telatar, Foschini and Gans [4, 23, 35] for MIMO flat-fading channels, later for multipath [36, 37] and correlated [38–40] fading channels, triggered a large amount of research on MIMO technology. These researches were mainly focused on channel coding, transceiver signal processing algorithms to develop practical schemes that achieve a large fraction of the promised capacity [41–43]. In general, the MIMO system design is strongly influenced by the CSI knowledge available on the transmitter side [44]. However, below we characterize the MIMO system design based on the CSI knowledge available on the receiver side.

1.4.1 Coherent channels

Design with no CSIT

Signal design with no CSIT has received much attention for many years because of its evident importance from a practical perspective. One of the first work considering this case was the delay diversity technique proposed by Seshadri *et al.* [45] for multiple transmit antenna system which transmits the same symbols through all the antennae, but applying a different delay at each antenna. Besides this approach, ST coding techniques have received a lot of attention. Tarokh *et al.* [24] and Guey *et al.* [46] derived the fundamental design criteria of the optimum ST codes for a Rayleigh flat-fading MIMO channel, providing both diversity and coding gain. Based on the same criteria, several ST codes are proposed, such as space-time trellis codes (STTCs) [24]. Tarokh *et al.* [47] later accounted for imperfect CSIR on the performances of the STTCs. A new metric for the Veterbi decoder was also proposed to improve the performance in the presence of imperfect CSIR. One artifact of STTC is the increase in the computational complexity both at the transmitter and at the receiver with the higher number of transmit and receive antennae and code rate. To address this problem, Tarokh *et al.* [48] considered a different approach, where they combined the STTC with beamforming at the receiver. The receiver structure was not optimal, which resulted in decreased diversity gain; however, the computational complexity was reduced dramatically.

The unaffordable decoder computational complexity, based on the maximum likelihood (ML) criterion, of STTC motivated the development of space-time block code (STBC) for MIMO channels. Alamouti [49] proposed block codes for a flat-fading channel with two transmit antennae and any number of receive antennae, which has very low decoding computational complexity. Alamouti's STBC was later generalized [50–52] for any number of transmit antennae based on orthogonal designs for both real and complex constellations. Full rate codes for any number of transmit antennae were designed using real constellations and for two transmit antennae using complex constellations. They have fast ML decoding and full diversity. Later, full-rate quasi-orthogonal STBCs for a larger number of transmit antennae were designed using complex constellations by Jafarkhani [53], Tirkkonen *et al.* [54] and Papadias *et al.* [55]. In quasi-orthogonal

STBC designs, the orthogonality is relaxed to provide s higher transmission rate. With the quasi-orthogonal structure, the quasi-orthogonal STBCs still enable fast ML decoding but do not achieve full diversity. The performance of these codes was better than that of the codes from orthogonal designs at a low SNR but worse at a high SNR. In order to improve the performances at higher SNRs, Su *et al.* [56] proposed a method where half of the symbols in a quasi-orthogonal design are chosen from a signal constellation set and the other half from its rotated constellation. Stoica *et al.* [57] presented a maximum SNR solution with no CSIT. There the idea was to transmit whole information about the most favored subchannel, which also provides very good bit error rate (BER) performance results.

SM is another MIMO transmission technique which can be used with no CSIT. The well-known SM techniques are Bell Lab's space-time (BLAST) [33] based structures. The most prominent ones are vertical-BLAST (V-BLAST) and diagonal-BLAST (D-BLAST). They both obtained full diversity and full rate. Implementation complexity of D-BLAST is higher compared to that of V-BLAST. In D-BLAST, the original stream to be transmitted is divided into M_T parallel substreams so that the symbols from each of them are transmitted sequentially through all the transmit antennae in successive channel use [33]. Whereas in V-BLAST, the substreams are mapped one to one from each symbol to each transmit antenna [58].

Design with perfect CSIT

If the channel is perfectly known on the transmitter side, the MIMO channel can be converted into a set of parallel, non-interfering SISO channels through a singular value decomposition (SVD) of the channel matrix [35]. The gains of these elementary spatial subchannels, commonly denoted as eigenmodes, are equal to the singular values of the MIMO channel matrix. To maximize the MI, the total available power should be distributed to eigenmodes based on the waterfilling (WF) principle [30, 59].

For a frequency selective MIMO channel, Scaglione *et al.* [60] divided the transmitted symbols into disjoint groups and then encoded each group using a matrix called linear precoder matrix. On the receiver side, the linear decoder matrix is applied to the received data to estimate the transmitted sym-

bols. The linear precoder/decoder matrices are designed jointly by minimizing the minimum mean-square error (MMSE), minimizing the determinant of the mean-square error (MSE) matrix, and maximizing the minimum eigenvalue of the SNR-like matrix. Numerous criteria can be found in the literature to design the precoders, e.g., maximizing the mutual information (MI) [61, 62] or cutoff rate (CR) [63, 64], minimizing the total MSE [65], minimum bit error probability (BEP) [66], maximizing the received SNR [57], and minimum Euclidean distance based designs [67, 68].

The capacity-optimal signaling strategy [59] and other criteria mentioned above were developed with an assumption of Gaussian input distribution, which is practically not feasible to implement, although capacity optimal. Furthermore, Lozano *et al.* [69] showed that a power allocation policy to parallel Gaussian channels with Gaussian input is sub-optimal for discrete inputs[3]. Therefore, numerous works [61, 62, 70–73] have considered the design of linear precoders for the discrete inputs over the MIMO fading channels as well.

1.4.2 Design for non-coherent channels with no CSIT

In fast-fading scenarios, however, fading coefficients can change into new, almost independent values before being learned by the receiver through training signals. This problem becomes even more acute when large numbers of transmit and receive antennae are being used by the system, which requires very long training sequences to estimate the fading coefficients. Even if the channel does not change very rapidly, for applications which require transmission of short control packets, long training sequences have a large overhead (in terms of the amount of time and power spent on them) and significantly reduce the efficiency of the system. A non-coherent detection scheme, where the receiver detects the transmitted symbols without having any information about the current realization of the channel, is more suitable for these fast-fading scenarios.

Motivated by this fact, numerous non-coherent channel ST code designs have been considered. When the transmitter and the receiver both have no access to the CSI, as shown by Marzetta and Hochwald [34], in the high SNR regime,

[3]The optimal policy allocates more power to the channels with high gain to support maximum rate and finite constellation, on the other hand, might not support that high rate. Thus, power allocated to that channel must be reduced, otherwise it would be wasted.

the capacity optimal signalling scheme is to transmit the mutually orthogonal data streams through different antennae. These types of codes are known as unitary space-time codes (USTCs). Based on previous results, USTC designs were presented in [74]. They also compared the performance of the codes with a coherent ML detector to the codes with a non-coherent ML detector and reported a 3 dB loss in terms of SNR. Later, Hochwald *et al.* [75] presented a systematic design of unitary codes based on Fourier and algebraic models. On the other hand, in a low SNR regime, a peaky signaling scheme [76–78] was found to be optimal.

For continuously fading channels, differential unitary space-time modulation has been proposed in [79]. In this scheme, the transmitted signal matrix at each time block was the product of the previously transmitted matrix and the current unitary data matrix. They also proposed a set of group-structured diagonal constellations called cyclic codes, and a quantity defined as diversity product was chosen as the design criterion of constellations for USTCs. Using the differential modulation approach, Tarokh and Jafarkhani [80] presented a differential extension of the Alamouti code using PSK constellations with a simple encoder and decoders. Another differential USTC construction similar to the one used in [79] was proposed by Hughes [81], where the focus was on group codes and two-antenna codes with cyclic and quaternionic structures explicitly designed. A similar approach [82] but with a more simplified analysis was carried out with the focus on the differential receiver. Hassibi *et al.* [83] presented a systematic differential code design using the Cayley transform. It enables to finding simple encoders based on linear mapping and transformation and low complex suboptimal receivers based on the resolution of a set of linear equations. Numerous methods have since been proposed to construct unitary ST signals [84–88] that leverage the unitary codes designed in [34].

1.4.3 Partially coherent channels with partial CSIT

In the previous two sections, transmission strategies in two extreme cases have been described. In a practical scenario, it may be too pessimistic that the receiver is totally unaware of CSI, and assuming that perfect CSIR might not be very realistic. Consequently, only partial or imperfect CSI is usually available at the receiver, which further implies that the transmitter can have only partial CSI in

the form of either mean or covariance of the channel estimate or both. Spectral efficiency and the performance of MIMO systems degrade as the quality of the channel estimates reduces from perfect to imperfect [89, 90]. Furthermore, Ray *et al.* [91] studied the maximum capacity loss due to the lack of receiver CSI for a wideband MIMO channel in Rayleigh-fading. The maximum penalty to be paid in terms of capacity not having CSI at the receiver is shown. However, the channel capacity with partial receiver CSI is an open problem, but useful bounds are known [89, 92]. Transmitter design including constellation and precoder design for this case has also received some attention. We briefly review the MIMO constellations and precoder design adapted to the partial CSIR below.

Constellation design

Numerous methods to design and construct the multiple antenna constellations adapted to the quality of channel estimated at the receiver, called partially coherent constellations (PCCs), have been investigated [93–96]. Baccarelli and Biagi [93] designed the STBCs by maximizing the minimum squared Euclidean distance and, at the same time, minimizing the maximum squared correlation between the codewords. They restricted the structure of the STBC to unitary matrices that "*self-match*" to channel estimation errors to guarantee "full-diversity", for any value of channel estimation error variance σ_E^2. They constructed the self-matching STBC by augmenting an arbitrary unitary matrix $\mathbf{U}$ with those codes $\mathbf{V}$ already designed for fully-coherent applications [25, 49, 97]. Similar to this approach of code constructions Giese and Skoglund [94] also restricted the structure of the STBC to a unitary matrix. They presented two approaches to construct the unitary STBC adapted to the level of CSIR. First, they used a gradient search method to designs unitary codes by optimizing the upper bound on the pairwise error probability (PEP). The second approach was based on a combination of constellations previously designed for coherent [25, 49, 97] and non-coherent [34, 75] communications, where more weight was given to the coherent or non-coherent constellations depending on the available CSIR.

Unlike the above constellation construction methods, Borran *et al.* [96] proposed constellations which were multi-level with multi-dimensional spherical constellations at each level. They showed that the new constellations provide significant performance improvement over the conventional single-antenna PSK and

QAM and multiple-antenna techniques such as the BLAST architecture and orthogonal transmit diversity (OTD) schemes when the estimation variance is comparable to the reciprocal of the SNR. Wu and Pätzold [95] proposed to using the asymptotic symbol error probability (ASEP) of orthogonal space-time block codes (OSTBC) as a criterion to design the constellations that match well with the level of the CSI error. All the constellation design criteria mentioned above were based on minimizing the average symbol error probability of uncoded constellations (when each block of symbols is decoded separately).

Precoder design

Much less literature exists concerning the transmission strategies with imperfect CSI at both ends. This scenario is of paramount importance in practical implementations and should be taken into account when designing a system. Towards this end, Palomar [98, Chapter 7] considered two different design philosophies: the worst-case and the stochastic (Bayesian) robust designs. In [99], Zhang *et al.* derived closed form robust designs including the minimum total MSE design with an assumption that the channel mean and the receiver correlation matrix were available to both ends. They also accounted for the channel correlation into the design. Under the same CSI assumptions, Serbetli and Yener [100] used the minimum total MSE criterion to design the precoder/decoder matrices. Unlike [99, 100], Ming and Blostein [101, 102] considered the joint design of a precoder/decoder matrix with an assumption that the channel mean and the transmitter correlation matrix were available to both ends. These works assumed that input distribution is Gaussian. However, in practice we use discrete input (QAM and PSK, etc.). Therefore, some works [61, 62, 70–73] consider the design of linear precoders for the discrete input over the MIMO fading channels. However, perfect CSIT/CSIR was assumed in [61, 70–73], and [62] assumes perfect CSIR and partial CSIT.

1.5 Aims and outline of the thesis

The focus of this thesis is on the design single-user MIMO PCCs and linear precoder matrices for partially coherent communication scenarios under a given average power constraint. We assume a block Rayleigh flat-fading channel where

the transmitter has access to the channel estimation error covariance matrix and the receiver has only an imperfect estimate of them. Furthermore, in order to use the PCCs with forward error control (FEC) codes, an algorithm is developed, corresponding to the PCC, to find the bit mapping scheme. Performances, with respect to MI, SER, peak-to-average power ratio (PAPR), BER, and frame error rate (FER) of the newly designed PCCs and precoders are evaluated and compared with those of Kullback-Leibler divergence (KLD)-optimized constellations and conventional QAM constellations and precoders. All the results presented in this thesis have been published, conditionally accepted or submitted for publication in peer reviewed international scientific journals.

We propose using CR as the primary criterion to design of the ST constellations and linear precoder matrices for a partially coherent MIMO channel. CR is a lower bound on channel capacity and determines the region of rates where a communication system can operate to achieve an arbitrarily small probability of error. Channel capacity is the maximum possible MI between input and output of the channel for all input distributions. Its maximization minimizes an upper bound on the codeword error probability over the ensemble of the binary channel codes assuming sequential decoding while it is independent on a specific code [103–105]. Although rates larger than the CR can be achieved (e.g., by turbo codes or low-density parity check codes with iterative decoding [106] or optimum Viterbi decoding of convolutional codes, etc.), it is still useful in predicting the performance [107]. CR has been proposed for non-coherent channels as a signal design criterion in [84, 87] and for companding channels in [108]. CR has also been proposed to design precoders [64] and optimal binary inputs with imperfect CSI [109].

A closed and tractable form of the mutual information for the MIMO fading channels with imperfect CSIR is not known [110]. Moreover, the corresponding capacity achieving input distribution is also an open problem [89, 92, 110]. Only upper and lower bounds on the MI are known, but those can be rather loose for certain non-Gaussian input distributions [89, 92]. Nevertheless, we propose using CR as a criterion for the MIMO constellation and precoder design. The CR expression is suitable for designing finite and discrete constellations and has a closed and analytically tractable form. Furthermore, maximizing the CR maximizes the MI of the channel.

Especially for single transmit antenna constellations, we also propose using the Bhattacharyya distance (BD) and upper bound (UB) on the average bit error probability (ABEP) as the design criteria. The BD, in a statistical context, measures the similarity of two discrete or continuous probability distributions. Moreover, the BD is a special case of the Chernoff distance, when the Chernoff parameter is assigned the value $\frac{1}{2}$. The BD determines the asymptotic exponential decay rate of the average pairwise error probability (APEP) of the ML detector. In terms of the problem of signal selection, Kailath [111] found that the BD is superior to the KLD. It has also been shown in [112] that the Bhattacharyya upper bound is indeed the tightest Chernoff bound when signals have equal priors. On the other hand, the UB on the ABEP criterion has been used to design PCCs when they are to be used in conjunction with FEC codes. The rationale for using an UB-ABEP expression as a constellation design criterion in this case seems obvious: it allows taking both the Hamming distance and PEPs into account in a single expression. Thus, a bit mapping can be fixed to the Gray in advance and constellation can be searched through numerical optimization.

Chapter 2, the results of which have been presented in [113–115], considers the ST codeword design for partially coherent i.i.d. MIMO channels. The BD and the CR are derived and used as the design criteria. The single antenna constellations are designed by maximizing the minimum BD and maximizing the CR. Constellation diagrams are presented for different values of the channel estimation error variance in order to study the impact of the imperfect CSIR on them. When channel coherence time is equal to one symbol interval, the multiple transmit antennae constellations are designed simultaneously across the transmit antennae by maximizing the CR. On the other hand, when the channel coherence time is equal to several symbol intervals, the USTCs are used as a signal matrix. The USTCs are constructed by leveraging the unitary codes designed in [93, 94]. Furthermore, there MI, SER and PAPR performances are compared to the performances of the KLD-based design constellations and conventional QAM constellations. In spite of the fact that CR, an information theoretic measure, characterizes predicted performance with long FEC codes, it is used in this chapter to investigate the uncoded SER performances. This is done in order to compare the performances with other existing non-information theoretic measures, such as KLD and APEP, which were used to measure the uncoded SER performances.

Chapter 3, the results of which have been documented in [116, 117], extends the design of the PCCs developed in Chapter 2 to a spatial correlated MIMO channel and there to performances with a practical coding scheme. The combined impact of the CSI estimation error and spatial correlation on the ST code design is studied in this chapter. Furthermore, using the PCCs with any FEC coding requires efficient bit mapping. An efficient bit mapping algorithm called modified bit switching algorithm (MBSA) is developed.

Two criteria, UB on the ABEP and CR expressions, are derived and used to design the single and multiple antenna PCCs, respectively. Then, two methodologies to design the constellation and bit mapping schemes in two steps are proposed. The first method, which is for the single transmit antenna case, starts with some known conventional two-dimensional (2-D) constellations (e.g., M-QAM) which already apply the Gray mapping and then optimize the constellation points by minimizing the UB-ABEP. The resulting constellation can straight-forwardly apply the Gray mapping and maintain its simplicity. In the second method, which is for multiple transmit antennae, the constellation is designed simultaneously across the transmit antennae using an approach similar to the one used in Chapter 2, which was based on maximizing the CR expression (other criteria can also be used, e.g., maximizing the minimum BD [113], KLD, etc.). The resulting symbols are subsequently mapped to a binary sequence using some efficient algorithms, e.g., tabu search or binary switching algorithm (BSA) [118]. One artifact for this method is the difficulty in its use when the cardinality of the constellation is large.

When the channel coherence time is equal to several symbol intervals, the CR-optimized OSTBCs [49] and USTCs are used as a signal matrix. Combining the turbo codes with the unitary ST codes was first considered in [119] but without optimized mapping. The effects of mapping on the error performance of the coded ST constellation have been studied in [120, 121] for bit-interleaved coded modulation and iterative decoding (BICM-ID). In [121], two different mapping rules were introduced for USTCs with iterative decoding. The results show good performance gain but their mapping rules were limited only to the unitary constellation obtained from the orthogonal designs. A faster algorithm to design the mapping rule based on the BSA was introduced in [120]. We present a MBSA to develop mapping rules for PCCs using a novel design metric suitable for partially coherent channels. The coded BER and FER performances of the

resulting PCCs are compared to those of the conventional QAM constellations with turbo codes.

Chapter 4, the results of which are presented in [122, 123], considers the problem of a single-user MIMO linear precoder matrix design for spatially correlated partially coherent Rayleigh-fading channels with discrete inputs. A major drawback of the PCC construction procedure, developed in Chapters 2 and 3, is that it has two-fold computational complexity. First, searching the constellation points itself, and, second, the search for a close-to-optimal, pseudo-Gray bit mapping scheme. Moreover, due to the nonlinear fashion in which the optimal ST signal is structured, it is expected that this feature inhibits the use of efficient suboptimal techniques like sphere detectors in the detection process. Furthermore, linear precoders are easily backword compatible with the existing conventional constellations and various wireless standards (e.g., 3^{rd} Generation Partnership Project (3GPP) Long Term Evolution (LTE), wireless local area network (WLAN), etc.) Because of these reasons, linear precoder design is consider as an alternative to PCC.

CR is proposed as a criterion for the MIMO linear precoder matrix design. It is suitable for readily available finite and discrete constellations and has a closed and analytically tractable form. A linear precoder is obtained by numerically maximizing the CR with respect to the precoder matrix with a given average power constraint. The precoder matrix is decomposed using SVD into the input shaping matrix, power loading matrix, and beamforming matrix. The beamforming matrix is found to coincide with the eigenvectors of the transmit correlation matrix. The power loading and input shaping matrices are solved numerically using the difference of convex (d.c.) programming algorithm and optimization under the unitary constraint, respectively. Precoders are designed to be used in conjunction with two MIMO transmission scheme: the SM and ST block transmission modes. The MI and FER performance of the CR-optimized precoders are compared to those of CR PCCs and conventional QAM constellations with turbo codes.

Chapter 5 concludes the thesis. The main results are summarized and suggestions for future research are presented.

1.6 Author's contribution

The thesis is based, in parts, on three journal papers [114, 117, 122], and four published conference papers [113, 115, 116, 123]. The first journal paper [114] is already been published, second one [117] to appear and third one [122] is under revision. The author has had the main responsibility for performing the analysis, developing the simulation software, generating the numerical results, and writing all the papers [113–117, 122, 123]. Other authors provided help, ideas, comments, and criticism during the process.

In sum, the main contributions of the thesis are:

- Derivation of CR and UB-ABEP expressions as a function of the channel estimation error covariance matrix for an i.i.d. and spatially correlated MIMO channel.
- UB-ABEP and CR expressions are used as design criteria to design the single transmit and multiple transmit antenna PCCs, respectively, under a given average power constraint.
- MBSA is proposed to find out the bit mapping schemes for the PCCs.
- Detailed performance evaluations of the resulting PCCs for various MIMO schemes (such as SM and ST coding) with and without FEC codes.
- CR expression, suitable for discrete input, is further modified to design the precoder matrices adapted to the imperfect CSIT and transmit and receive correlations.
- A difference of convex (d.c.) decomposition of the CR expression with respect to the precoder matrices is derived.
- Detailed two-step iterative algorithm (the first step concerns the prismatic branch-and-bound (BnB) algorithm and the second step the self-tuning Riemannian steepest descent (SD) algorithm) is presented to solve the CR expression for the precoder matrix.
- Detailed performance evaluations of the resulting CR-optimized precoders for various MIMO schemes (such as SM and ST coding) with FEC codes.

2 Partially coherent constellation design in i.i.d. channels

In this chapter, we consider the problem of ST constellation design for a MIMO channel with partial CSIR and CSI estimation error variance available perfectly via feedback[4] from the receiver to the transmitter. We assume i.i.d. Rayleigh flat-fading channels. Furthermore, the receiver CSI estimate is assumed to be an unbiased Gaussian random variable with a variance known by both the receiver and the transmitter. The BD and CR expressions as a function of channel estimation error variance are derived and proposed as constellation design criteria. No outer code is used during the performance evaluations of the newly designed constellations.

The chapter is organized as follows: The assumptions and system model are described in Section 2.1. The detailed derivations of the design criteria, signal set construction method and constellation design with additional PAPR constraint on the signal set are presented in Section 2.2. The details of the numerical optimization method are presented in Section 2.3. The MI, PAPR and numerical SER results are presented in Section 2.4. Section 2.5 concludes the chapter.

2.1 System model

We consider a communication system with M_T transmit and M_R receiver antennae in a block Rayleigh flat-fading channel with coherence time of $T = T_t + T_d$ symbol intervals, where $T_t \in \mathbb{Z}_+$ and $T_d \in \mathbb{Z}_+$ are the training symbol and data transmission time in discrete symbol intervals, respectively. The matrix of the received symbols can be expressed as

$$\mathbf{R}_d \quad = \quad \mathbf{S}_d\mathbf{H} + \mathbf{W}_d, \tag{1}$$

where $\mathbf{R}_d \in \mathbb{C}^{T_d \times M_R}$, $\mathbf{S}_d \in \mathcal{S} \subset \mathbb{C}^{T_d \times M_T}$ is the transmitted symbol[5], $\mathcal{S}$ is the

[4]It should be noted that the transmission of CSI estimation variance from the receiver via a feedback link to the transmitter will reduce the spectral efficiency of the system.

modulation signal matrix alphabet with L elements or $\mathcal{S} = \{\mathbf{S}_{d,1}, \mathbf{S}_{d,2}, \ldots \mathbf{S}_{d,L}\}$, $\mathbf{H} \in \mathbb{C}^{M_T \times M_R}$ is the channel response and $\mathbf{W}_d \in \mathbb{C}^{T_d \times M_R}$ the additive white Gaussian noise (AWGN) matrix. Here, we capture the effect of $\mathrm{SNR_d}$ factor in $\mathbf{S}_d$, and use the power normalization

$$\frac{1}{T_d} \sum_{t=1}^{T_d} \sum_{m=1}^{M_T} \mathbb{E}[|s_{tm}|^2] \quad = \quad P_d, \tag{2}$$

where s_{tm} is the element at the tth row and mth column of the signal matrix $\mathbf{S}$. As we will see in Section 2.2, the structure of the optimal constellation depends on the value of the $\mathrm{SNR_d}$, and constellation of the same size at different $\mathrm{SNR_d}$ are not necessarily scaled versions of each other. The elements of $\mathbf{H}$ and $\mathbf{W}_d$ are modeled as i.i.d. circularly-symmetric complex Gaussian random variables from the distribution $\mathcal{CN}(0,1)$ with $\mathbf{w} \triangleq \mathrm{vec}\,(\mathbf{W}_d)$ and $\mathbf{h} \triangleq \mathrm{vec}(\mathbf{H})$. The channel $\mathbf{H}$ stays constant during the transmission of the signal matrix $\mathbf{S}$ (hereinafter we drop the subscript d for convenience). We also assume that the receiver has computed an estimate $\hat{\mathbf{H}}$ of the channel matrix $\mathbf{H}$. We model the channel as [96], [124]

$$\mathbf{H} \quad = \quad \hat{\mathbf{H}} + \tilde{\mathbf{H}}, \tag{3}$$

where $\hat{\mathbf{H}} \sim \mathcal{CN}(\mathbf{0}, (1-\sigma_E^2)\mathbf{I})$ is the estimate known to the receiver and $\tilde{\mathbf{H}} \sim \mathcal{CN}(\mathbf{0}, \sigma_E^2\mathbf{I})$ is the unknown channel component, which can be viewed as an additive channel estimation error. We can further assume that the entries of $\hat{\mathbf{H}}$ are independent from the entries of $\tilde{\mathbf{H}}$. This can be obtained, e.g., by using a linear MMSE (LMMSE) estimator[6]. Parameter $\sigma_E^2 \in [0,1]$ is the channel estimation variance per channel coefficient. By setting σ_E^2 equal to zero or one, this model reduces to the coherent and non-coherent system models, respectively.

The conditional PDF of the received signal is [96]

$$p\left(\mathbf{R}_d|\mathbf{S}, \hat{\mathbf{H}}\right) = \frac{\exp\left\{-\mathrm{tr}\left[(\mathbf{I}_{T_d} + \sigma_E^2 \mathbf{S}\mathbf{S}^H)^{-1}(\mathbf{R}_d - \mathbf{S}\hat{\mathbf{H}})(\mathbf{R}_d - \mathbf{S}\hat{\mathbf{H}})^H\right]\right\}}{\pi^{T_d M_R}|(\mathbf{I}_{T_d} + \sigma_E^2 \mathbf{S}\mathbf{S}^H)|^{M_R}}. \tag{4}$$

[5]Note that $\mathbf{S}_d$ is a dedicated part of the actual transmitted symbol for data transmission sent over T_d symbol intervals. We assume that the receiver will estimate the channel from dedicated training symbols sent over a training period in addition to T_t [124].

[6]Transmitting the training signal with longer sequences and/or a higher power level will increase the estimation accuracy at the cost of more resources allocated to the control signalling and less to the data payload. Therefore, in this section, we have kept the communication resources (i.e., power and rate) allocation to the training symbols minimum.

The ML detection finds the signal matrix that maximizes the above expression for the given received signal matrix and channel estimate. The ML detector is

$$\hat{\mathbf{S}}_{ML} = \arg\max_{\mathbf{S}\in\mathcal{S}} p\left(\mathbf{R}_d|\mathbf{S},\hat{\mathbf{H}}\right). \tag{5}$$

2.2 Constellation design

In this section, we first derive the cutoff rate expression and adopt it as an ST constellation design criterion for a partially coherent channel.

2.2.1 Cutoff rate matched to partially coherent channel

The CR for the discrete input of cardinality L and continuous output channel under the additional assumption of partial CSI is given by [105]

$$R_0 = \max_{\{\pi_i\}_{i=1}^{L}} -\log \int\int \left[\sum_i \pi_i \sqrt{p(\mathbf{R}_d,\hat{\mathbf{H}}|\mathbf{S}_i)}\right]^2 d\hat{\mathbf{H}} d\mathbf{R}_d, \tag{6}$$

where $p(\mathbf{R}_d,\hat{\mathbf{H}}|\mathbf{S}_i)$ is the joint PDF of matrix $\mathbf{R}_d$ and partial CSI matrix $\hat{\mathbf{H}}$, when $\mathbf{S}_i$ is transmitted and π_i is the probability distribution over the set of signal matrices $\mathcal{S}$.[7] The cutoff rate for the partially coherent MIMO channel is given below.

Proposition 1 *The cutoff rate of the partially coherent channel with discrete input values and continuous output with the channel estimation variance σ_E^2 is given by (7)*

$$R_0 = \max_{\{\pi_i\}_{i=1}^{L},\{\boldsymbol{S}_i\}_{i=1}^{L}} -\log \left\{ \sum_i \pi_i \sum_j \pi_j \left(\frac{|\boldsymbol{I}_{M_T} + \sigma_E^2 \boldsymbol{S}_i^H \boldsymbol{S}_i|^{1/2} |\boldsymbol{I}_{M_T} + \sigma_E^2 \boldsymbol{S}_j^H \boldsymbol{S}_j|^{1/2}}{\left|\boldsymbol{I}_{T_d} + \frac{1}{2}\sigma_E^2(\boldsymbol{S}_i\boldsymbol{S}_i^H + \boldsymbol{S}_j\boldsymbol{S}_j^H) + \frac{1}{4}(1-\sigma_E^2)(\boldsymbol{S}_i - \boldsymbol{S}_j)(\boldsymbol{S}_i - \boldsymbol{S}_j)^H\right|} \right)^{M_R} \right\}, \tag{7}$$

where $\{\boldsymbol{S}_i\}_{i=1}^{L}$ is the constellation set with corresponding probabilities $\{\pi_i\}_{i=1}^{L}$.

Proof. Appendix 2. ■

[7] Note that by definition (6), the CR implies finding the probabilities of the constellation points maximizing certain expression.

The inner expression of the CR in (7) is the Bhattacharyya bound on the probability of error between any two signal matrices $\mathbf{S}_i, \mathbf{S}_j \in \mathcal{S}$, as a function of CSI estimation error σ_E^2, or

$$\rho_{\text{uncor}}(i,j) \triangleq \sqrt{|\mathbf{I}_{T_d} + \sigma_E^2 \mathbf{S}_i \mathbf{S}_i^H|}\sqrt{|\mathbf{I}_{T_d} + \sigma_E^2 \mathbf{S}_j \mathbf{S}_j^H|} \cdot \frac{1}{\left|\mathbf{I}_{T_d} + \frac{1}{2}\sigma_E^2(\mathbf{S}_i\mathbf{S}_i^H + \mathbf{S}_j\mathbf{S}_j^H) + \frac{1}{4}(1-\sigma_E^2)(\mathbf{S}_i - \mathbf{S}_j)(\mathbf{S}_i - \mathbf{S}_j)^H\right|} = e^{-\mathcal{B}(\mathbf{S}_i \| \mathbf{S}_j)}, \quad (8)$$

where $\mathcal{B}(\mathbf{S}_i \| \mathbf{S}_j) = -\log \rho_{\text{uncor}}(i,j)$ is the BD between the two signals [125]. The usefulness of (8) can be seen later in deriving Propositions 2 and 3.

For $\sigma_E^2 = 0$ or perfect CSIR, i.e., coherent communication, (7) reduces to

$$R_0 = \max_{\{\pi_i\}_{i=1}^L, \{\mathbf{S}_i\}_{i=1}^L} -\log \left\{ \sum_i \pi_i \sum_j \pi_j \left(\frac{1}{|\mathbf{I}_{M_T} + \frac{1}{4}(\mathbf{S}_i - \mathbf{S}_j)^H(\mathbf{S}_i - \mathbf{S}_j)|} \right)^{M_R} \right\}, \quad (9)$$

which is the same performance criterion as given in [24] for coherent ST codes with equal transmission probabilities, and results in *rank* and *determinant* design criteria. For $\sigma_E^2 = 1$ or no CSIR, i.e., non-coherent communication, (7) reduces to

$$R_0 = \max_{\{\pi_i\}_{i=1}^L, \{\mathbf{S}_i\}_{i=1}^L} -\log \left\{ \sum_i \pi_i \sum_j \pi_j \left(\frac{\sqrt{|\mathbf{I}_{T_d} + \mathbf{S}_i\mathbf{S}_i^H|}\sqrt{|\mathbf{I}_{T_d} + \mathbf{S}_j\mathbf{S}_j^H|}}{|\mathbf{I}_{T_d} + \frac{1}{2}(\mathbf{S}_i\mathbf{S}_i^H + \mathbf{S}_j\mathbf{S}_j^H)|} \right)^{M_R} \right\}, \quad (10)$$

which is the same performance criterion as the one in [87] and [84] for non-coherent space-time constellation design. We can infer from (9) and (10) that an optimal CR for the intermediate values of σ_E^2 is a combination of the coherent and non-coherent CR expressions.

Now we discuss few remarks on the BD which are useful in interpreting the constellation obtained through CR maximization:

Remark 1: The minimum BD between two signal matrices $\mathcal{B}(\mathbf{S}_i \| \mathbf{S}_j)$ is proportional to the Euclidean distance when perfect CSI is available at the receiver, i.e., $\log|\mathbf{I}_{T_d} + \frac{1}{4}(\mathbf{S}_i - \mathbf{S}_j)(\mathbf{S}_i - \mathbf{S}_j)^H|$.

Remark 2: A set of signal matrices which achieve the cutoff rate have a maximum value of minimum $\mathcal{B}(\mathbf{S}_i \| \mathbf{S}_j)$.

Remark 3: For the non-coherent channel (no CSIT), the minimum BD between two signal matrices is proportional to the squared norm of $\|\mathbf{S}_i\mathbf{S}_i^H - \mathbf{S}_j\mathbf{S}_j^H\|^2$ of the matrix outer product difference [84].

We refer to the argument of $\max(\cdot)$ in (7) as the cutoff rate expression and denote it as ϱ. For the equiprobable signal set with probabilities $\{\pi_i\}_{i=1}^{L} = 1/L$, the ST constellation design can be now formulated as the following continuous optimization problem (for fixed L, elements of $\mathbf{S}$ can take any values on complex plane)

$$\begin{array}{ll} \underset{\{\mathbf{S}_i\}_{i=1}^{L}}{\text{maximize}} & \varrho \\ \text{subject to} & \frac{1}{L}\sum_{i=1}^{L} \|\mathbf{S}_i\|^2 = T_d P_d \end{array} \tag{11}$$

where the maximization is with respect to the signal matrices.

The cutoff rate (11) is obviously not a convex function in the coordinates of the signal points. There are several approaches to approximate a non-convex function, for example, grid search, simulated annealing, SD, etc., but the solution is not guaranteed to be optimal. The cutoff rate R_0 and the rate-achieving signal set can be iteratively computed using (11).

We now discuss two properties of the solution to (11); similar properties have been discussed in [84] for non-coherent constellations under peak power constraint. First, we give the relation between the expected BD of the rate-optimal constellation and the largest possible minimum BD of any constellation of identical dimension. Define this latter distance as

$$\mathcal{B}_{\min}^{\star\star} = \underset{\{\mathbf{S}_i\}_{i=1}^{L},\, \frac{1}{L}\sum_{i=1}^{L}\|\mathbf{S}_i\|^2 = T_d P_d}{\text{maximize}} \; \min_{i \neq j} \mathcal{B}(\mathbf{S}_i \| \mathbf{S}_j). \tag{12}$$

A constellation whose minimum BD $\mathcal{B}_{\min}$ attains $\mathcal{B}_{\min}^{\star\star}$ is said to be distance-optimal.

Proposition 2 *Let $\{\boldsymbol{S}_i^{\star}\}_{i=1}^{L}$ be the set of constellation points that attain the cutoff rate R_0. Then*

$$\mathcal{B}_{ave}^{\star\star} \geq \mathcal{B}_{\min}^{\star\star}, \tag{13}$$

where $\mathcal{B}_{ave}^{\star\star} = \sum_{i \neq j} \mathcal{B}(\boldsymbol{S}_i^{\star} \| \boldsymbol{S}_j^{\star})/L^2$ is the expected value.

Proof. Denote the argument of $\log(\cdot)$ in (7) for the cutoff rate optimized signal set as

$$Q^{\star} = \sum_{i \neq j} \pi_i \pi_j e^{-M_R \mathcal{B}(\mathbf{S}_i^{\star} \| \mathbf{S}_j^{\star})} + \sum_{i} \pi_i^2. \tag{14}$$

For an equiprobable signal set, (14) becomes

$$Q^{\star} = \frac{1}{L^2} \sum_{i \neq j} e^{-M_R \mathcal{B}(\mathbf{S}_i^{\star} \| \mathbf{S}_j^{\star})} + \frac{1}{L}. \tag{15}$$

For any other equiprobable constellation of identical dimension

$$
\begin{aligned}
Q^{\star} &= \min_{\{\mathbf{S}_i\}_{i=1}^{K}} \left\{ \frac{1}{L^2} \sum_{i \neq j} e^{-M_R \mathcal{B}(\mathbf{S}_i \| \mathbf{S}_j)} + \frac{1}{L} \right\} && (16) \\
&\leq \min_{\{\mathbf{S}_i\}_{i=1}^{K}} \{ e^{-M_R \min\limits_{i \neq j} \mathcal{B}(\mathbf{S}_i \| \mathbf{S}_j)} \} \frac{(L-1)}{L} + \frac{1}{L} \\
&= \frac{L-1}{L} e^{\{-M_R \max\limits_{\{\mathbf{S}_i\}_{i=1}^{L}} \min\limits_{i \neq j} \mathcal{B}(\mathbf{S}_i \| \mathbf{S}_j)\}} + \frac{1}{L} \\
&= \frac{L-1}{L} e^{-M_R \mathcal{B}^{\star\star}_{\min}} + \frac{1}{L}. && (17)
\end{aligned}
$$

Using (15) and (16) we get,

$$
\frac{\sum_{i \neq j} e^{-M_R \mathcal{B}(\mathbf{S}_i^{\star} \| \mathbf{S}_j^{\star})}}{L^2} \leq e^{-M_R \mathcal{B}^{\star\star}_{\min}} \frac{L-1}{L} \tag{18a}
$$

$$
e^{-M_R \mathcal{B}^{\star\star}_{ave}} \leq e^{-M_R \mathcal{B}^{\star\star}_{\min}} \frac{L-1}{L}. \tag{18b}
$$

Equation (18b) is obtained by applying Jensen's inequality to the left-hand side of (18a), taking logarithm to both sides of (18b), and Proposition 2 follows. ■

Lemma 1 *[126] Let P_e represent the average error probability of the ML detector, then*

$$
P_e \leq \beta e^{-\mathcal{B}^{\star\star}_{ave}} - \frac{1}{2}, \tag{19}
$$

where $\beta > 0$ and $\mathcal{B}^{\star\star}_{ave}$ is an expected BD defined as in Proposition 2.

Remark 4: The relationship between the expected BD and P_e (Lemma 1) in combination with Proposition 2 follows tight upper bound over P_e

$$
P_e \leq \beta e^{-\mathcal{B}^{\star\star}_{ave}} - \frac{1}{2} \leq \beta e^{-\mathcal{B}^{\star\star}_{\min}} - \frac{1}{2}, \tag{20}
$$

which implies that maximizing the CR is a better criterion for constellation design than maximizing the minimum BD.

Proposition 3 *If the number of receive antennae is $M_R \geq \frac{\log(L-1)}{\mathcal{B}^{\star\star}_{\min}}$, the optimal cutoff rate obtained by constellation of size L is bounded as*

$$
\log L - \log 2 \leq R_0 \leq \log L. \tag{21}
$$

Proof. Using an inequality $\left(\sum_i \pi_i \sqrt{p(\mathbf{R}_d, \hat{\mathbf{H}}|\mathbf{S}_i)}\right)^2 \geq \sum_i \pi_i^2 p(\mathbf{R}_d, \hat{\mathbf{H}}|\mathbf{S}_i)$ in (6), we get the upper bound on R_0

$$R_0 \leq \max_{\{\pi_i\}_{i=1}^L} -\log \sum_i \pi_i^2 \leq \log L \tag{22}$$

where the last line follows from the inequality $\sum_i \pi_i^2 \geq 1/L$, for any set of probabilities $\{\pi_i\}_{i=1}^L$, with equality when $\pi_i = 1/L$.

Taking negative logarithm to both sides of (16) with $M_R \geq \frac{\log(L-1)}{\mathcal{B}^{\star\star}_{\min}}$, we get

$$R_0 \geq \log L - \log 2. \tag{23}$$

which is a lower bound on R_0. ■

2.2.2 Special cases

Single transmit antenna and T_d = 1

In this section, we present two criteria to design single transmit antenna (M_T = 1) constellations in a fast fading environment (T_d = 1): first, constellation design by maximizing the minimum $\mathcal{B}(\mathbf{S}_i \| \mathbf{S}_j)$, and second, by maximizing the CR (7). Fast fading is an important benchmark, although it does not necessarily happen as such in practice. Consedering the observation of Footnote 1, it can also be approximately valid in practice. Each ST codeword $\mathbf{S}$ is now simply a complex scalar s, e.g., (7) becomes:

$$R_0 = \max_{\{s_i\}_{i=1}^L} -\log \left\{ \frac{1}{L^2} \sum_i \sum_j \frac{\sqrt{1+\sigma_E^2|s_i|^2} \cdot \sqrt{1+\sigma_E^2|s_j|^2}}{1 + \frac{1}{2}\sigma_E^2(|s_i|^2 + |s_j|^2) + \frac{1}{4}(1-\sigma_E^2)|s_i - s_j|^2} \right\}. \tag{24}$$

To find a close-to-optimal BD-based constellation with average power P_d, we solve (12). For signal construction, we will adopt the idea of multilevel circular constellations as described in [96]. We consider constellations which consist of points on concentric circles, and solve the optimization problem to find the optimum values for the number of circles, their radii, and the number of constellation points on each circle.

An example of a 16-point BD PCCs design at $\mathrm{SNR_d}$ per bit of 10 dB and for σ_E^2 with values of 0 and 0.3 is shown in Fig. 2. Next, to find a CR-optimized

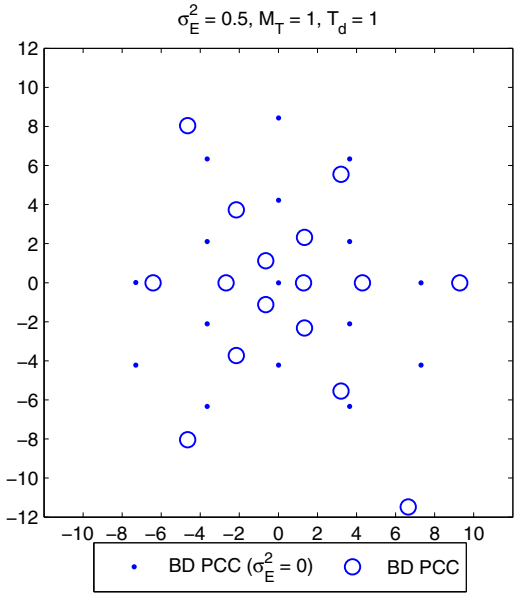

Fig. 2. Partially coherent constellation (BD-optimized) of size $L = 16$ designed for $M_T = 1$, $T_d = 1$, $E_b/N_0 = 10$ dB and for fixed $\sigma_E^2 = 0.5$.

constellation, we solve the following optimization problem:

$$\begin{aligned} &\underset{\{s_i\}_{i=1}^{L}}{\text{maximize}} \quad \varrho \\ &\text{subject to} \quad \tfrac{1}{L}\sum_{i=1}^{L} |s_i|^2 = T_d P_d. \end{aligned} \tag{25}$$

For signal construction, in this case, we perform numerical optimization for which Matlab's [127] optimization toolbox program `fmincon` is used. The program `fmincon` solves nonlinear constrained optimization problems (e.g., (25)) and is based on the sequential quadratic programming (SQP) algorithm. In this algorithm, the function solves a quadratic programming (QP) subproblem in each major SQP iteration step. Figs. 3 and 4 show the 16-point PCCs for $\mathrm{SNR_d}$ per bit of 10 dB and for σ_E^2 with values of 0, 0.3 and 0.5, respectively. In all cases, the constellation points lie on concentric circles. It has been observed for several other PCCs obtained at different values of σ_E^2 and $\mathrm{SNR_d}$ that the majority of points lie in close vicinity of the origin. The reason for this is that as the amplitude decreases, the numerator of (7) decreases in order to maximize the cutoff rate. This phenomenon becomes more dominant at higher values of σ_E^2

or low values of $\mathrm{SNR_d}$. At low-to-medium $\mathrm{SNR_d}$ regime or high values of σ_E^2 ($\geq$ 0.4) and starting with L equiprobable random constellation points, many of the amplitudes are assigned the value 0 in the resulting CR PCCs. Therefore, the cardinality reduces to $K \leq L$. Since multiple points are assigned zero amplitude, these points will coincide at the origin and yield one point with correspondingly higher probability, e.g., CR PCCs in Fig. 4. It is also observed that the resulting CR PCCs always have a point at the origin, which is often not feasible in practice.

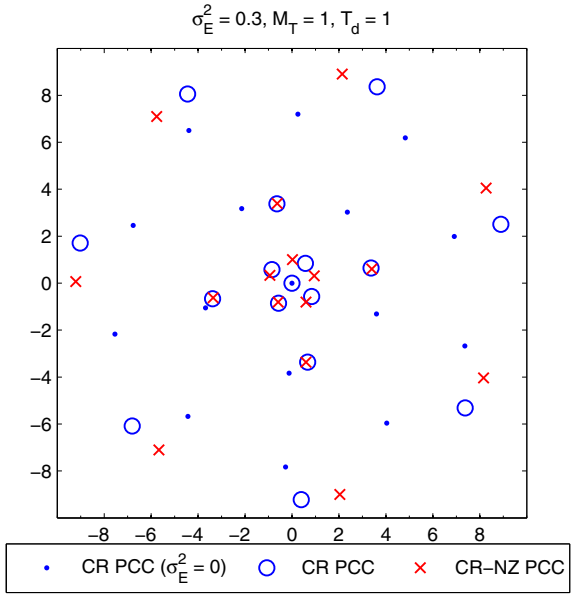

Fig. 3. Partially coherent constellation (cutoff rate-optimized and cutoff rate-optimized with non-zero amplitudes) of size $L = 16$ designed for $M_T = 1$, $T_d = 1$, $E_b/N_0 = 10$ dB and for fixed $\sigma_E^2 = 0.3$, [114] (©2012 IEEE).

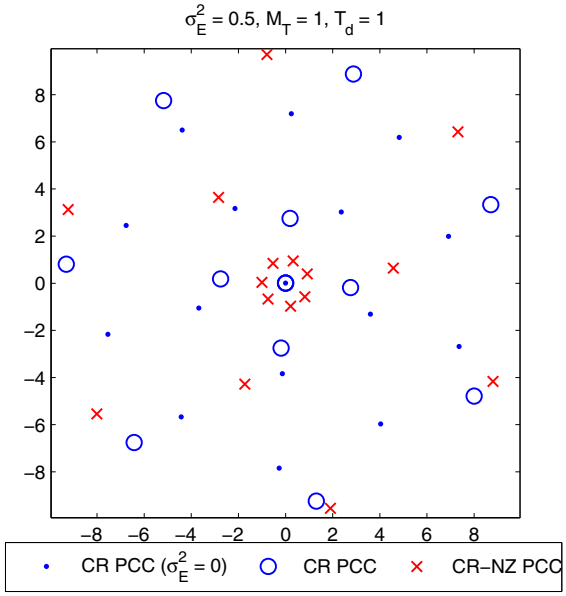

Fig. 4. Partially coherent constellation (cutoff rate-optimized and cutoff rate-optimized with non-zero amplitudes) of size $L = 16$ designed for $M_T = 1$, $T_d = 1$, $E_b/N_0 = 10$ dB and for fixed $\sigma_E^2 = 0.5$, [114] (©2012 IEEE).

To overcome the problems discussed above, we solve the optimization problem with an additional constraint that energy of every point must be larger than some positive constant $\varepsilon > 0$ ($|s_i|^2 \geq \varepsilon$), chosen such that the resulting PCCs should have distinct points and cutoff rate higher than conventional M-QAM and PCCs obtained by KLD-based design for fixed $\mathrm{SNR_d}$. The resulting cutoff rate, non-zero amplitude (CR-NZ) PCCs can also be seen in Figs. 3 and 4 for $\varepsilon = 1$ (obtained from several trials) with average power constraint $\frac{1}{L}\sum_{i=1}^{L}|s_i|^2 = T_d P_d$.

Multiple transmit antennae and T_d = 1

We will now design the constellations with multiple transmit antennae ($M_T \geq 2$) and in a fast-fading environment. Each $\mathbf{S}$ will now be a complex row vector

and (7) reduces to

$$R_0 = \max_{\{\mathbf{s}_i\}_{i=1}^{L}} -\log\left\{\frac{1}{L^2}\sum_i\sum_j \frac{\sqrt{1+\sigma_E^2||\mathbf{s}_i||^2}\sqrt{1+\sigma_E^2||\mathbf{s}_j||^2}}{1+\frac{1}{2}\sigma_E^2(||\mathbf{s}_i||^2+||\mathbf{s}_j||^2)+\frac{1}{4}(1-\sigma_E^2)||\mathbf{s}_i-\mathbf{s}_j||^2}\right\}. \quad (26)$$

To find a close-to-optimal constellation with average power P_d, we use (25) with replacing the complex scalar s with the complex row vector $\mathbf{s}$. Like in [96], the proposed constellations are jointly designed across transmit antennae. With $T_d = 1$, each transmit matrix will have a unit rank, independent of the number of transmit antennae, and, thus, is not able to provide any transmit diversity gain.

In both cases discussed above, signal set construction is started by first randomly selecting $2L$ initial points according to a uniform probability density inside a $2M_T$-dimensional real sphere (or L points inside an M_T-dimensional complex sphere centered at the origin). The SQP algorithm was tested for different values of CSI estimation variance σ_E^2 and for various values of L. The algorithm always converged in less than 3,000 iterations. Numerous local optima were found by taking several random starts, many of which were merely rotations or other symmetric modifications of each other. The number of optimization variables in the problem is $2LM_T$. In each major SQP iteration step, a QP subproblem with computational complexity of $\mathcal{O}(8L^3M_T^3)$ [128] has to be solved. This is the dominating component in terms of computational complexity. Computational complexity gets higher with large values of T_d, since more constellation points L need to be found and have huge decoding complexity. Note that since the optimization process is independent of the number of the receive antennae M_R, the complexity term is independent of it. For relatively small size constellations and transmit antennae, e.g., $L = 32$ and $M_T = 4$, the algorithm solves the optimization problem with a tractable complexity.

Multiple transmit antennae and $T_d \geq 2$

We will design the ST block code with block lengths of several symbol intervals which can be applicable to a KLD-based design [96] as well. We constrain the signal matrix to be unitary to guarantee transmit diversity. Unitary codes are optimal in terms of capacity [34] in the absence of CSI, and they have very simple ML decoding algorithms with perfect CSI [52]. We propose that the

ST constellations have the structure $\mathcal{S} = \{\Phi_i \mathbf{D}_i\}_{i=1}^{L}$, where $\Phi_i \in \mathbb{C}^{T_d \times M_T}$ is a matrix with orthonormal columns (i.e., $\Phi_i^H \Phi_i = \mathbf{I}_{M_T}$) and $\mathbf{D}_i \in \mathbb{R}^{M_T \times M_T}$ is a diagonal matrix with nonnegative and equal entries (i.e., $\mathbf{D}_i = \sqrt{d_i}\mathbf{I}_{M_T}$). Thus, any $T_d \times M_T$ transmitted matrix symbol $\mathbf{S}$ having the structure $\mathcal{S} = \{\Phi_i \mathbf{D}_i\}_{i=1}^{L}$ can be used in this framework. The rationale for the above choice is that the amplitudes of the signal matrix can now vary in order to maximize the cutoff rate. Assuming the above code structure, we can write $\mathbf{S}_i^H \mathbf{S}_i = d_i \mathbf{I}_{M_T}, i = 1 \ldots L$. When $T_d \geq 2$ and $M_T \geq 2$, the cutoff rate in (7) will reduce to

$$R_0 \geq \max_{\{d_i\}_{i=1}^{L}} -\log \left\{ \frac{1}{L^2} \sum_i \sum_j \left[\frac{(1+\sigma_E^2 d_i)^{1/2}(1+\sigma_E^2 d_j)^{1/2}}{(1+\frac{1}{2}\sigma_E^2 d_i)(1+\frac{1}{2}\sigma_E^2 d_j)} \right]^{M_T} \right. \\ \left. \frac{1}{\prod_{k=1}^{M_T}(1-\alpha_{i,j}\lambda_{i,j}^k)} \frac{1}{\left(1+\frac{1-\sigma_E^2}{4}[M_T(d_i+d_j)-(d_i d_j)^{\frac{1}{2}}\mathrm{tr}(\Phi_i\Phi_j^H+\Phi_j\Phi_i^H)]\right)} \right\}, \tag{27}$$

where $\lambda_{i,j}^k$ are eigenvalues of the matrix $\Phi_j^H \Phi_i \Phi_i^H \Phi_j$ and

$$\alpha_{i,j} = \frac{\sigma_E^4}{4} \frac{d_i d_j}{(1+\frac{1}{2}\sigma_E^2 d_i)(1+\frac{1}{2}\sigma_E^2 d_j)}. \tag{28}$$

Detailed derivation of (27) is given in Appendix III.

We solve the following optimization problem to find a close-to-optimal constellation with average power P_d over $\{d_i\}_{i=1}^{L}$, by leveraging $\{\Phi_i\}_{i=1}^{L}$ that are proposed in [94], [93] for the partially coherent channel:

$$\begin{array}{ll} \underset{\{d_i\}_{i=1}^{L}}{\text{maximize}} & \varrho \\ \text{subject to} & \frac{M_T}{L}\sum_{i=1}^{L} d_i^2 = T_d P_d. \end{array} \tag{29}$$

In [94] and [93], the proposed unitary matrix code $\{\mathbf{S}_i\}_{i=1}^{L}$ has all the columns of square norm equal to $\frac{T_d P_d}{M_T}$ which are not cutoff rate optimal because fixed norm will not give the largest minimum BD.

2.2.3 Constellation design criterion with PAPR constraint

In the previous section, we have assumed the average power constraint on signal set matrices. In this section, we constrain the PAPR, defined as the ratio of the peak energy of any signal matrix to the average energy or power, below a given threshold.

Adding a PAPR constraint, the design in (11) can be reformulated as the following optimization problem:

$$\begin{array}{ll} \underset{\{\mathbf{S}_i\}_{i=1}^{L}}{\text{maximize}} & \varrho \\ \text{subject to} & \frac{1}{L}\sum_{i=1}^{L}\|\mathbf{S}_i\|^2 = T_d P_d, \\ & \max\{\|\mathbf{S}_i\|^2\}_{i=1}^{L} \leq T_d P_d P_{\text{PAPR}}, \end{array} \tag{30}$$

where the maximization is with respect to the signal matrices, and P_{PAPR} is the PAPR threshold power specified by the designer. The nonlinear constrained optimization problem (30) can be numerically solved in the same way as discussed in the previous section to solve (11).

2.3 Numerical optimization

The CR (7) expressions are obviously not convex functions in the coordinates of the signal points and their optimization does not lead to a closed form solution for the optimal constellations. There are several approaches to approximate a non-convex function, for example, grid search, simulated annealing, SD, etc., but the solution is not guaranteed to be optimal. The CR and the optimal signal set can be iteratively computed using (47).

The algorithm used in this chapter is SQP [128]. The complex vector $\mathbf{x} \in \mathbb{C}^{LM_T}$ has to be transformed into the real vector $\mathbf{x}' \in \mathbb{R}^{2LM_T}$ before optimization. Starting from an initial vector $\mathbf{x}_0$, a quadratic approximation (i.e., QP subproblem) of the objective function (e.g., CR) at the point $\mathbf{x}_0$ is calculated and minimized. A line search is performed in the calculated direction of the function minimum. This is repeated iteratively until the stopping condition is fulfilled. For the QP subproblem, analytical values for CR at $\mathbf{x}_0$ and its first derivative and an approximation of the Hessian matrix $\mathbf{W}_{Hess}$ are necessary. The approximation of the Hessian $\mathbf{W}_{Hess}$ is determined using the Broyden-Fletcher-Goldfarb-Shanno (BFGS) algorithm, also called a Quasi-Newton update [128].

There are three stopping conditions**:** *i)* a small enough value of the objective function derivative (e.g., 10^{-10}), *ii)* the maximum number of iterations, and *iii)* a minimum function value. The algorithm iterates until one of the stopping conditions is fulfilled and sets $\mathbf{x}_k$, where k is the current iteration index, as a local optimal solution.

In each major SQP iteration step, a QP subproblem with computational complexity of $\mathcal{O}(8L^3M_T^3)$ [128] has to be solved. This is the dominating component in terms of computational complexity. Computational complexity gets higher with large values of T_d, since more constellation points $L = 2^{RT_d}$, where R is the uncoded transmission rate, need to be found and have huge decoding complexity. Note that although the optimization process depends on the number of receive antennae M_R, its impact on the complexity term is negligible. For relatively small size constellations and a small number of transmit antennae, the algorithm solves the optimization problem with a reasonable complexity (e.g., for $L = 32$ and $M_T = 4$, the complexity order would be $\approx 10^7$). The algorithm always converges in less than 3,000 iterations. Furthermore, low order PCCs, which can be computed with a reasonable complexity, are recommended to be used when a considerable amount of CSI estimation errors exists at the receiver input [113, 129]. Moreover, the PCCs can be computed off-line and made available to both the transmitter and the receiver in order to use them in a real system, thus avoiding the delay caused in computing them.

2.4 Numerical results and discussion

Mutual information, SER and PAPR have been used as performance metrics to compare the performance with conventional M-QAM and M-PSK, existing Borran's [96] PCC and self-match unitary constellations [93]. In all numerical examples, the constellations are optimized for a particular $\mathrm{SNR_d}$ value. To obtain the mutual information of the constellation, we use a Monte-Carlo computer simulation. The mutual information with a discrete-input and continuous-output channel is given as

$$\mathcal{I}(\mathbf{R}_d; \mathbf{S}|\hat{\mathbf{H}}) = \sum_i \pi_i \mathbb{E}_{p(\mathbf{R}_d|\mathbf{S}_i,\hat{\mathbf{H}})} \left[\log \left(\frac{p(\mathbf{R}_d|\mathbf{S}_i, \hat{\mathbf{H}})}{\sum_j \pi_j p(\mathbf{R}_d|\mathbf{S}_j, \hat{\mathbf{H}})} \right) \right]. \tag{31}$$

2.4.1 Single transmit antenna partially coherent constellations

Performances of the single transmit antenna PCCs are considered in this section. First, we evaluate the performance of the BD-optimized constellation BD PCC for $M_T = 1$, $M_R = 1$, $T_d = 1$. The SER versus $\mathrm{SNR_d}$ performances of the 4-point

BD PCC to those of the KL PCC and the conventional 4-QAM are presented in Fig. 5. It can be observed that the BD PCC has better gains than the 4-QAM and slightly better than the KL PCC while 4-QAM shows error floor.

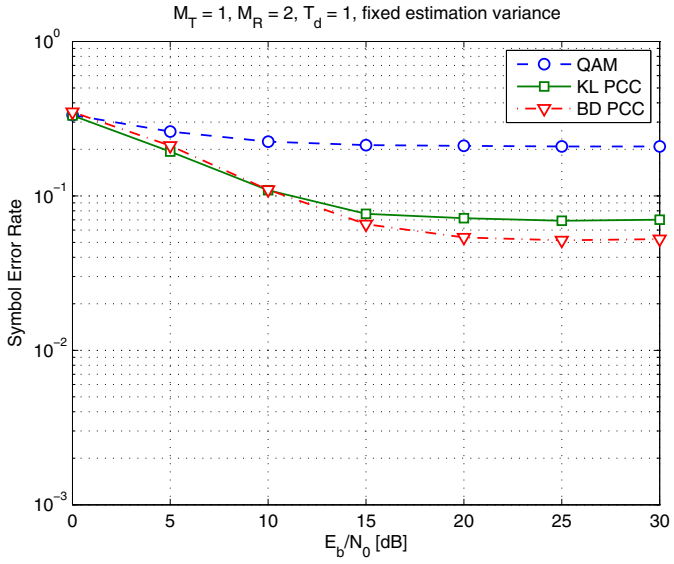

Fig. 5. Symbol error rate versus $\mathrm{SNR_d}$ per bit with $L = 4$, $M_R = 2$, $M_T = 1$ and fixed $\sigma_E^2 = 0.5$, [113] (©2010 IEEE).

Now, we evaluate the MI and SER values of the 16-point CR-optimized constellations for $M_T = 1$, $M_R = 1$, $T_d = 1$. In Fig. 6, the mutual information values are plotted versus $\mathrm{SNR_d}$ per bit for various channel estimation variances which are assumed to be fixed over $\mathrm{SNR_d}$. It is observed that with estimation variances of a small value equal to 0.3, the CR PCC and the KL PCC have the same mutual information and at the intermediate value of 0.5 and larger value of 0.7, the CR PCC has higher mutual information than the KL PCC. In all cases, the CR PCC shows better mutual information than the 16-QAM, especially at higher $\mathrm{SNR_d}$.

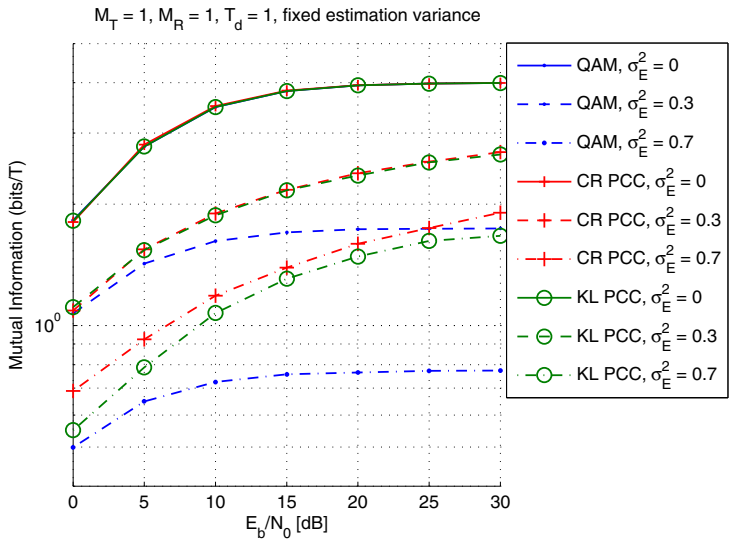

Fig. 6. Mutual information versus $\mathrm{SNR_d}$ per bit with $L = 16$, $M_T = 1$, $M_R = 1$, $T_d = 1$, and for various fixed $\sigma_E^2 \in \{0, 0.3, 0.5, 0.7\}$, [114] (©2012 IEEE).

The SER performance of the cutoff rate non-zero CR-NZ PCC is compared to that of the KL PCC and 16-QAM in Fig. 7. For the estimation variance values of 0, 0.1 and 0.3, the performance of the CR-NZ and the KL PCCs are similar and shows significant gain over the conventional 16-QAM at high $\mathrm{SNR_d}$.

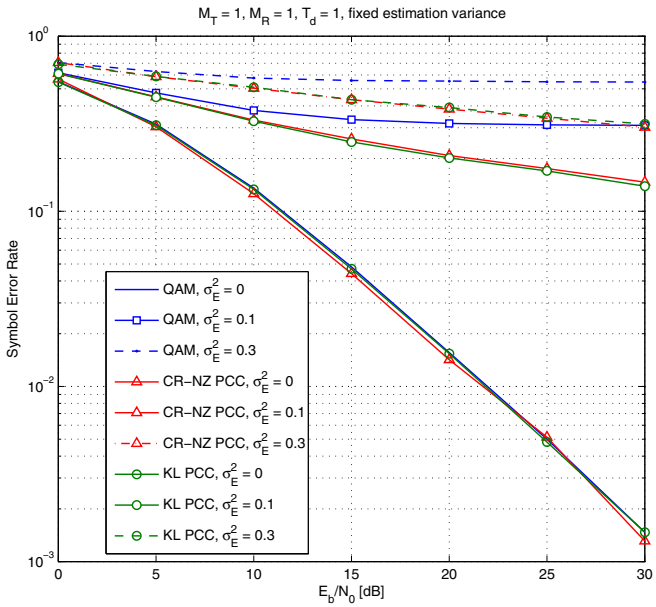

Fig. 7. Symbol error rate versus $\mathrm{SNR_d}$ per bit with $L = 16$, $M_T = 1$, $M_R = 1$, $T_d = 1$, and for various fixed $\sigma_E^2 \in \{0, 0.1, 0.3\}$, [114] (©2012 IEEE).

In Fig. 8, the PAPR of CR PCC is compared to those of the KL PCC and 16-QAM constellations versus $\mathrm{SNR_d}$ for an estimation variance value equal to 0.3. It is observed that the cutoff rate-based constellation has PAPR values lower than the KL PCC.

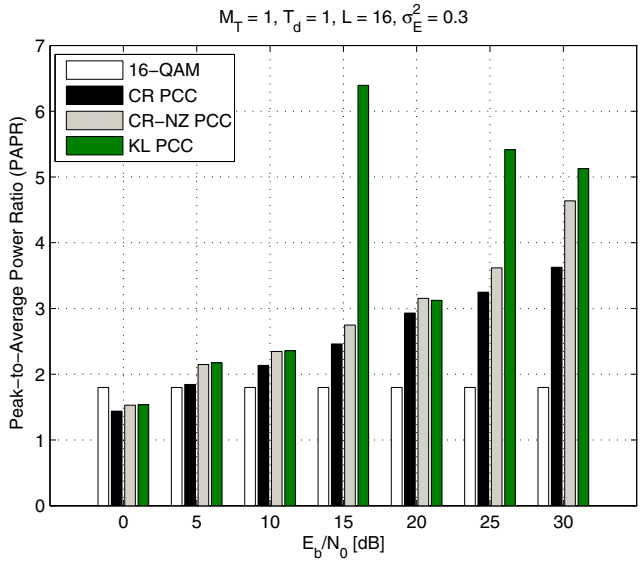

Fig. 8. PAPR versus $\mathrm{SNR_d}$ per bit with $L = 16$, $M_T = 1$, $M_R = 1$, $T_d = 1$, and for fixed $\sigma_E^2 = 0.3$, [114] (©2012 IEEE).

The assumption of a fixed estimation variance for all $\mathrm{SNR_d}$ values is not always realistic. As the $\mathrm{SNR_d}$ increases, the estimation variance typically reduces with training-based channel estimation. To evaluate the performance of the CR PCC with $\mathrm{SNR_d}$ dependent estimation variance [124] ($\sigma_E^2 = 1/(1+\mathrm{SNR_d})$) as would be the case with training-based LMMSE estimation, we keep the system configuration the same as in the previous cases. In Fig. 10, the mutual information values of the CR PCC and the CR-NZ PCC are compared to those of the KL PCC and conventional M-QAM. In a higher $\mathrm{SNR_d}$ region, as expected, all constellations have the same mutual information, because the estimation variance will have very low values. In a low $\mathrm{SNR_d}$ region[8], the CR PCC and CR-NZ PCC have higher mutual information as compared to that of the KL PCC and 16-QAM constellations. Similar behavior as for the $L = 16$ points PCC is observed for the $L = 4$ points CR PCC and 4-QAM. The case for the

[8]In a low $\mathrm{SNR_d}$ region where the channel estimation variance attains very high values (> 0.8), the channel no longer can be considered as a partially coherent channel. Moreover, the optimal signaling at low $\mathrm{SNR_d}$ achieves same capacity as the coherent case [130].

$L = 2$ is not shown here, but it has also similar behavior. Now if we look into Fig. 9, which compares the PAPR values of the CR PCC to those of the KL PCC and 16-QAM constellations at different $\mathrm{SNR_d}$ values for $\mathrm{SNR_d}$ dependent estimation variance, we observe that in the low $\mathrm{SNR_d}$ region, the resulting cut-off rate-optimized constellations get peaky to achieve high mutual information values; this is an expected result from [34] for non-coherent channels. Even in this region, the PAPR values of the CR PCC can be brought down, for example, to 1.8 (which is same as for 16-QAM by using (30) and shown in Fig. 9 but at the expense of low MI values as shown in Fig. 10). In the medium-to-high $\mathrm{SNR_d}$ region, cutoff rate-optimized constellations have low PAPR values; even lower than the conventional QAM constellations.

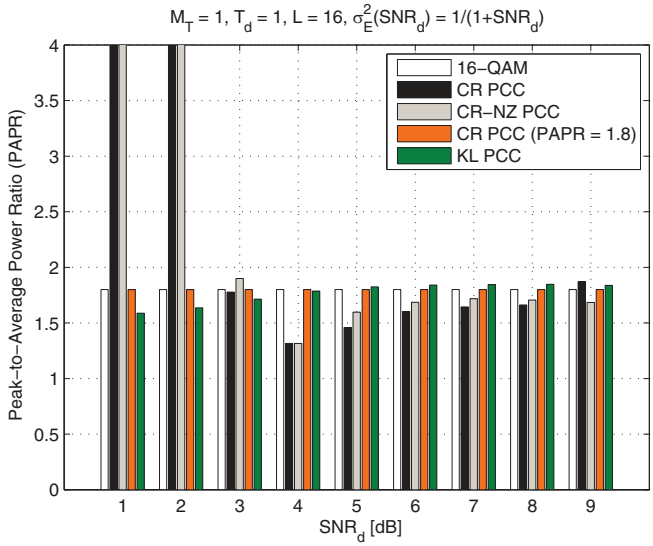

Fig. 9. PAPR versus $\mathrm{SNR_d}$ per symbol with $L = 16$, $M_T = 1$, $M_R = 1$, $T_d = 1$, and for $\mathrm{SNR_d}$ dependent σ_E^2. (Note: Vertical axis has been truncated in order to magnify the low values of PAPR). [114] (© IEEE).

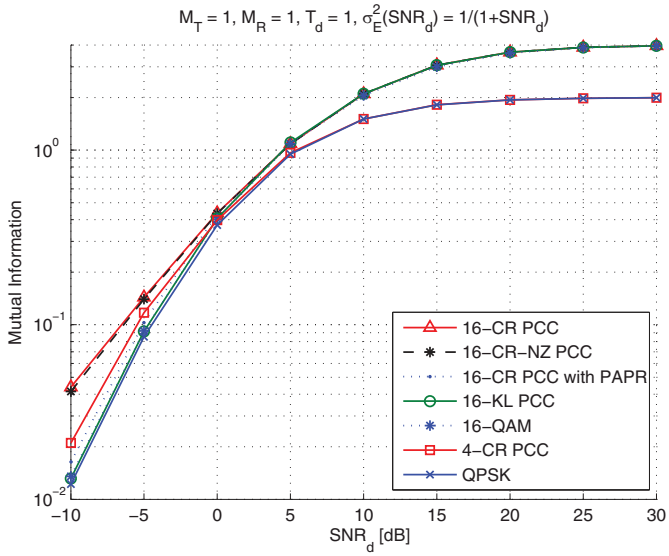

Fig. 10. Mutual information versus $\mathbf{SNR_d}$ per symbol with $L = \{4, 16\}$, $M_T = 1$, $M_R = 1$, $T_d = 1$, and $\mathbf{SNR_d}$ dependent σ_E^2, [114] (©2012 IEEE).

As mentioned in Section 2.2.2, it is observed in Fig. 4 that the resulting CR PCC has a lower number of constellation points, i.e., 12 with respect to the initial 16 equiprobable points before the start of the optimization process. It has one point at the origin with a probability of $5/16$ and the rest of the points with an equal probability of $1/16$. Since the resulting constellation points are no more equiprobable, variable-length bit assignment could be used [131]. In order to keep the implementation simple and backward compatible, we compare the SER performance of the CR-NZ PCC to those of the KL PCC and 16-QAM constellations with $\mathrm{SNR_d}$ dependent estimation variance in Fig. 11. At all $\mathrm{SNR_d}$ points, the proposed CR-NZ PCC outperforms the conventional one. The performance of the CR-based constellations is better than that of the constellation based on the KLD. The difference becomes more pronounced as the number of receive antennae increases.

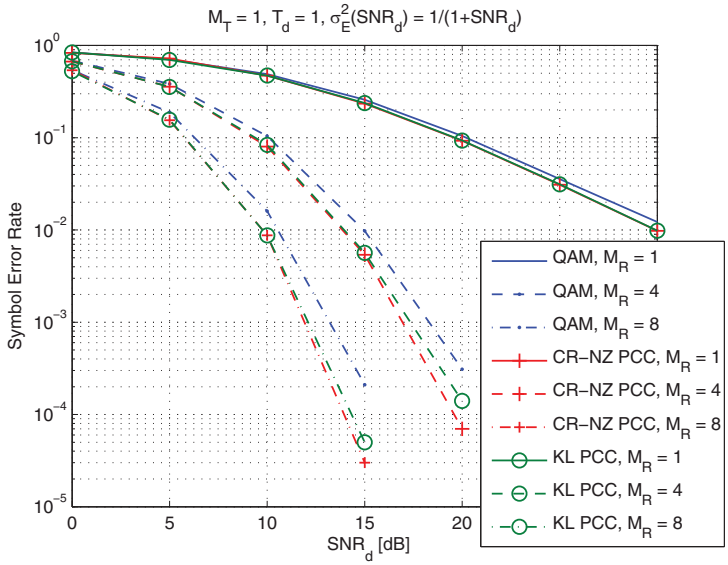

Fig. 11. Symbol error rate versus $\mathbf{SNR_d}$ per symbol with $L = 16$, $M_T = 1$, $M_R = \{1, 4, 8\}$, $T_d = 1$, and $\mathbf{SNR_d}$ dependent σ_E^2, [114] (©2012 IEEE).

So far we have seen the performances of PCCs which are obtained by using a different constellation optimized for different $\mathrm{SNR_d}$ values. These PCCs might be useful for systems which use adaptive modulation techniques, etc. For systems where using different constellations for different $\mathrm{SNR_d}$ might not be applicable, we have designed a PCC at some $\mathrm{SNR_d}$ (e.g., 10 dB and 15 dB), for fixed σ_E^2, and use its appropriately scaled version at all $\mathrm{SNR_d}$ values to plot the SER performance in Fig. 12. Its performance is observed to be slightly degraded than of that obtained by the constellation designed at different values of the $\mathrm{SNR_d}$ but it still gives remarkable gains compared to 16-QAM.

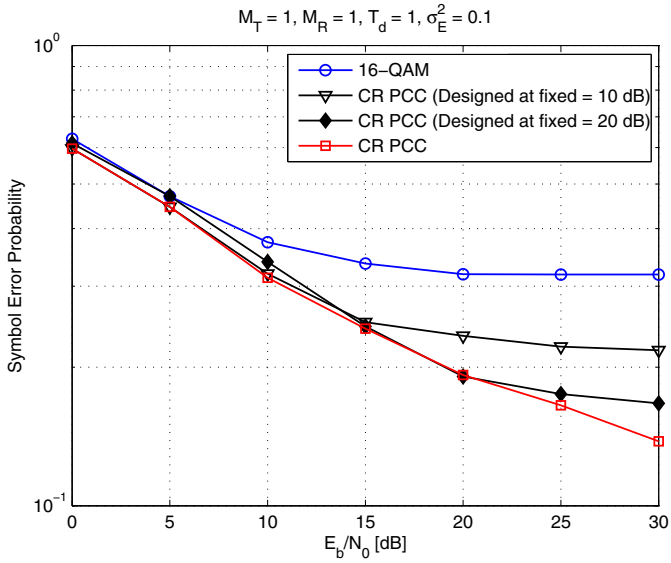

Fig. 12. SER versus SNR_d per bit with $L = 16$, $M_T = 1$, $M_R = 1$, $T_d = 1$, and $\sigma_E^2 = 0.1$, [114] (©2012 IEEE).

2.4.2 Multiple transmit antenna partially coherent constellations

We now consider the constellation design for the $M_T = 2$, $M_R = 1$, $T_d = 1$ system configuration and evaluate the mutual information values of the CR PCC with the QAM constellations. Mutual information values versus SNR_d per bit is plotted in Fig. 13 for fixed estimation variance values of 0, 0.05, 0.3 and 0.5. In order to compare the performance, we use a 16-point CR PCC designed jointly for two transmit antennae for our case and two independent 4-QAM for two transmit antennae as baseline for comparison so that they have the same spectral efficiency of 4 bits/T. We can see a similar performance as we have seen in the single transmit antenna case. As estimation variance increases, the CR PCC shows higher mutual information compared to that of the QAM constellations.

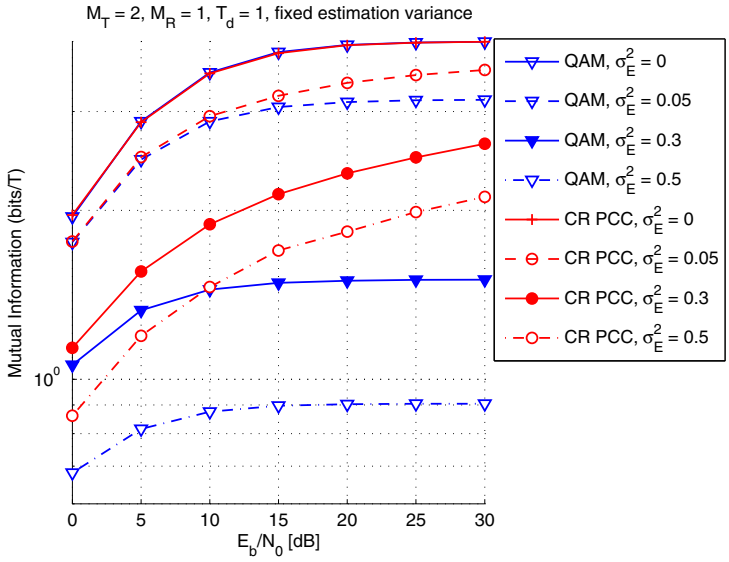

Fig. 13. Mutual information versus $\mathrm{SNR_d}$ per bit with $L = 16$, $M_T = 2$, $M_R = 1$, $T_d = 1$, and for fixed $\sigma_E^2 \in \{0, 0.05, 0.3, 0.5\}$, [114] (©2012 IEEE).

The SER performance for the same system configuration as that in Fig. 13 but with $M_R = 2$ and for fixed estimation variance values of 0 and 0.05 is plotted in Fig. 14. We compare the performances of the CR PCC designed for different values of $L = 4$, 16, and 64 to that of a spatial multiplexing scheme, transmitting two independent conventional binary phase-shift keying (BPSK), 4-QAM and 8-PSK symbols to two transmit antennae, respectively. As expected, the CR PCC shows significantly better gains compared to the conventional constellations even with perfect CSIR. We can also observe that the performance plots experience error floor for the case of non-zero estimation variances, which is more prominent in the 16-QAM constellation than in the CR PCCs, especially at high $\mathrm{SNR_d}$. The error floor at high $\mathrm{SNR_d}$ is due to the presence of $\sigma_E^2 \mathbf{S}\mathbf{S}^H$ term in the covariance matrix of the received symbols matrix (4), which is a self-interference that does not decrease as the $\mathrm{SNR_d}$ increase. The flooring effect can be obviated by using an $\mathrm{SNR_d}$ dependent estimation variance, e.g., as shown in Fig. 11.

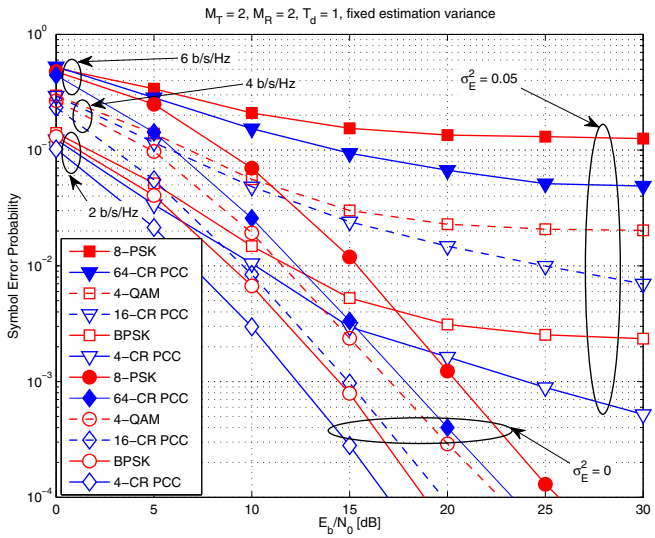

Fig. 14. Symbol error rate versus $\mathrm{SNR_d}$ per bit with $L = \{4, 16, 64\}$, $M_T = 2$, $M_R = 2$, $T_d = 1$, and for fixed $\sigma_E^2 \in \{0, 0.05\}$, [114] (©2012 IEEE).

2.4.3 Partially coherent space-time constellations

Finally, we evaluate the performance of the ST constellations for $T_d > 1$. In this section, we present the performance results of two CR-optimized ST constellations. First, the ST constellations are designed by leveraging the self-match unitary constellations [93], and second, they are designed by leveraging the unitary code obtained by combining the non-coherent [75] and coherent codes by Giese and Skoglund [94].

The performance of the cutoff rate, self-match (CR-SM) and the cutoff rate, self-match with non-zero amplitude (CR-SM-NZ) for the $M_T = 2$, $M_R = 1$, $T_d = 8$ system configuration with an $\mathrm{SNR_d}$ dependent estimation variance is considered first. The CR-SM-NZ ST constellations are obtained with an additional constraint that the energy of each matrix of a ST constellation set must be larger than some positive constant $\varepsilon > 0$ ($d_i^2 \geq \varepsilon$). In this example, we have used $\varepsilon = 1$ (obtained from several trials) at a $\mathrm{SNR_d}$ of 10 dB. The self-match unitary constellations are used in this example, as they are easy to construct,

guarantee full diversity and do not exhibit an error-floor with channel estimation error [93]. The mutual information versus $\mathrm{SNR_d}$ is plotted in Fig. 15. The mutual information of the CR-SM and CR-SM-NZ constellation are compared to that of the self-match unitary constellations. It is observed that the CR-SM has higher mutual information at all $\mathrm{SNR_d}$ values and especially in the low $\mathrm{SNR_d}$ region. Comparison is also made with the ST constellation with non-zero amplitudes (CR-SM-NZ), which shows to have very minimal degradation in mutual information as of the CR-SM.

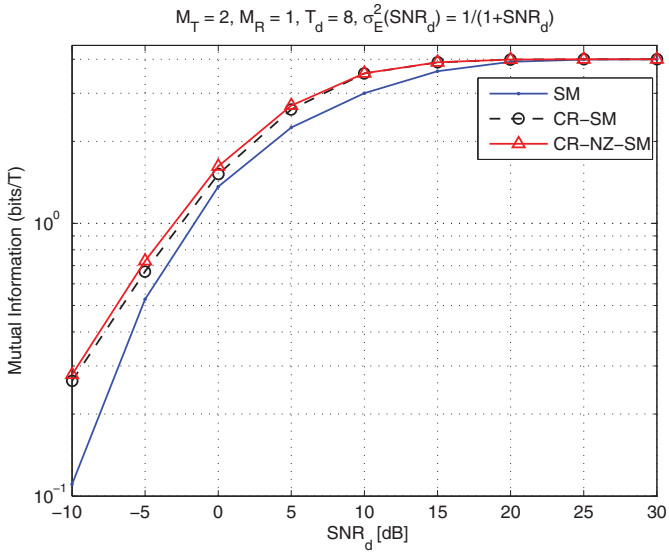

Fig. 15. Mutual information versus $\mathrm{SNR_d}$ per symbol with $L = 16$, $M_T = 2$, $M_R = 1$, $T_d = 8$, and for $\mathrm{SNR_d}$ dependent σ_E^2, [114] (©2012 IEEE).

The corresponding block error rate performance is compared in Fig. 16. The CR-SM constellation exhibits significantly better performance compared to that of the SM constellations over entire $\mathrm{SNR_d}$ region.

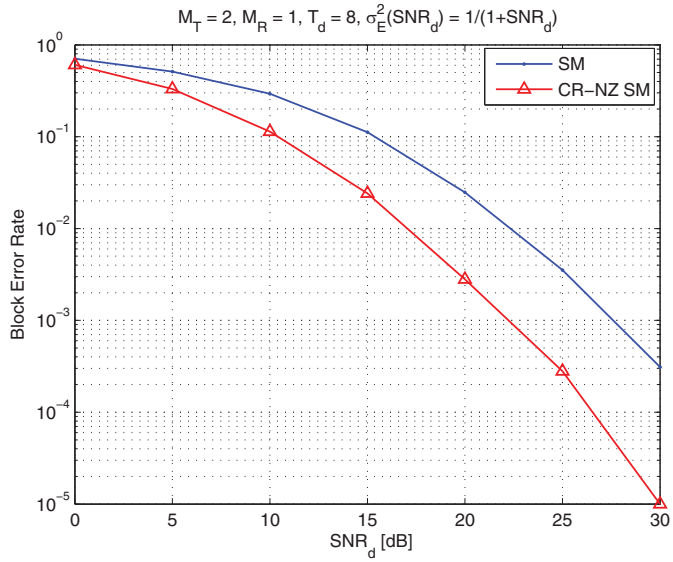

Fig. 16. Block error rate versus $\mathbf{SNR_d}$ per block with $L = 16$, $M_T = 2$, $M_R = 1$, $T_d = 8$, and for $\mathbf{SNR_d}$ dependent σ_E^2, [114] (©2012 IEEE).

Next, we consider the performance of the CR-optimized ST constellations, leverages Giese and Skoglund [94] unitary codes, for the $M_T = 2$, $M_R = 2$, $T_d = 4$ system configuration with spectral efficiency or code rate $R = 1$ bits/s per channel use. In this example, we compare the performance of a purely non-coherent code (16 unitary code) with a signal set based on combining 8 non-coherent codes with 2 coherent codes, and a constellation combining 4 non-coherent codes with 4 coherent codes. The idea of adaptively determining the number of coherent and non-coherent component codes is dependent on the quality of the channel estimate, i.e., estimation variance σ_E^2. For the non-coherent case ($\sigma_E^2 = 1$), the inter-subspace distance between two signals Φ_i and Φ_j depends upon the principal angles between the subspace spanned by Φ_i and Φ_j. For the coherent case ($\sigma_E^2 = 0$), two signals in the same subspace have vanishing inter-subspace and non-vanishing intra-subspace distances since it depends upon the singular values of the difference $\Phi_i - \Phi_j$. In other words, a higher estimation variance will involve more non-coherent components to achieve a large inter-subspace distance and less coherent component codes, and vice versa.

The block error rate (BLER) versus estimation variance performance of the combined codes designed for SNR = 10 dB per block is compared in Fig. 17. All the three CR-optimized constellation sets exhibit better performance compared to that of the constellation sets proposed in [94] over different values of channel estimation variance (σ_E^2).

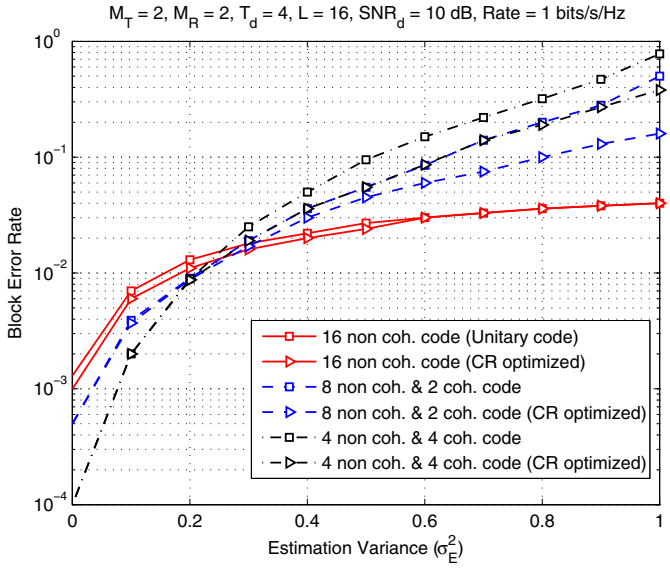

Fig. 17. Block error rate (BLER) versus estimation variance (σ_E^2) with $L = 16$, $M_T = 2$, $M_R = 2$, $T_d = 4$, and combined codes designed for $\mathbf{SNR_d} = 10$ dB per block, [115] (©2013 VDE VERLAG GMBH).

2.5 Conclusion

The ST constellation design matched to imperfect CSIR in a Rayleigh-fading channel has been considered. The cutoff rate as a function of the channel estimation variance has been proposed as a design criterion to obtain partially coherent ST constellations. The resulting CR-optimized PCCs have the largest minimum BD and are close to rate-optimal for a very large number of receive antennae. We have also demonstrated the shape and structure of the resulting constellations matched to channel estimation errors. The resulting constellations

are shown to have higher MI in low or medium SNR regimes compared to those of the KLD-based PCCs, USTCs and conventional QAM constellations. Numerical results also demonstrated that SER performance of the new constellations is similar to that of the KLD-based PCCs [96] and have better performance compared to unitary codes [93, 94]. The resulting single transmit antenna constellations are also shown to have lower PAPR values compared to those of KLD-based PCCs. Another signal set construction method is discussed with additional constraints. It gives control over the constellation's PAPR values and takes care that no signal points have a zero amplitude.

One key benefit of using CR-based optimization is that it yields a computation framework which can be straightforwardly solved for ST block code design for block lengths of several symbol intervals. This problem proved out to be a difficult one with the KLD-based design [96]. Moreover, the code construction method used in the KLD and the BD-based design is computationally more intensive as it involves an exhaustive search in order to obtain the optimized constellations.

3 Partially coherent constellation design in spatially correlated channels

As discussed in Section 1.1, apart from imperfect CSIR, the presence of spatial correlation also degrades the performance of the MIMO system. To reduce the performance losses incurred due to imperfect CSIR and spatial correlation, various designs have been proposed, such as the precoder design [16, 101, 102] and robust ST codes [132]. In this chapter, we study the combined impact of the CSI estimation error and spatial correlation on the ST code design. We consider non-CSIT schemes, and our goal is to use partial CSIT (channel estimation covariance matrix, transmit and receive correlation matrices) to design the transmitted ST codes and the corresponding bit mapping schemes to adapt to the available accuracy of the CSIR.

This chapter is organized as follows: The assumptions, the system model, and the Kronecker channel model for correlated channel and LMMSE channel estimation method are detailed in Section 3.1. Detailed derivations of the UB-ABEP and CR expressions for a spatially correlated MIMO channel with partial CSIR, two methodologies for signal set construction, and an efficient bit-mapping algorithm MBSA are presented in Section 3.2. The details of the numerical optimization method are presented in Section 3.3. The numerical coded BER and FER results are presented in Section 3.4. Section 3.5 concludes the chapter.

3.1 System model

Consider a similar communication system (1) as the one considered in Chapter 2 with a given power constraint (2).

We model the channel correlation with the Kronecker model [9, 133, 134], i.e., $\mathbf{H} = \mathbf{R}_T^{1/2}\mathbf{H}_w\mathbf{R}_R^{1/2}$, where $\mathbf{H}_w$ is a spatially white matrix whose entries are i.i.d. $\mathcal{CN}(0,1)$. Matrices $\mathbf{R}_T$ and $\mathbf{R}_R$ represent normalized transmit and receive correlation with eigenvalues $\{\lambda_T^i\}_{i=1}^{M_T}$ and $\{\lambda_R^i\}_{i=1}^{M_R}$, respectively. The normalizations in (1) are assumed to be such that $\sum_{i=1}^{M_T}\lambda_T^i = M_T$ and $\sum_{i=1}^{M_R}\lambda_R^i = M_R$.

We assume that $\mathbf{R}_T$ and $\mathbf{R}_R$ are measured accurately at the receiver and are fed back to the transmitter via an error-free feedback link. However, in practice

correlation matrices are estimated as in [135–137] with sufficiently high accuracy. Now, the receiver computes an estimate $\hat{\mathbf{H}}_w$ of the channel matrix $\mathbf{H}_w$ using the well-established orthogonal training method [138]. The received signal matrix in T_t time slots can be written as

$$\mathbf{Y}_t \quad = \quad \mathbf{S}_t\mathbf{R}_T^{1/2}\mathbf{H}_w\mathbf{R}_R^{1/2} + \mathbf{W}_t, \tag{32}$$

where $\mathbf{S}_t$ is a known $\mathbb{C}^{M_T \times M_T}$ orthogonal training symbol matrix with total energy, i.e., $\mathrm{tr}(\mathbf{S}_t\mathbf{S}_t^H) = P_t = \mathrm{SNR}_t$, and $\mathbf{W}_t$ is the AWGN noise matrix, during the training period, from the distribution $\mathcal{CN}(0, \mathbf{I})$. Let $\mathbf{S}_t = \mathbf{A}\mathbf{R}_T^{-1/2}$, where $\mathbf{A}$ is a unitary matrix scaled by $\sqrt{P_t/\mathrm{tr}(\mathbf{R}_T^{-1})}$ for equal power allocation to the transmit antennae. Pre-multiplying both sides of (32) by $\mathbf{A}^{-1}$ and then post-multiplying the resultant equation by $\mathbf{R}_R^{-1/2}$, we get

$$\mathbf{G}_w \quad = \quad \mathbf{A}^{-1}\mathbf{Y}_t\mathbf{R}_R^{-1/2} = \mathbf{H}_w + \underbrace{\mathbf{A}^{-1}\mathbf{W}_t\mathbf{R}_R^{-1/2}}_{\mathbf{W}_0}. \tag{33}$$

The LMMSE estimation [138] of $\mathbf{H}_w$ is performed on (33) to obtain

$$\hat{\mathbf{h}}_w = \mathrm{vec}(\hat{\mathbf{H}}_w) = [\mathbf{I}_{M_R M_T} + (\sigma_{ce}^2\mathbf{R}_R^{-1} \otimes \mathbf{I}_{M_T})]^{-1}\mathrm{vec}(\mathbf{G}_w) \tag{34}$$

and in the matrix version $\hat{\mathbf{H}}_w = \mathbf{G}_w[\mathbf{I}_{M_R} + \sigma_{ce}^2\mathbf{R}_R^{-1}]^{-1}$, where $\sigma_{ce}^2 = \mathrm{tr}(\mathbf{R}_T^{-1})/P_t$. Similarly, the channel estimation error vector and the corresponding matrix version are given by

$$\tilde{\mathbf{h}}_w = \mathbf{h}_w - \hat{\mathbf{h}}_w = \mathrm{vec}(\tilde{\mathbf{H}}_w) = [\mathbf{I}_{M_R} + \sigma_{ce}^{-2}\mathbf{R}_R]^{-1/2} \otimes \mathbf{I}_{M_T}\mathrm{vec}(\mathbf{E}_w) \tag{35}$$

$$\tilde{\mathbf{H}}_w = \mathbf{E}_w[\mathbf{I}_{M_R} + \sigma_{ce}^{-2}\mathbf{R}_R]^{-1/2}, \tag{36}$$

where $\mathbf{E}_w$ is a random matrix with i.i.d. complex Gaussian entries having $\mathcal{CN}(0, 1)$, and is independent of $\hat{\mathbf{H}}_w$. A detailed derivation of (35) is given in Appendix 4. By the orthogonality principle $\hat{\mathbf{h}}_w$ and $\tilde{\mathbf{h}}_w$ are uncorrelated.

The CSI model based on the model above becomes

$$\mathbf{H} = \hat{\mathbf{H}} + \tilde{\mathbf{H}} = \mathbf{R}_T^{1/2}\hat{\mathbf{H}}_w\mathbf{R}_R^{1/2} + \mathbf{R}_T^{1/2}\tilde{\mathbf{H}}_w\mathbf{R}_R^{1/2} \tag{37a}$$

$$= \mathbf{R}_T^{1/2}\mathbf{G}_w(\underbrace{[\mathbf{I}_{M_R} + \sigma_{ce}^2\mathbf{R}_R^{-1}]^{-2}\mathbf{R}_R}_{=\bar{\mathbf{R}}_R\cdot\hat{\mathbf{R}}_R})^{1/2} + \mathbf{R}_T^{1/2}\mathbf{E}_w(\underbrace{[\mathbf{I}_{M_R} + \sigma_{ce}^{-2}\mathbf{R}_R]^{-1}\mathbf{R}_R}_{\tilde{\mathbf{R}}_R})^{1/2}, \tag{37b}$$

where $\bar{\mathbf{R}}_R = [\mathbf{I}_{M_R} + \sigma_{ce}^2\mathbf{R}_R^{-1}]^{-1}$ and $\hat{\mathbf{R}}_R = [\mathbf{I}_{M_R} + \sigma_{ce}^2\mathbf{R}_R^{-1}]^{-1}\mathbf{R}_R$.

Substituting the eigenvalue decompositions (EVDs) for $\mathbf{R}_T = \mathbf{U}_T \Lambda_T \mathbf{U}_T^H$, $\bar{\mathbf{R}}_R = \mathbf{U}_R \bar{\Lambda}_R \mathbf{U}_R^H$, $\hat{\mathbf{R}}_R = \mathbf{U}_R \hat{\Lambda}_R \mathbf{U}_R^H$ and $\tilde{\mathbf{R}}_R = \mathbf{U}_R \tilde{\Lambda}_R \mathbf{U}_R^H$, where $\mathbf{U}_T$ and $\mathbf{U}_R$ are the transmit and receive unitary matrices of the EVDs of R_T and R_R, respectively, we get

$$\begin{aligned}\mathbf{H} &= \mathbf{U}_T \underbrace{\Lambda_T^{1/2} \mathbf{U}_T^H \mathbf{G}_w \mathbf{U}_R \bar{\Lambda}_R^{1/2} \hat{\Lambda}_R^{1/2}}_{\hat{\mathbf{H}}} \mathbf{U}_R^H + \mathbf{U}_T \underbrace{\Lambda_T^{1/2} \mathbf{U}_T^H \mathbf{E}_w \mathbf{U}_R \tilde{\Lambda}_R^{1/2}}_{\tilde{\mathbf{H}}} \mathbf{U}_R^H \\ &= \mathbf{U}_T \hat{\tilde{\mathbf{H}}} \mathbf{U}_R^H + \mathbf{U}_T \tilde{\tilde{\mathbf{H}}} \mathbf{U}_R^H.\end{aligned} \tag{38}$$

After post-multiplying (1) by $\mathbf{U}_R$, denoting $\mathbf{S}_d \mathbf{U}_T$ by $\mathbf{X}$, and denoting $\mathbf{R}_d \mathbf{U}_R$ by $\mathbf{Y}$, we get

$$\mathbf{Y} \quad = \quad \mathbf{X} \hat{\tilde{\mathbf{H}}} + \mathbf{X} \tilde{\tilde{\mathbf{H}}} + \mathbf{N} \tag{39}$$

which represents the sufficient statistics of the received signal. The precoded constellation $\{\mathbf{X}\}$ satisfies the same average-power constraint as the original constellation $\{\mathbf{S}_d\}$, and $\mathbf{N}$ has i.i.d. circularly symmetric $\mathcal{CN}(0,1)$ entries, since it has the same distribution as $\mathbf{W}_d$.

Applying the vec operation to (39), we get

$$\mathbf{y} \quad = \quad \mathbf{Z} \hat{\tilde{\mathbf{h}}} + \mathbf{Z} \tilde{\tilde{\mathbf{h}}} + \mathbf{n}, \tag{40}$$

where $\mathbf{Z} = \mathbf{I}_{M_R} \otimes \mathbf{X}$. The conditional probability density function (PDF) of the received signal conditioned on given $\hat{\tilde{\mathbf{h}}}$ and $\mathbf{Z}_i$ being sent is [96]

$$p_i(\mathbf{y}) = p\left(\mathbf{y} | \mathbf{Z}_i, \hat{\tilde{\mathbf{h}}}\right) = \frac{\exp\left\{-(\mathbf{y} - \mathbf{Z}_i \hat{\tilde{\mathbf{h}}})^H (\mathbf{I}_{T_d M_R} + \mathbf{Z}_i \tilde{\Sigma} \mathbf{Z}_i^H)^{-1} (\mathbf{y} - \mathbf{Z}_i \hat{\tilde{\mathbf{h}}})\right\}}{\pi^{TM_R} |(\mathbf{I}_{T_d M_R} + \mathbf{Z}_i \tilde{\Sigma} \mathbf{Z}_i^H)|}, \tag{41}$$

where $\tilde{\Sigma} = \mathbb{E}[\mathrm{vec}(\tilde{\tilde{\mathbf{H}}}) \mathrm{vec}(\tilde{\tilde{\mathbf{H}}})^H] = (\tilde{\Lambda}_R \otimes \Lambda_T)$ is a correlation matrix of $\tilde{\tilde{\mathbf{H}}}$, which is the same as that of $\tilde{\mathbf{H}}$.

In the remainder of the chapter, we will assume that $\mathbf{R}_T$, $\mathbf{R}_R$, and σ_{ce}^2 are known to the receiver and the transmitter, which further implies knowledge of the estimation covariance matrix $\tilde{\Sigma}$ at the transmitter.

We have used a channel model different from the one used in [116], which had a genie-provided estimate at the receiver. However, the analysis presented in this section can also be applied to the channel model in [116].

3.2 Constellation design

In this section, we use upper bound on the ABEP (UB-ABEP) and CR expressions as constellation design criteria for partially coherent channels for single and multiple transmit antennae, respectively. The error rate performance of the coded system depends on the bit mapping as well. Thus, we also need to design the bit mapping (close to the Gray mapping), along with the constellation points to minimize the error rate. We propose two methodologies to design the constellations and bit mapping schemes in two steps. The first one is for the single transmit antenna case, where the design of a 2-D constellation is of interest. In this method, we minimize the UB-ABEP with a given average transmit power and the Gray mapping constraint on the constellation set. The rationale for using a UB-ABEP expression as a constellation design criterion in this case seems obvious: it allows taking both the Hamming distance and pairwise error probabilities PEPs into account in a single expression. We start with some known conventional 2-D constellations (e.g., M-QAM) which readily apply the Gray mapping in the first step and then optimize the constellation points by minimizing the UB-ABEP in the second step. The resulting constellation can maintain the same Gray mapping and its simplicity. The second method is for multiple transmit antennae where constellations are designed simultaneously across the transmit antennae and allowed to differ from an antenna to another. In this method, we start with some $\mathbb{R}^{2M_T}$ vector and optimize it by maximizing the CR under the average transmit power constraint in the first step. In the second step, the resulting symbols are then mapped to a binary sequence using the MBSA.

It should be noted that the UB-ABEP expression is a suitable design criterion for the single transmit antenna as 2-D constellations (e.g., M-QAM, M-PSK etc.), where the Gray mapping can be used as initial starting points of the iterative optimization. In the multiple transmit antenna case, on the other hand, we design the constellations simultaneously across the transmit antennae. The approach then gives rise to the need for higher dimensional constellations (e.g., 4-D constellations for two transmit antennae). Since the 4-D or higher dimensional constellations which readily apply the Gray mapping are not available, their bit mapping schemes must also be designed. Thus, the CR expression is a useful design criterion. As in [114], the CR criterion can also be used to design the 2-D constellations. However, their bit mappings result often in non-Gray mappings.

This deteriorates their bit error performance as compared to the constellations designed using the UB-ABEP criterion. We overcome the problem by a specific bit mapping design.

3.2.1 Single transmit antenna

We now derive a UB-ABEP expression and use it for designing the constellation for the single transmit antenna case. Using the relationship between the average BEP and the PEPs for the codebook of size L [139],

$$\bar{P}_b = \sum_{i=1}^{L} \sum_{j \neq i} \frac{d(\mathbf{X}_i, \mathbf{X}_j)}{\log_2 L} \pi_i \Pr\{\mathbf{X}_i \rightarrow \mathbf{X}_j\}, \tag{42}$$

where $d(\mathbf{X}_i, \mathbf{X}_j)$ is the Hamming distance between binary sequences representing $\mathbf{X}_i$ and $\mathbf{X}_j$, $\Pr\{\mathbf{X}_i \rightarrow \mathbf{X}_j\}$ is the PEP of transmitting $\mathbf{X}_i$ and detecting $\mathbf{X}_j$. π_i is the transmission probability of $\mathbf{X}_i$ and is equal to $\frac{1}{L}$ for the equiprobable inputs, which is the case here. In the above equation, the PEPs can be approximated[9] as

$$\Pr(\mathbf{X}_i \rightarrow \mathbf{X}_j) \approx \Pr_{p_i}\{\mathbf{y} : p_j(\mathbf{y}) > p_i(\mathbf{y})\}, \tag{43}$$

where $p_i(\mathbf{y})$ is a conditional PDF as defined in (41) and $\Pr_{p_i}$ is used to denote the probability with respect to the probability density function $p_i(\mathbf{y})$. One would like to select the signals by minimizing the PEP. Unfortunately, minimizing the PEP and even the Chernoff distance [29], which determines the asymptotic exponential decay rate of the APEP of the ML detector, is usually not analytically tractable. To circumvent this problem, we use the BD between two conditional distributions, which is a special case of the Chernoff distance, when the Chernoff parameter is assigned the value $\frac{1}{2}$. We refer to $P_e = \pi_i \Pr_{p_i}\{\mathbf{y} : p_j(\mathbf{y}) > p_i(\mathbf{y})\} + \pi_j \Pr_{p_j}\{\mathbf{y} : p_i(\mathbf{y}) > p_j(\mathbf{y})\}$ as the APEP between $\mathbf{X}_i$ and $\mathbf{X}_j$.

The Bhattacharyya coefficient and the BD $\mathcal{B}(i,j)$ between $p_i(\mathbf{y})$ and $p_j(\mathbf{y})$ are defined as [111] $\rho(i,j) = \int_{-\infty}^{\infty} \sqrt{p_i(\mathbf{y}) p_j(\mathbf{y})} dy$, and $\mathcal{B}(i,j) = -\log \rho(i,j)$, respectively.

[9]When there are only two decision points (i.e., L =2), (14) should be an equality. For more than two decision points (i.e., L >2), the equality no longer holds, however, we can still use them as an approximation for the PEP.

The relation between the Bhattacharyya coefficient and the APEP is [140]

$$\frac{1}{2}\min(\pi_i,\pi_j)\rho(i,j)^2 \le P_e \le \sqrt{\pi_i\pi_j}\rho(i,j), \tag{44}$$

where π_i and π_j are the *a priori* probabilities of the codewords, which are assumed to be equal. Based on (44), with equal priors, minimizing the maximum P_e is equivalent to maximizing the minimum $\mathcal{B}(i,j)$ among all pairs i,j. The next proposition is an extension of our result for the i.i.d. channel [113, 114] to the correlated channel.

Proposition 4 *The Bhattacharyya coefficient between the pair of symbols $\boldsymbol{X}_i$ and $\boldsymbol{X}_j$ is given by*

$$\rho_{\text{cor}}(i,j) = \prod_{n=1}^{M_R} \frac{|\boldsymbol{I}_{T_d} + \boldsymbol{X}_i\Lambda_T\boldsymbol{X}_i^H\tilde{\lambda}_R^n|^{\frac{1}{2}}|\boldsymbol{I}_{T_d} + \boldsymbol{X}_j\Lambda_T\boldsymbol{X}_j^H\tilde{\lambda}_R^n|^{\frac{1}{2}}}{|\boldsymbol{I}_{T_d} + \frac{1}{2}(\boldsymbol{X}_i\Lambda_T\boldsymbol{X}_i^H + \boldsymbol{X}_j\Lambda_T\boldsymbol{X}_j^H)\tilde{\lambda}_R^n + \frac{1}{4}(\boldsymbol{X}_i-\boldsymbol{X}_j)\Lambda_T(\boldsymbol{X}_i-\boldsymbol{X}_j)^H\hat{\lambda}_R^n|}, \tag{45}$$

where $\tilde{\lambda}_R^n$ and $\hat{\lambda}_R^n$ are the eigenvalues of $\tilde{\boldsymbol{R}}_R$ and $\hat{\boldsymbol{R}}_R$ respectively, and $\{\boldsymbol{X}_i\}_{i=1}^L$ is the constellation set with equiprobable transmit probabilities.

Proof. See Appendix 5. ∎

Using (42), (44) and Proposition 1, an UB-ABEP is given by

$$\bar{P}_b \le \frac{1}{L}\sum_{i=1}^{L-1}\sum_{j=i+1}^{L}\frac{d(\mathbf{X}_i,\mathbf{X}_j)}{\log_2 L}\rho_{\text{cor}}(i,j) = \bar{P}_b^{UB}. \tag{46}$$

Adopting the UB-ABEP expression (46) as the design criterion, the signal set design can be formulated as the following optimization problem:

$$\begin{array}{ll} \underset{\{\mathbf{X}_i\}_{i=1}^L}{\text{minimize}} & \bar{P}_b^{UB} \\ \text{subject to} & \frac{1}{L}\sum_{i=1}^{L}\|\mathbf{X}_i\|^2 = T_dP_d \\ & \text{Gray mapping.} \end{array} \tag{47}$$

For the single transmit antenna case and with $T_d = 1$ each $\mathbf{X}$ will now be a complex scalar.

For the numerical optimization, we use Matlab's [127] optimization toolbox program `fmincon`. The program `fmincon` solves nonlinear constrained optimization problems (e.g., (47)) and is based on the SQP algorithm. In this algorithm, the function solves a QP subproblem in each major SQP iteration step. Fig. 18

shows the constellation diagrams of the M-BEP PCC (M-points PCCs designed by minimizing the UB-ABEP), for $M = 16$, designed with the $(E_b/N_0)_d = 10$ dB along with its bit mapping and 16-QAM constellation for structural comparison. In this case, we used the Gray-mapped 16-QAM as an initial guess to the optimization problem and finding the optimized 16-BEP PCC. It can be seen that the majority of the points are shifted towards the origin as compared to those of 16-QAM. The reason for this is that as the amplitude decreases, the variance of the received signal decreases as it depends on the strength of the transmitted symbol. It has been observed that this phenomenon becomes more dominant at low values of $\mathrm{SNR_t}$ (e.g., structure of the 16-BEP PCC designed at $(E_b/N_0)_d$ of 10 dB and $\mathrm{SNR_t}$ of 3.7 dB as shown in Fig. 19).

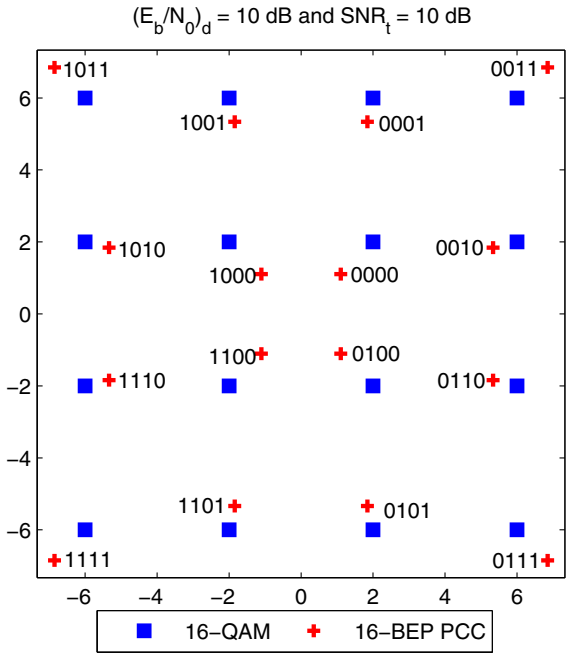

Fig. 18. Constellation diagram: 16-QAM and partially coherent constellation (BEP-optimized) of size $L = 16$ designed for $M_T = 1$, $T_d = 1$, $(E_b/N_0)_d$ of 10 dB and for fixed $\mathrm{SNR_t} = 10$ dB, [117] (©2013 IEEE).

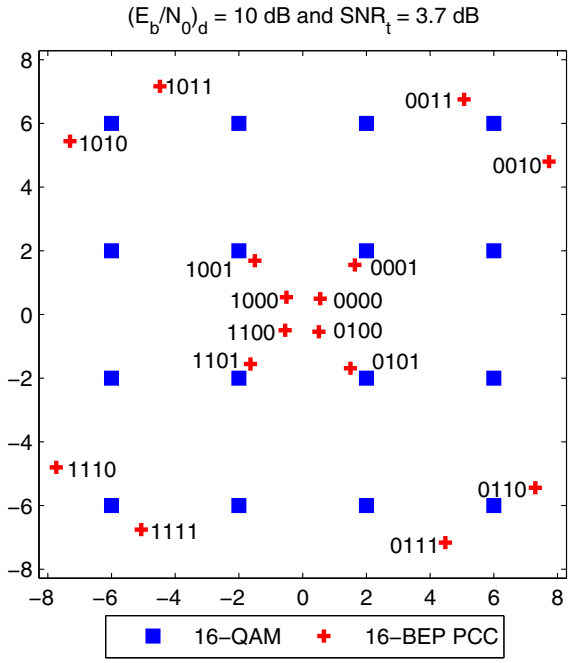

Fig. 19. Constellation diagram: 16-QAM and partially coherent constellation (BEP-optimized) of size $L = 16$ designed for $M_T = 1$, $T_d = 1$, $(E_b/N_0)_d$ of 10 dB and for fixed $\mathrm{SNR_t} = 3.7$ dB, [117] (©2013 IEEE).

3.2.2 Multiple transmit antennae

We derive next the CR expression and use it as a constellation design criterion for the multiple transmit antenna case. The next proposition is an extension of our result for the i.i.d. channel in Chapter 2 to the correlated channel.

Proposition 5 *The CR of the partially coherent spatially correlated channel with discrete input values and continuous output is given by*

$$R_0 \quad = \quad \max_{\{\pi_i\}_{i=1}^{L},\{\boldsymbol{X}_i\}_{i=1}^{L}} -\log\left(\sum_i \pi_i \sum_j \pi_j \rho_{\mathrm{cor}}(i,j)\right), \tag{48}$$

where $\{\boldsymbol{X}_i\}_{i=1}^{L}$ is the constellation set with corresponding probabilities $\{\pi_i\}_{i=1}^{L}$.

Proof. Using the relation between the CR and BD [114] results in (48). ■

We refer to the argument of $\max(\cdot)$ in (48) as the cutoff rate expression and denote it as ϱ. For the equiprobable signal set with probabilities $\{\pi_i\}_{i=1}^{L} = 1/L$, the ST constellation design can be now formulated as the following continuous optimization problem (for fixed L, elements of $\mathbf{X}$ can take any values on the complex plane):

$$\begin{array}{ll} \underset{\{\mathbf{X}_i\}_{i=1}^{L}}{\text{maximize}} & \varrho \\ \text{subject to} & \frac{1}{L}\sum_{i=1}^{L} \|\mathbf{X}_i\|^2 = T_d P_d, \end{array} \tag{49}$$

where the maximization is with respect to the signal matrices.

Spatial multiplexing ($M_T \geq 2$ and $T_d = 1$)

We will now design the constellations with multiple transmit antennae ($M_T \geq 2$) and fast fading environment. Like in [96] and Chapter 2, the proposed constellations are jointly designed across the transmit antennae. With $T_d = 1$ each $\mathbf{X}$ will now be a complex row vector $\mathbf{x}$.

To find a close-to-optimal constellation with average power P_d, we use (49), replacing the complex $\mathbf{X}$ matrix with the complex row vector $\mathbf{x}$. Moreover, with $T_d = 1$, each transmit matrix will have a unit rank, independent of the number of transmit antennae, and, thus, is not able to provide any transmit diversity gain.

Space-time codes ($M_T \geq 2$ and $T_d \geq 2$)

We will design the ST block codes, with block length of several intervals and for more than one transmit antennae, to guarantee transmit diversity.

Orthogonal ST codes OSTBCs were first proposed for two transmit antennae [49] and later extended to an arbitrary number of transmit antennae [52]. The OSTBCs are of particular interest here due to their simple decoding while providing diversity gain. The OSTBC matrix used in all related works, including [49, 52], draws its symbols either from the conventional M-QAM or M-PSK constellation or 2-D constellation as designed in [95]. Let us take the example of the Alamouti code, with spectral efficiency $R = 2$ bits/s/Hz, given by

$$\mathbf{X}_{2\times 2} = \begin{bmatrix} s_1 & s_2 \\ -s_2^* & s_1^* \end{bmatrix}. \tag{50}$$

In this case, the non-zero entries, i.e., s_1 and s_2 are drawn from a 4-QAM constellation. We propose to jointly design s_1 and s_2 for the OSTBC matrix. In order to achieve the spectral efficiency = 2 bits/s/Hz, we need 16 such combinations to form 16 different Alamouti codes. Furthermore, this approach can also be extended to other OSTBCs, e.g., $\mathbf{X}_{4\times 3}$, $\mathbf{X}_{4\times 4}$ and golden codes [141], etc. Close-to-optimal OSTBC matrices with average power P_d can be obtained by solving the continuous optimization problem (49). Furthermore, as the number of non-zero and distinct entries increases, the optimization complexity increases.

Unitary matrix codes We constrain herein the STBC to be a unitary one belonging to the class of optimal ST codes in terms of capacity [34] in the absence of CSIR and having very simple ML decoding algorithms with perfect CSI [52]. We propose that the ST constellations have the structure $\mathcal{S} = \{\Phi_i \mathbf{D}_i\}_{i=1}^{L}$, where $\Phi_i \in \mathbb{C}^{T_d \times M_T}$ is a matrix with orthonormal columns (i.e., $\Phi_i^H \Phi_i = \mathbf{I}_{M_T}$), and $\mathbf{D}_i \in \mathbb{R}^{M_T \times M_T}$ is a diagonal matrix with nonnegative and equal entries (i.e., $\mathbf{D}_i = \sqrt{d_i}\mathbf{I}_{M_T}$). In this way, we allow the amplitudes of the signal matrix to vary in order to maximize the cutoff rate. Assuming the above code structure, we can write $\mathbf{S}_i^H \mathbf{S}_i = d_i \mathbf{I}_{M_T}, i = 1 \dots L$. When $T_d \geq 2$ and $M_T \geq 2$, the Bhattacharyya coefficient in (45) will reduce to

$$\rho_{\text{cor}}(i,j) = \prod_{n=1}^{M_R} \frac{|\mathbf{I}_{T_d} + d_i \Phi_i \Lambda_T \Phi_i^H \tilde{\lambda}_R^n|^{\frac{1}{2}} |\mathbf{I}_{T_d} + d_j \Phi_j \Lambda_T \Phi_j^H \tilde{\lambda}_R^n|^{\frac{1}{2}}}{|\mathbf{I}_{T_d} + \frac{1}{2}(d_i \Phi_i \Lambda_T \Phi_i^H + d_j \Phi_j \Lambda_T \Phi_j^H)\tilde{\lambda}_R^n + \frac{1}{4}\delta\Phi \Lambda_T \delta\Phi^H \hat{\lambda}_R^n|}, \quad (51)$$

where $\delta\Phi = \sqrt{d_i}\Phi_i - \sqrt{d_j}\Phi_j$.

We solve the following optimization problem to find a close-to-optimal constellation with the average power P_d over $\{d_i\}_{i=1}^{L}$, by leveraging combined noncoherent and coherent unitary codes proposed in [94] for the partially coherent channel:

$$\begin{aligned} &\underset{\{d_i\}_{i=1}^{L}}{\text{maximize}} && \varrho \\ &\text{subject to} && \tfrac{M_T}{L} \textstyle\sum_{i=1}^{L} d_i^2 = T_d P_d. \end{aligned} \quad (52)$$

Constellation mapping

In this section, we design the bit mapping scheme for the resulting PCCs designed in previous sections for multiple transmit antennae. As mentioned above, the optimal bit mapping is crucial for the performance of the decoder. Therefore,

we propose a novel MBSA, which is a modified version of the BSA [118]. The BSA was first used to perform index optimization vector quantization and then for symbol mapping optimization in [142] for QAM and PSK and in [120] for ST constellations in the BICM-ID scheme.

The main goal of the algorithm is to find the optimized mapping with minimum total cost as described below. The total cost of a mapping is the sum of the individual costs of the symbols, as each symbol has a cost based on its location in the mapping. Furthermore, switching between the symbols, indices change the individual costs. This results either in an increment or a decrement of the total cost. Both the BSA and MBSA start with some random mapping assigned to the symbols. Then, in the case of the BSA, the algorithm constructs a new mapping on each iteration (called the current mapped array) by sorting the symbols according to the decreasing order of their individual costs. Now the symbol with the highest cost switches its index with other symbols indices, and calculates the total cost change for each symbol switching. If the lowest total cost from all of the index switchings is lower than the initial total cost, the corresponding index switching is performed to update the current mapped array, and the iteration continues for the remaining $(L-1)$ symbols. However, in the case of MBSA, the algorithm constructs the current mapped array in the same way as done in the BSA on each iteration. The symbol index with the highest individual cost is switched with all the other symbols indices. The total cost for each index switching is calculated and the switching associated to the lowest total cost is stored in an array (called switching array). Then the symbol index with the second highest individual cost switches with the rest of the symbols indices. The total cost for each index switching is calculated and the switching associated to the lowest total cost is stored in a switching array and so on for $L(L-1)$ times, until no more indices are left in the current mapped array. The algorithm then selects the indices switching such that it has the lowest total minimum cost to update the current mapped array, and the iteration continues for the remaining $(L-1)$ symbol times. In this way, the MBSA allows to searching for the mapping with a lower total cost at the end of every iteration unlike the BSA, which stops searching when it gets its first total cost lower than the initial total cost. Thus, the MBSA converges to the mapping with better local optimal values compared to those obtained using the BSA at the cost of L times search complexity. For more insight on the MBSA, a pseudo code is given in

Algorithm 1. The total cost function used in the MBSA is given by

$$\mathrm{C} \quad = \quad \sum_i \mathrm{C}(\mathbf{X}_i), \tag{53}$$

where $\mathrm{C}(\mathbf{X}_i)$ is the cost for individual symbols and is defined as

$$\mathrm{C}(\mathbf{X}_i) \quad = \quad \frac{1}{L} \sum_j \frac{d(\mathbf{X}_i, \mathbf{X}_j)}{\log_2 L} \Pr(\mathbf{X}_j \to \mathbf{X}_i). \tag{54}$$

The UB-ABEP given in (46) is used to calculate the total cost function. The MBSA converges to a local optimal mapping, so to find the close-to-global-optimal mapping, we started the algorithm with 10–15 different initial mappings chosen randomly.

3.2.3 Special case of i.i.d. channels

In this section, we will reproduce the CR for the uncorrelated and i.i.d. channels of Chapter 2. Assuming the fading coefficients are uncorrelated (i.e., $\mathbf{R}_T = \mathbf{R}_R = \mathbf{I}$), the Bhattacharyya coefficient (45) will reduce to the form [113]

$$\rho_{\mathrm{uncor}}(i,j) = \left(\frac{|\mathbf{I}_{T_d} + \sigma_E^2 \mathbf{X}_i \mathbf{X}_i^H|^{\frac{1}{2}} |\mathbf{I}_{T_d} + \sigma_E^2 \mathbf{X}_j \mathbf{X}_j^H|^{\frac{1}{2}}}{|\mathbf{I}_{T_d} + \frac{1}{2}\sigma_E^2 (\mathbf{X}_i \mathbf{X}_i^H + \mathbf{X}_j \mathbf{X}_j^H) + \frac{1}{4}(1-\sigma_E^2)(\mathbf{X}_i - \mathbf{X}_j)(\mathbf{X}_i - \mathbf{X}_j)^H|} \right)^{M_R}, \tag{55}$$

where $\sigma_E^2 = \sigma_{ce}^2/(1+\sigma_{ce}^2)$ is the estimation variance per channel coefficient. An UB-ABEP and CR can be rewritten as

$$\bar{P}_b \leq \frac{1}{L} \sum_{i=1}^{L-1} \sum_{j=i+1}^{L} \frac{d(\mathbf{X}_i, \mathbf{X}_j)}{\log_2 L} \rho_{\mathrm{uncor}}(i,j), \tag{56}$$

$$R_0 \quad = \quad \max_{\{\pi_i\}_{i=1}^L, \{\mathbf{X}_i\}_{i=1}^L} -\log \left(\sum_i \pi_i \sum_j \pi_j \rho_{\mathrm{uncor}}(i,j) \right), \tag{57}$$

respectively.

It is important to note that the number of receive antennae in the uncorrelated and i.i.d. channels does not have any role in the numerical optimization but does in the correlated channel case. As a result, the structures of the PCCs differ from each other although obtained at the same value of $(E_b/N_0)_d$.

Algorithm 1 MODIFIED BINARY SWITCHING ALGORITHM.

Input: Input constellation set $\mathcal{S} \in \{\mathbf{S}_i : 0 \leq i \leq L-1\}$

Procedures: Procedures used in the algorithm–

- **INITIALIZATION():** Assign some random indices to the each constellation point of the set.
- **SORT_INDICES():** Construct an array $\mathbf{a}_{L\times 1}$ of the indices of constellation points stored in a decreasing order of *Cost*.
- **SWITCH_INDEX(i, j):** Swap the index assignments of the constellation points $\mathbf{S}_i$ and $\mathbf{S}_j$ in $\mathcal{S}$.
- **UPDATE_COST():** Calculate the cost of individual points and total cost D_π of the constellation set.

Output: Permuted version of the constellation set $\mathcal{S}$

INITIALIZATION()
for ($k = 1$ to L) **do**
  D_π = **UPDATE_COST**()
  $\mathbf{a}$ = **SORT_INDICES**()
  $\delta^\star = \mathbf{0}$, $\mathbf{j}^\star = \mathbf{0}$
  for ($i = 1$ to L) **do**
    for ($j = 1$ to L) **do**
      if ($j \neq [\mathbf{a}]_i$) **then**
        SWITCH_INDEX($[\mathbf{a}]_i, j$)
        $D_{\pi'}$ = **UPDATE_COST**()
        $\delta = D_{\pi'}$ - D_π
        if ($\delta < 0$) **then**
          if ($|\delta| > [\delta^\star]_i$) **then**
            $[\delta^\star]_i = |\delta|$
            $[\mathbf{j}^\star]_i = j$
        SWITCH_INDEX(j, $[\mathbf{a}]_i$)
  $[a, b]$ = **MAX**($\delta^\star$)
  $\delta^{'} = a$
  $j^{'} = [\mathbf{j}^\star]_b$
  if $\delta^{'} == 0$ **then**
    BREAK
  else
    SWITCH_INDEX($j^{'}, [\mathbf{a}]_b$)

3.3 Numerical optimization

Similar to the CR expression for i.i.d. channels in Chapter 2, the UB-ABEP (46) and CR (48) expressions for the correlation channel are not also convex functions in the coordinates of the signal points and its optimization does not lead to a closed form solution for the optimal constellations. There are several approaches to approximate a non-convex function, for example, grid search, simulated annealing, SD, etc., but the solution is not guaranteed to be optimal. The UB-ABEP, CR and their corresponding optimal signal set can be iteratively computed using (47) and (49), respectively. The algorithm used in this chapter is same as the one used in Chapter 3, i.e., SQP [128].

As far as algorithm complexity is concern, low order PCCs, which can be computed with a reasonable complexity, are recommended to be used when a considerable amount of CSI estimation errors exists at the receiver input [113, 129]. Moreover, the PCCs can be computed off-line and made available to both the transmitter and the receiver in order to use them in a real system, thus avoiding the delay caused by computing them.

3.4 Numerical results and discussion

Coded FER and BER have been used as performance metrics to compare the performance of the resulting PCCs with the M-QAM and combined unitary constellation [94]. In all the presented simulated examples, the constellations are optimized for the true SNR value unless otherwise stated. For the Monte Carlo computer simulation, we considered the turbo-coded system with frames of length equal to 512 symbols. The exponentially correlated fading model is considered on both the transmit and the receive sides. The transmit and receive correlation matrix is given by $(\mathbf{R}_{\{T,R\}})_{i,j} = \rho_{\{T,R\}}^{|i-j|}$ for $i, j \in \{1, \cdots, M_{\{T,R\}}\}$, where $\rho_{\{T,R\}}$ denotes the normalized correlation coefficient of the channel and satisfies $0 \leq \rho_{\{T,R\}} < 1$. The values used for ρ_T and ρ_R in the simulations are 0.30 and 0.45, respectively.

At the receiver, the knowledge of the channel estimation covariance matrix $\tilde{\Sigma}$ is also considered to be available to the decoding metric as in [143]. The decoder estimates the log-likelihood ratios (LLRs) of the coded bit for soft decision decoding from the modulated symbols. Let us denote the transmitted bits of each signal $\mathbf{b} = \{b_1, \ldots, b_N\}$. The LLR for the l^{th} bit in $\mathbf{b}$ is given by

$$L(b_l) = \log \frac{\sum_{\mathbf{X}^+:\mathbf{X}=f(b),b_l=1} p\left(\mathbf{Y}|\mathbf{X}^+, \bar{\hat{\mathbf{H}}}\right)}{\sum_{\mathbf{X}^-:\mathbf{X}=f(b),b_l=0} p\left(\mathbf{Y}|\mathbf{X}^-, \bar{\hat{\mathbf{H}}}\right)}. \tag{58}$$

3.4.1 Single transmit antenna partially coherent constellations

We first compare the uncoded system's, with no outer codes, SER and BER performance of the 16-BEP PCCs to that of 16-CR PCCs (16-points PCCs designed by maximizing the CR) and the conventional 16-QAM constellations in the i.i.d. channel. The BEP PCCs and 16-QAM constellations are Gray-mapped while the CR PCC has MBSA-optimized bit-mapping. The uncoded SER and BER versus $(E_b/N_0)_d$ for $M_T = 1$, $M_R = 1$, $T_d = 1$ and at fixed value of training power or $\text{SNR}_\text{t} = 10$ dB are plotted in Fig. 20. As expected, the CR PCCs and BEP PCCs show SER and BER gains compared to the QAM constellations. However, the BEP PCC show better BER and worse SER gains compared to the CR PCC. The reason for this is that the CR PCC are designed without taking the bit mapping into account. Moreover, their structure does not allow the use of the Gray mapping even after the MBSA optimization. In the same figure, a similar effect can also be observed for the coded FER versus $(E_b/N_0)_d$ performance curve with turbo code rate $R_c = \frac{1}{2}$.

We now evaluate the FER performance of the 16-BEP PCCs and fixed (non $(E_b/N_0)_d$ dependent) 16-BEP PCCs designed at $(E_b/N_0)_d$ of 10 dB and 5 dB with $M_T = 1$, $M_R = 2$, $T_d = 1$. In Fig. 21, the FER versus $(E_b/N_0)_d$ for fixed SNR_t values of 3.7 dB and 10 dB are plotted with the R_c of $\frac{1}{2}$ and $\frac{2}{3}$, respectively. It is observed that for a SNR_t value equal to 3.7 dB, the BEP PCCs show better gain as compared to that of 16-QAM. The performance significantly improves when the value of SNR_t further increases to 10 dB. The fixed BEP PCCs in this example are appropriately scaled at all $(E_b/N_0)_d$ values and have negligible performance loss compared to the substantial gains obtained over the conventional 16-QAM.

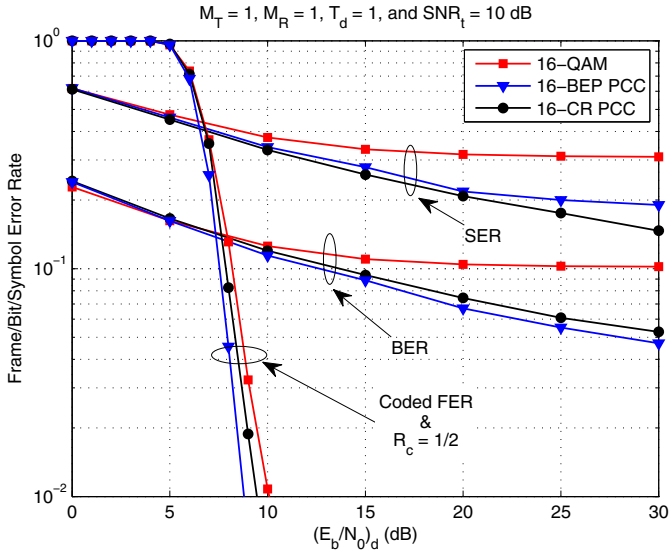

Fig. 20. Coded FER and uncoded SER & BER of SISO system versus $(E_b/N_0)_d$ for fixed $\mathbf{SNR_t} = 10$ dB with $L = 16$, $M_T = 1$, $M_R = 1$ and $T_d = 1$, [117] (©2013 IEEE).

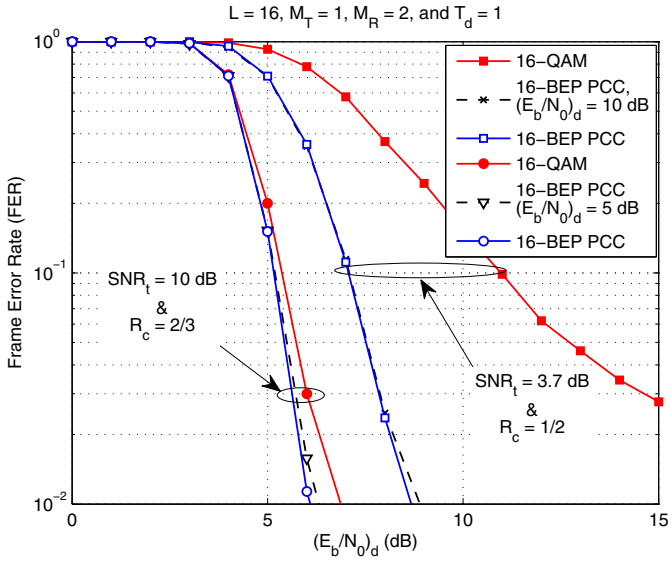

Fig. 21. Decoded FER of SIMO system versus $(E_b/N_0)_d$ for fixed $\mathbf{SNR_t} \in \{3.7, 10\}$ dB with $L = 16$, $M_T = 1$, $M_R = 2$ and $T_d = 1$. The 16-BEP PCC, $(E_b/N_0)_d \in \{5, 10\}$ dB are the fixed (non-$\mathbf{SNR_d}$ dependent) constellations designed at 10 dB and 5 dB $(E_b/N_0)_d$, [117] (©2013 IEEE).

In the examples presented so far, we used the PCCs matched to the quality of CSI (error statistics) provided by the receiver to the transmitter while assuming that the communication resource (i.e., power and rate) allocation to the training symbols fixed. This is done in order to increase the robustness and study the performance of the PCC against imperfect CSIR. However, the LMMSE based channel estimation algorithms give inversely decreasing MSE versus SNR if the training transmit power and overhead is kept fixed. In Fig. 22, we evaluate the performances of the 16- and 64-BEP PCC with $\mathrm{SNR_d}$ dependent channel estimation, i.e., $\mathrm{SNR_t} = \mathrm{SNR_d}$ or $P_t = P_d$ and with different numbers of receive antennae. Although the estimation covariance is a decreasing function of the SNR, the coded FER performances of the BEP PCCs are better than that of the conventional constellations. As can be expected, the performance gets even better with higher order (i.e., $L = 64$) PCCs and with a large number of receive antennae.

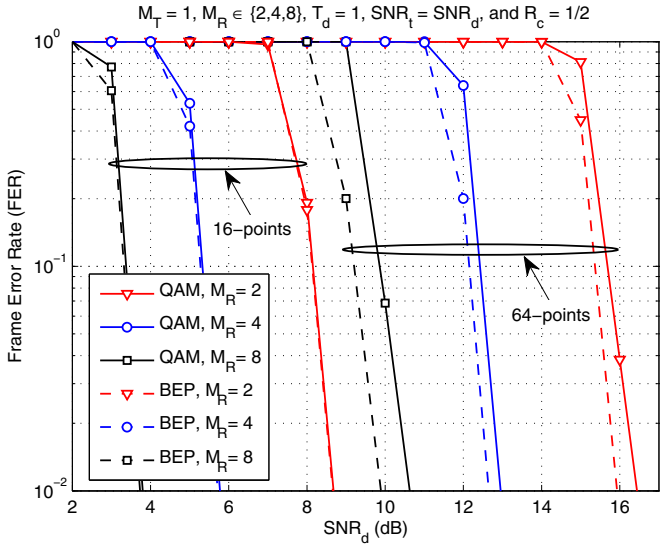

Fig. 22. Decoded FER of SIMO system versus $\mathrm{SNR_d}$ for signal-to-noise dependent channel estimation covariance (i.e., $\mathrm{SNR_t} = \mathrm{SNR_d}$) with $L \in \{16, 64\}$, $M_T = 1$, $M_R \in \{2, 4, 8\}$, and $T_d = 1$, [117] (©2013 IEEE).

3.4.2 *Multiple transmit antennae partially coherent constellations*

Now we evaluate the performance of the multiple transmit antennae constellations for $M_T = 2$, $M_R = 2$, $T_d = 1$ and for fixed SNR_t values of 3.7 dB, 8 dB and 10 dB. In order to have a fair performance comparison, we use a 16-CR PCC designed jointly for two transmit antennae for our case and two independent 4-QAM for two transmit antennae as a baseline for comparison so that they have the same spectral efficiency $R = 4$ bits/T. In Fig. 23, their FER versus $(E_b/N_0)_d$ performances with $R_c = \frac{1}{2}$ are plotted. The bit mapping used for the CR PCCs is optimized using the MBSA. It can be observed that at $\text{SNR}_\text{t} = 3.7$ dB, where channel estimation covariance has small values, the CR PCCs have significant performance gain compared to that of the conventional 4-QAM (spatial multiplexed). Performance gains of the CR PCCs naturally reduces for higher values of SNR_t, i.e. 8 dB and 10 dB, but still show significant as compared to the conventional constellations.

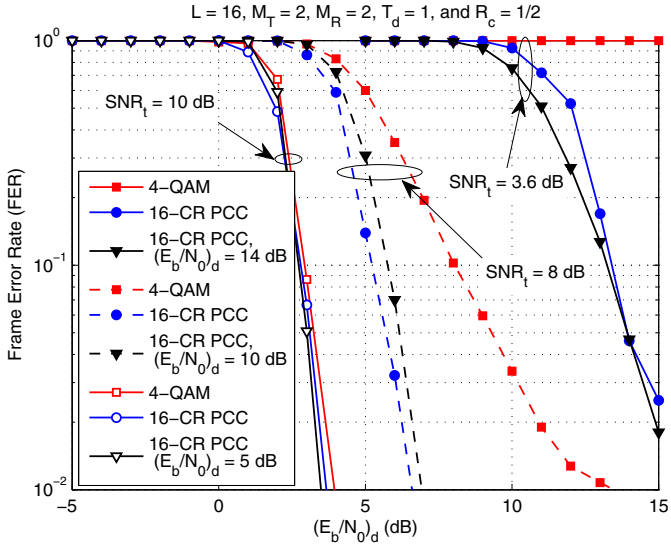

Fig. 23. Decoded FER of MIMO system versus $(E_b/N_0)_d$ for fixed $\text{SNR}_\text{t} \in \{3.7, 8, 10\}$ dB with $L = 16$, $M_T = 2$, $M_R = 2$ and $T_d = 1$. The 16-CR PCC, $(E_b/N_0)_d \in \{5, 10, 14\}$ dB are the fixed (non-SNR_d dependent) constellations designed at 5 dB, 10 dB and 14 dB $(E_b/N_0)_d$, [117] (©2013 IEEE).

The coded FER performances of the CR PCC designed at fixed value of $(E_b/N_0)_d \in \{5, 10, 14\}$ dB are also shown in Fig. 23. They show substantial performance gains compared to the conventional constellations and slight losses compared to the CR PCCs. However, at some $(E_b/N_0)_d$ values, their performances get better as compared to the CR PCC designed for different values of $(E_b/N_0)_d$. This performance loss for CR PCC is due to the bit mapping (obtained using the MBSA) assigned to it. The MBSA converges to a local mapping, and mapping can be good for a CR PCC designed for some value of $(E_b/N_0)_d$ and worse for some other CR PCC designed for a different value of $(E_b/N_0)_d$. In this example, the CR PCC designed at $(E_b/N_0)_d = 14$ dB seems to have a better mapping compared to those of CR PCCs designed for different values of $(E_b/N_0)_d$.

The effects of different values of channel transmit and receive correlations on the error performance are depicted in Fig. 24. The performances of the 16-CR PCC with the conventional constellations for $M_T = 2$, $M_R = 2$, $T_d = 1$, $R_c = 1/2$ and for a fixed $\mathrm{SNR_t}$ value of 8 dB are shown. As expected, both constellations show better performances at lower values of channel correlations (i.e., $\{\rho_T, \rho_R\} \in [\{0, 0\}, \{0.3, 0.45\}]$) than at higher ones $\{0.5, 0.7\}$. We can also observe that the performances of the 16-CR PCC are significantly better than those of the conventional constellations. The reason for this is that the design criterion is a function of both the channel estimation covariance and channel correlation matrices. Thus, the resulting CR PCC, which is adapted to both the channel estimation covariance and the channel correlation matrices, jointly compensates for the degradation caused by the imperfect channel estimation and channel correlations.

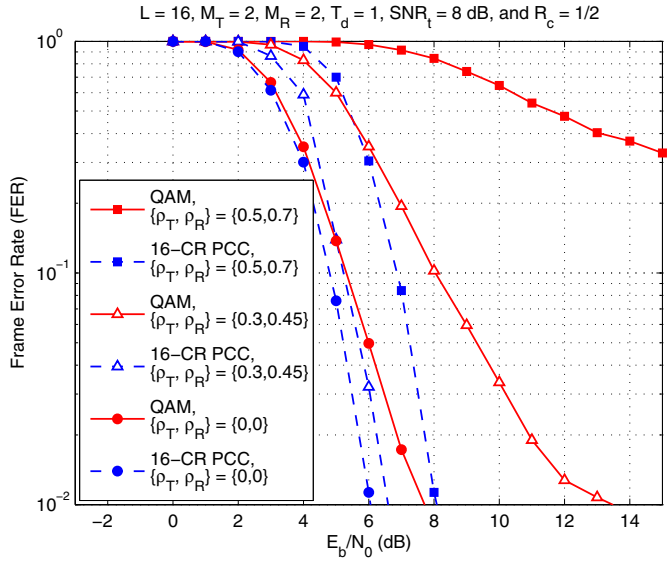

Fig. 24. Decoded FER of MIMO system versus $(E_b/N_0)_d$ for fixed $\text{SNR}_\text{t} = 8$ dB with $L = 16$, $M_T = 2$, $M_R = 2$, $T_d = 1$ and different values of transmit and receive correlations, i.e., $\{\rho_T, \rho_R\} = [\{0, 0\}, \{0.3, 0.45\}, \{0.5, 0.7\}]$, [117] (©2013 IEEE).

In Table 1, we have compared the total $\text{SNR} = \text{SNR}_\text{d} + \text{SNR}_\text{t}$ or the total power required by the CR PCCs with the conventional constellations in order to achieve the target $\text{FER} = 10^{-1}$ for various values of $L \in \{2, 4, 6\}$ under different values of training power $\text{SNR}_\text{t} \in \{12, 10, 8, 3.7\}$ dBs. The system parameters are $M_T = 2$, $M_R = 2$, $T_d = 1$, and $R_c = \frac{1}{2}$. The mark "-" in the table means that the target FER is not achieved. It can be seen from the table that the total SNR required by the CR PCCs is always less than that of the conventional constellations. For $R = 2$ bits/T, the target FER is achieved by the 4-CR PCC designed for $\text{SNR}_\text{t} = 3.7$ dB at $\text{SNR} = 13.98$ dB, whereas the conventional constellation required 1.7 dB more in total SNR and an SNR_t value of 8 dB. Thus, using the 4-CR PCC we can save some power on the training symbols. As expected, the constellation with a larger number of symbol points needs a higher training SNR_t to achieve the target. Nevertheless, the CR PCC designed for $\text{SNR}_\text{t} = 12$ dB saves 0.28 dB and 2.21 dB in total SNR as compared to that of QAM for $R = 4$ bits/T and $R = 6$ bits/T, respectively. Moreover, the

conventional constellations of higher spectral efficiencies (i.e., $R = 6$ bits/T) for $\mathrm{SNR_t} = 10$, 8 and 3.7 dB never achieve the target FER, whereas the CR PCC does achieve it, except for $\mathrm{SNR_t} = 3.7$ dB.

Table 1. Comparison of total SNR = $\mathbf{SNR_d}$ + $\mathbf{SNR_t}$ required by CR PCC with QAM in MIMO system to achieve FER = 10^{-1} for $\mathbf{SNR_t} \in \{12, 10, 8, 3.7\}$ dB with $M_T = 2$, $M_R = 2$, $T_d = 1$, and spectral efficiencies $R \in \{2, 4, 6\}$ bits/T, [117] (©2013 IEEE).

Total SNR, spectral efficiency	$\mathrm{SNR_t}$ = 12 dB		$\mathrm{SNR_t}$ = 10 dB		$\mathrm{SNR_t}$ = 8 dB		$\mathrm{SNR_t}$ = 3.7 dB	
	CR PCC	QAM	CR PCC	QAM	CR PCC	QAM	CR PCC	QAM
SNR, R=2 bits/T	17.63	17.65	15.95	16.39	14.88	15.68	13.98	27.13
SNR, R=4 bits/T	26.20	26.48	26.61	27.37	27.11	29.86	30.76	-
SNR, R=6 bits/T	37.80	40.01	44.86	-	50.50	-	-	-

3.4.3 Partially coherent space-time constellations

Finally, we evaluate the performance of the ST constellations for $M_T = 2$, $M_R = 2$, $T_d \geq 2$. The $\mathrm{SNR_t}$ is fixed for all values of $(E_b/N_0)_d$ used in the simulation. In this section, we present two examples, one for $T_d = 2$ and another for $T_d = 4$. In the first example, we use the Alamouti codes as an OSTBC and compare its performance with the CR-optimized OSTBC. In Fig. 25, we evaluate the FER versus $(E_b/N_0)_d$ performance of the Alamouti code, which chooses its symbols from two independent conventional constellations with the one which chooses its symbols from CR PCCs designed jointly across the M_T transmit antennae. The turbo code rate used here is $R_c = \frac{2}{3}$ and $\mathrm{SNR_t} = 3.7$ dB. For a fair comparison, we use 4-QAM (2 bits/T) constellations corresponding to the 16-CR PCC. The Alamouti code which uses a CR-optimized 16-CR PCC observed significant performance gain as compared to the one using the 4-QAM. The performances of 16-CR PCCs designed at fixed $(E_b/N_0)_d$ values of 10 dB and 6 dB are also shown in the same figure. As expected, their gains are substantial as compared to those of the 4-QAM constellation and show slight loss compared to the CR PCCs. It should be pointed out that the imperfect CSIR lose the diversity offered by Alamouti codes with perfect CSIR. However, Alamouti codes using CR PCC achieve diversity.

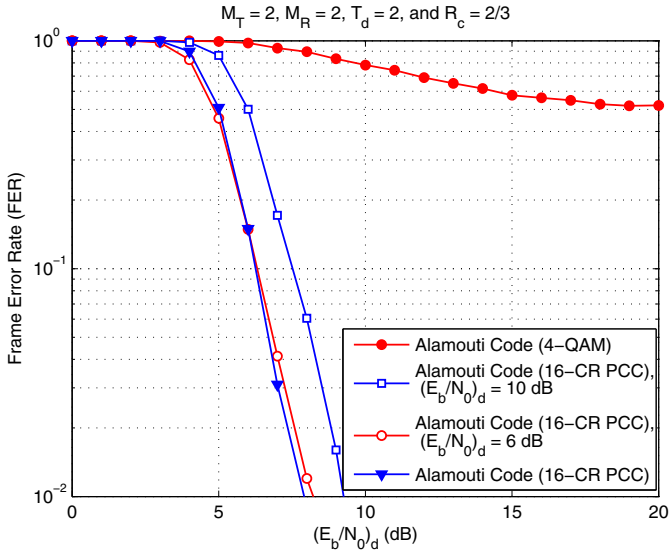

Fig. 25. Decoded FER of MIMO system versus $(E_b/N_0)_d$ for fixed $\mathrm{SNR_t} = 3.7$ dB with $L = 16$, $M_T = 2$, $M_R = 2$ and $T_d = 2$. The 16-CR PCC, $(E_b/N_0)_d \in \{6, 10\}$ dB are the fixed (non-$\mathrm{SNR_d}$ dependent) constellations designed at 6 dB and 10 dB $(E_b/N_0)_d$, [117] (©2013 IEEE).

In the second example, we have used the unitary ST constellations obtained by solving (52). Here, each ST constellation has the structure $\mathcal{S} = \{\Phi_i \mathbf{D}_i\}_{i=1}^{L}$, where Φ_i is a unitary matrix and is already known. In this example, we use the unitary matrices which were found by Giese and Skoglund [94], as they were designed for the partially coherent channels. Another unitary matrix designed for the partially coherent channels proposed in [93] could also be used in this example. The unitary matrices [94] are obtained by combining non-coherent [75] and coherent codes. The idea of adaptively determining the number of coherent and non-coherent component codes goes according to the weighting factor (estimation covariance or $\mathrm{SNR_t}$) between their intra-subspace and inter-subspace distances [94]. For the non-coherent case ($\mathrm{SNR_t} = 0$), the inter-subspace distance between two signals $\Phi_i$and Φ_j depends upon the principal angles between the subspace spanned by Φ_i and Φ_j. For the coherent case (high $\mathrm{SNR_t}$), two signals in the same subspace have vanishing inter-subspace and non-vanishing

intra-subspace distance, since it depends upon the singular values of the difference $\Phi_i - \Phi_j$. In other words, higher estimation variance will involve more non-coherent components to achieve a large inter-subspace distance and less coherent component codes and vice versa. In this example, we compare the performance of a purely non-coherent code (16 unitary code) to that of a signal set based on combining eight non-coherent codes with two coherent codes, and a constellation combining four non-coherent codes with four coherent codes. The dominance of all three constellation sets in various regions of $\mathrm{SNR_t}$ is shown in the inset of Fig. 26 for both the unitary codes of [94] and their corresponding CR-optimized constellation sets.

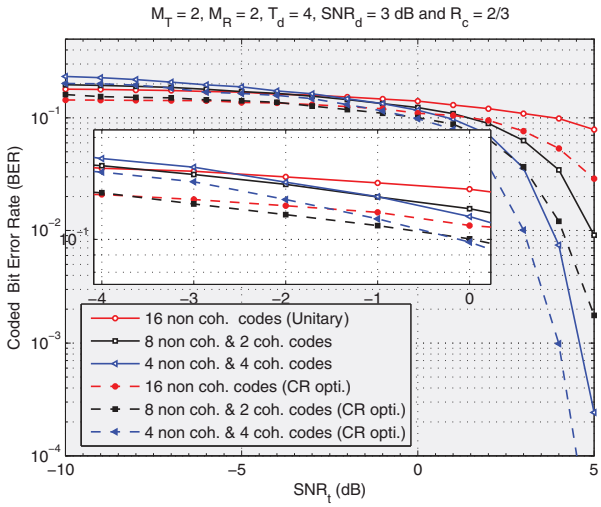

Fig. 26. Decoded BER of MIMO system versus training $\mathrm{SNR_t}$ for the codes designed at $\mathrm{SNR_d}$ per block of 3 dB with $L = 16$, $M_T = 2$, $M_R = 2$, $T_d = 4$, [117] (©2013 IEEE).

The coded BER versus $\mathrm{SNR_t}$ performance of the combined codes, designed at $\mathrm{SNR_d}$ per block of 3 dB, are compared in Fig. 26 with $R_c = \frac{2}{3}$. All three CR-optimized constellation sets exhibit significantly better performance compared to that of the constellation sets proposed by [94] over the entire $\mathrm{SNR_t}$ region.

3.5 Conclusion

The space-time constellation design and bit mapping schemes with imperfect CSIR for a spatially correlated Rayleigh-fading channel were considered. The UB-ABEP and CR as a function of channel estimation variance have been proposed as design criteria to obtain partially coherent ST constellations. The UB-ABEP and CR expressions for the partially coherent and spatially correlated channel were derived. Two effective bit mapping schemes were presented. First, for the single transmit antenna case, which maintains the Gray mapping, and second, for the multiple transmit antennae using the MBSA. Numerical results demonstrated the effectiveness of the optimized constellations and optimized bit mapping. The resulting constellations were shown to have significantly better FER gains and improved power efficiencies compared to those of the conventional constellations with turbo codes.

4 Linear precoder design for partially coherent correlated channels

In this chapter, we consider the single-user MIMO linear precoder matrix design, as an alternative to PCCs, for imperfectly estimated CSIR with the assumption that the second order statistics of the CSI error covariance matrix are available at the transmitter via an error-free feedback link. The designed linear precoder is adapted to both the quality of the channel estimate at the receiver and the transmiter/receiver antenna correlation.

This chapter is organized as follows: The assumptions and system and channel models are detailed in Section 4.1. A generic closed and tractable form of CR expression is derived and used in the optimization problem to design the linear precoder matrices for various MIMO transmission schemes such as SM and STBC (e.g., OSTBC and USTC). These are presented in Section 4.2. The details of the numerical optimization methods based on the branch-and-bound (BnB) and self-tuning Riemannian SD algorithms are presented in Section 4.3. Numerical-coded BER, FER, and MI performance results of the CR-optimized precoder matrices in conjunction with SM and STBC (e.g., Alamouti and unitary codes) are presented in Section 4.4. Section 4.5 concludes the chapter.

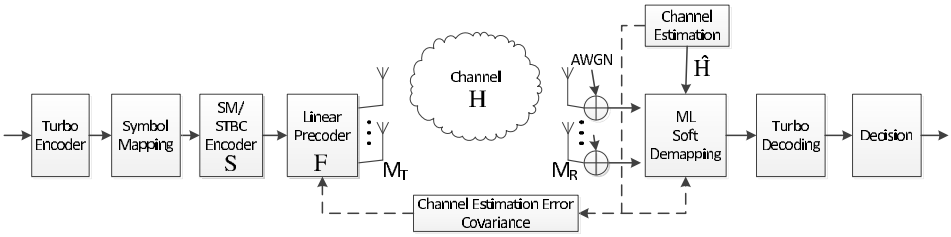

Fig. 27. Block diagram of the MIMO system with a linear precoder F at the transmitter.

4.1 System model

In this chapter as well we have considered the same communication system as the one in Chapters 2 and 3, but with an additional linear precoding block, after the SM/STBC encoder block, on the transmitter side as shown in Fig. 27. The matrix of the received data symbols can be expressed as

$$\mathbf{R}_d \quad = \quad \mathbf{SFH} + \mathbf{W}_d, \tag{59}$$

where $\mathbf{R}_d \in \mathbb{C}^{T_d \times M_R}$, $\mathbf{S} \in \mathcal{S} \subset \mathbb{C}^{T_d \times M_T}$ is a data codeword matrix used to transmit symbol vector $\mathbf{s} = [s_0, s_1, \cdots, s_{K-1}]^T \in \mathcal{S}^K$, where $s_i \in \mathcal{S}$, $\mathcal{S}$ is a set of signal alphabets such as M-level QAM or PSK, satisfying $\mathbb{E}[|s_i|^2] = 1$. $\mathbf{F} \in \mathbb{C}^{M_T \times M_T}$ is a linear precoder matrix, $\mathbf{H} \in \mathbb{C}^{M_T \times M_R}$ is the channel response assumed to be constant during transmission of the codeword matrix $\mathbf{S}$, and $\mathbf{W}_d \in \mathbb{C}^{T_d \times M_R}$ is an additive complex circularly symmetric white Gaussian noise (WGN) matrix with zero mean and element-wise unit variance. Here, we capture the effect of data signal-to-noise ratio ($\mathrm{SNR_d}$) factor in $\mathbf{F}$ thus, $\mathrm{SNR_d}$ $= P_d$, and use the power normalization

$$\mathbb{E}[||\mathbf{SF}||^2] \quad = \quad T_d P_d. \tag{60}$$

The model of imperfect channel estimation used in this chapter is the same as in Chapter 3.

After post-multiplying (59) by $\mathbf{U}_R$, denoting $\mathbf{SFU}_T$ by $\mathbf{X}$, and denoting $\mathbf{R}_d\mathbf{U}_R$ by $\mathbf{Y}$, we get

$$\mathbf{Y} \quad = \quad \mathbf{X}\hat{\hat{\mathbf{H}}} + \mathbf{X}\tilde{\tilde{\mathbf{H}}} + \mathbf{N} \tag{61}$$

which represents the sufficient statistics of the received signal. The unitary transformed codeword matrix $\{\mathbf{X}\}$ satisfies the same average-power constraint as the original precoded codeword matrix $\{\mathbf{SF}\}$, and $\mathbf{N}$ has i.i.d. circularly symmetric $\mathcal{CN}(0,1)$ entries, since it has the same distribution as $\mathbf{W}_d$.

Applying the vec operation to (61), we get

$$\mathbf{y} \quad = \quad \mathbf{Z}\hat{\hat{\mathbf{h}}} + \mathbf{Z}\tilde{\tilde{\mathbf{h}}} + \mathbf{n}, \tag{62}$$

where $\mathbf{Z} = \mathbf{I}_{M_R} \otimes \mathbf{X}$. The conditional probability density function (PDF) of the received signal conditioned on given $\hat{\hat{\mathbf{H}}}$ and $\mathbf{X}_i$ being sent is [96]

$$p_i(\mathbf{y}) = p\left(\mathbf{y}|\mathbf{Z}_i, \hat{\hat{\mathbf{h}}}\right) = \frac{\exp\left\{-(\mathbf{y} - \mathbf{Z}_i\hat{\hat{\mathbf{h}}})^H(\mathbf{I}_{T_d M_R} + \mathbf{Z}_i\tilde{\Sigma}\mathbf{Z}_i^H)^{-1}(\mathbf{y} - \mathbf{Z}_i\hat{\hat{\mathbf{h}}})\right\}}{\pi^{TM_R}|(\mathbf{I}_{T_d M_R} + \mathbf{Z}_i\tilde{\Sigma}\mathbf{Z}_i^H)|}, \tag{63}$$

where $\tilde{\Sigma} = \mathbb{E}[\text{vec}(\tilde{\tilde{\mathbf{H}}})\text{vec}(\tilde{\tilde{\mathbf{H}}})^H] = (\tilde{\Lambda}_R \otimes \Lambda_T)$ is a correlation matrix of $\tilde{\tilde{\mathbf{H}}}$, which is the same as that of $\tilde{\mathbf{H}}$.

In the remainder of the chapter, we will assume that $\mathbf{R}_T$, $\mathbf{R}_R$, and σ_{ce}^2 are known to the receiver and the transmitter, which further implies knowledge of the estimation covariance matrix $\tilde{\Sigma}$ at the transmitter.

4.2 Precoder design

In this section, we derive the cutoff rate (CR) expression as a function of the estimated channel covariance matrix and adopt it as a linear precoder design criterion for a doubly correlated partially coherent channels.

4.2.1 Cutoff rate matched to a partially coherent channel

In the following proposition, we use the relationship between the Bhattacharyya coefficient and the CR [114] to derive the CR expression.

Proposition 6 *The Bhattacharyya coefficient $\rho_{\text{cor}}(i,j)$ between the pair of codewords $\boldsymbol{S}_i$ and $\boldsymbol{S}_j$ and cutoff rate R_0, in bits per channel use, for a doubly correlated partially coherent channels with the discrete inputs and continuous output are given by*

$$\rho_{\text{cor}}(i,j) = \prod_{n=1}^{M_R} |\boldsymbol{I}_{T_d} + \boldsymbol{S}_i \boldsymbol{F} \boldsymbol{R}_T \boldsymbol{F}^H \boldsymbol{S}_i^H \tilde{\lambda}_R^n|^{\frac{1}{2}} |\boldsymbol{I}_{T_d} + \boldsymbol{S}_j \boldsymbol{F} \boldsymbol{R}_T \boldsymbol{F}^H \boldsymbol{S}_j^H \tilde{\lambda}_R^n|^{\frac{1}{2}} \frac{1}{|\boldsymbol{I}_{T_d} + \frac{1}{2}(\boldsymbol{S}_i \boldsymbol{F} \boldsymbol{R}_T \boldsymbol{F}^H \boldsymbol{S}_i^H + \boldsymbol{S}_j \boldsymbol{F} \boldsymbol{R}_T \boldsymbol{F}^H \boldsymbol{S}_j^H)\tilde{\lambda}_R^n + \frac{1}{4}(\boldsymbol{S}_i - \boldsymbol{S}_j)\boldsymbol{F} \boldsymbol{R}_T \boldsymbol{F}^H (\boldsymbol{S}_i - \boldsymbol{S}_j)^H \hat{\lambda}_R^n|}, \tag{64}$$

and

$$R_0 = \max_{\{\pi_i\}_{i=1}^L} \underbrace{-\log\left(\sum_i \pi_i \sum_j \pi_j \rho_{\text{cor}}(i,j)\right)}_{\varrho}, \tag{65}$$

respectively, where $\tilde{\lambda}_R^n$ and $\hat{\lambda}_R^n$ are the eigenvalues of $\tilde{\boldsymbol{R}}_R$ and $\hat{\boldsymbol{R}}_R$ and$\{\boldsymbol{X}_i\}_{i=1}^L$ is the constellation set with corresponding probabilities $\{\pi_i\}_{i=1}^L$.

Proof. Derivations of the Bhattacharyya coefficient and the cutoff rate follow the same line of steps as presented in Appendix 5. Replacing each codeword matrix $\mathbf{X}$ in Proposition 4 with $\mathbf{SFU}_T$ results in (64) and (65). ■

We refer to the argument of $\max(\cdot)$ in (65) as the CR expression and denote it as ϱ. For the equiprobable signal set with transmission probabilities $\{\pi_i\}_{i=1}^{L} = 1/L$, the linear precoder design can be now formulated as the following continuous optimization problem (for fixed L, elements of $\mathbf{S}$ can take any values from any constellation set, e.g., M-QAM, M-PSK)

$$\begin{aligned} \underset{\mathbf{F}}{\text{maximize}} \quad & \varrho \\ \text{subject to} \quad & \text{tr}\{\mathbf{S}_i\mathbf{F}\mathbf{F}^H\mathbf{S}_i^H\} = T_d P_d, \end{aligned} \tag{66}$$

where the maximization is with respect to the precoding matrix $\mathbf{F}$.

Without loss of generality, we write $\mathbf{F} = \mathbf{V}_F\Lambda_F\mathbf{U}_F^H$, which is the SVD of matrix $\mathbf{F}$. In order to find a close-to-optimal linear precoder matrix $\mathbf{F}$, we need to find three matrices: the input-shaping matrix ($\mathbf{V}_F$), power loading matrix (Λ_F), and beamforming matrix ($\mathbf{U}_F$). For the case of the Gaussian input distributions, the unitary matrix $\mathbf{V}_F$ is always assumed to be an identity matrix [144] and moreover, for any unitary matrix $\mathbf{V}_F$, with non-Gaussian input, the following relationship holds: $\mathcal{I}(\mathbf{x};\mathbf{y}) \neq \mathcal{I}(\mathbf{V}_F\mathbf{x};\mathbf{y})$ in general [145]. Thus, by properly designing the unitary matrix $\mathbf{V}_F$, for the non-Gaussian inputs, we may improve the average mutual information.

Proposition 7 *The beamforming matrix $\boldsymbol{U}_F$ of a linear precoder matrix $\boldsymbol{F}$ that maximizes the cutoff rate, for a doubly correlated partially coherent channel, coincides with the eigenvectors of the transmit correlation matrix $\boldsymbol{R}_T$*

Proof. By setting $\mathbf{X}_i\mathbf{V}_F = \tilde{\mathbf{X}}_i$, we can write $\mathbf{X}_i\mathbf{V}\Lambda_F\mathbf{U}_F^H\mathbf{R}_T\mathbf{U}_F\Lambda_F\mathbf{V}_F^H\mathbf{X}_i^H$ as $\tilde{\mathbf{X}}_i\Lambda_F\mathbf{U}_F^H\mathbf{R}_T\mathbf{U}_F\Lambda_F\tilde{\mathbf{X}}_i^H$. Now consider the EVD of $\Lambda_F\mathbf{U}_F^H\mathbf{R}_T\mathbf{U}_F\Lambda_F = \mathbf{Q}\mathbf{D}\mathbf{Q}^H$, where $\mathbf{D}$ and $\mathbf{Q}$ are diagonal and unitary matrices, respectively. Furthermore, the diagonal matrix $\mathbf{D}$ can be written as $\mathbf{Q}^H\Lambda\mathbf{U}^H\mathbf{R}_T\mathbf{U}_F\Lambda\mathbf{Q}$.

There exists a matrix $\mathbf{M} = \mathbf{U}_T\Lambda_M$ such that $\mathbf{M}^H\mathbf{R}_T\mathbf{M} = \mathbf{D}$ and $\text{tr}\{\mathbf{M}\mathbf{M}^H\} \leq \text{tr}\{\Lambda_F\Lambda_F^H\} = \text{tr}\{\mathbf{F}\mathbf{F}^H\}$. We can write

$$\mathbf{F}\mathbf{R}_T\mathbf{F}^H = \mathbf{V}_F\underbrace{\Lambda_F\mathbf{U}^H\mathbf{R}_T\mathbf{U}_F\Lambda}_{=\mathbf{Q}\mathbf{D}\mathbf{Q}^H}\mathbf{V}_F^H = \underbrace{\mathbf{V}_F\mathbf{Q}\mathbf{M}^H}_{=\tilde{\mathbf{F}}}\mathbf{R}_T\mathbf{M}\mathbf{Q}^H\mathbf{V}_F^H = \tilde{\mathbf{F}}\mathbf{R}_T\tilde{\mathbf{F}}^H \tag{67}$$

Now, $\tilde{\mathbf{F}} = \mathbf{V}_F\mathbf{Q}\mathbf{M}^H = \mathbf{V}_F\mathbf{Q}\Lambda_M^H\mathbf{U}_T^H = \tilde{\mathbf{V}}_F\Lambda_M^H\mathbf{U}_T^H$, where $\mathbf{V}_F\mathbf{Q} = \tilde{\mathbf{V}}_F$, means that the beamforming matrix $\mathbf{U}_F$ of a linear precoder matrix must coincide with eigenvectors $\mathbf{U}_T$ of the transmit correlation matrix $\mathbf{R}_T$ with lower transmit power, $\text{tr}\{\tilde{\mathbf{F}}\tilde{\mathbf{F}}^H\} \leq \text{tr}\{\mathbf{F}\mathbf{F}^H\}$. ■

Using the results from Proposition 6 and Proposition 7, the Bhattacharyya coefficient can be rewritten as

$$\rho_{\text{cor}}(i,j) = \prod_{n=1}^{M_R} |\mathbf{I}_{T_d} + \mathbf{S}_i \mathbf{V}_F \Lambda \mathbf{V}_F^H \mathbf{S}_i^H \tilde{\lambda}_R^n|^{\frac{1}{2}} |\mathbf{I}_{T_d} + \mathbf{S}_j \mathbf{V}_F \Lambda \mathbf{V}_F^H \mathbf{S}_j^H \tilde{\lambda}_R^n|^{\frac{1}{2}} \frac{1}{|\mathbf{I}_{T_d} + \frac{1}{2}(\mathbf{S}_i \mathbf{V}_F \Lambda \mathbf{V}_F^H \mathbf{X}_i^H + \mathbf{S}_j \mathbf{V}_F \Lambda \mathbf{V}_F^H \mathbf{S}_j^H)\tilde{\lambda}_R^n + \frac{1}{4}(\mathbf{S}_i - \mathbf{S}_j)\mathbf{V}_F \Lambda \mathbf{V}_F^H (\mathbf{X}_i - \mathbf{X}_j)^H \hat{\lambda}_R^n|}, \tag{68}$$

where $\Lambda = \Lambda_F^2 \Lambda_T$, subject to the average power constraint, i.e., $\text{tr}\{\Lambda_F \Lambda_F^H\} \leq T_d P_d$ and $\mathbf{V}_F \mathbf{V}_F^H = \mathbf{V}_F^H \mathbf{V}_F = \mathbf{I}$.

We will now rewrite the CR optimization problem (66) with two new variables, i.e., Λ_F and $\mathbf{V}_F$ as

$$\begin{aligned} \underset{\Lambda_F, \mathbf{V}_F}{\text{maximize}} \quad & \varrho \\ \text{subject to} \quad & \text{tr}\{\mathbf{S}_i \mathbf{V}_F \Lambda_F^2 \mathbf{V}_F^H \mathbf{S}_i^H\} \leq T_d P_d \\ & \mathbf{V}_F \mathbf{V}_F^H = \mathbf{V}_F^H \mathbf{V}_F = \mathbf{I}, \end{aligned} \tag{69}$$

where the maximization is now with respect to the diagonal power loading matrix Λ_F and unitary input-shaping matrix $\mathbf{V}_F$. The CR expression in (69) is not a convex function with respect to the $\mathbf{V}_F$ and Λ_F and moreover, its optimization does not lead to a closed form solution for the linear precoders. There are several approaches to approximate non-convex functions, e.g., gradient search, SD, etc. However, the solution is not guaranteed to be optimal. Since there are two matrices to be optimized in (69), we solve them in an iterative manner. Before addressing numerical solutions in Section 4.3, we consider two special cases as examples.

4.2.2 Special cases

We will now find the linear precoding matrices by solving (69) for two MIMO schemes, i.e., spatial multiplexing and space-time coding.

Spatial multiplexing ($M_T \geq 2$ and $T_d = 1$)

In this MIMO scheme, each transmit antenna draws its symbols independently from the conventional M-QAM or M-PSK constellations. With $T_d = 1$, each $\mathbf{S}$ in (68) will be replaced by a complex row vector $\mathbf{s}$, and the power constraint becomes $\text{tr}\{\Lambda_F^2\} \leq T_d P_d$.

Space-time codes ($M_T \geq 2$ and $T_d \geq 2$)

– *Orthogonal ST codes:* Herein, we use the OSTBC, designed to exploit the spatial diversity of the MIMO systems [49, 52], as a codeword matrix. The OSTBCs are of particular interest here due to their simple decoding while providing diversity gain. Precoder design combined with OSTBCs was previously studied in [146–149] with perfect CSIR and statistical CSIT and in [150, 151] with imperfect CSIR and partial CSIT (correlation matrix). However, the channel assumption in this chapter is different from [150, 151], as we have considered the covariance of the estimated channel is available as CSIT.

Assume that K independent complex symbols are transmitted simultaneously over T_d periods of time, i.e., the rate R of the code is K/T_d, and

$$\mathbf{S}^H\mathbf{S} = a\sum_{i=0}^{K-1}|x_i|^2\mathbf{I}, \tag{70}$$

where $a = 1$, if $\mathbf{S} \in \{\mathcal{G}_2, \mathcal{H}_3, \mathcal{H}_4\}$ and $a = 2$ if $\mathbf{S} \in \{\mathcal{G}_3, \mathcal{G}_4\}$[10] [25]. Close-to-optimal Λ_F and $\mathbf{V}_F$ matrices, with power constraint $aK\mathrm{tr}\{\Lambda_F^2\} \leq T_dP_d$, can be obtained by solving the optimization problem (69). Furthermore, the complexity of the optimization increases with the number of transmit antennae.

– *Unitary ST codes:* We constrain herein the ST block code to be a unitary one. The unitary space-time codes (USTC) [34, 74] are capacity optimal signals for non-coherent channels. Moreover, they have very simple ML decoding algorithms with perfect CSIR [97]. Recently, novel unitary signals or codes were designed for the partially coherent channels in [93, 94] and their improved form in [114]. Very little attention has been paid on the precoder design combined with the USTCs, while examples are [152, 153].

We consider the unitary ST codes $\mathcal{S} = \{\Phi_i\}_{i=1}^{L}$, where $\Phi_i \in \mathbb{C}^{T_d \times M_T}$ is a matrix with orthonormal columns (i.e., $\Phi_i^H\Phi_i = \mathbf{I}_{M_T}$ and $\Phi_i\Phi_i^H \neq \mathbf{I}_{T_d}$). In this case, close-to-optimal Λ_F and $\mathbf{V}_F$ matrices, with a power constraint $\mathrm{tr}\{\Lambda_F^2\} \leq T_dP_d/M_T$, can be obtained by solving the optimization problem (69).

[10] $\mathcal{G}_2, \mathcal{G}_3, \mathcal{G}_4, \mathcal{H}_3$ and, $\mathcal{H}_4$ are space-time block codes with rate R of 1, 1/2, 1/2, 3/4 and 3/4, respectively and subscripts denote the number of transmit antennae.

4.2.3 Difference of convex (d.c.) formulation

Let us now fix $\mathbf{V}_F$ and focus on optimizing the Λ_F which is calculated as $\Lambda^{1/2}\Lambda_T^{-1/2}$. Substituting $\tilde{\mathbf{X}}_i = \mathbf{S}_i\mathbf{V}_F$, the CR expression can be rewritten as

$$R_0 = -\log\left(\frac{1}{L^2}\sum_i\sum_j\prod_{n=1}^{M_R} \frac{|\mathbf{I}_{T_d} + \tilde{\mathbf{X}}_i\Lambda\tilde{\mathbf{X}}_i^H\tilde{\lambda}_R^n|^{\frac{1}{2}}|\mathbf{I}_{T_d} + \tilde{\mathbf{X}}_j\Lambda\tilde{\mathbf{X}}_j^H\tilde{\lambda}_R^n|^{\frac{1}{2}}}{|\mathbf{I}_{T_d} + \frac{1}{2}(\tilde{\mathbf{X}}_i\Lambda\tilde{\mathbf{X}}_i^H + \tilde{\mathbf{X}}_j\Lambda\tilde{\mathbf{X}}_j^H)\tilde{\lambda}_R^n + \frac{1}{4}(\tilde{\mathbf{X}}_i - \tilde{\mathbf{X}}_j)\Lambda(\tilde{\mathbf{X}}_i - \tilde{\mathbf{X}}_j)^H\hat{\lambda}_R^n|}\right). \tag{71}$$

We now decompose (71) into a d.c. form.

Theorem 1 *For a given $\boldsymbol{V}_F$, maximizing the cutoff rate with respect to Λ in (71) can be decomposed as a difference of two convex functions, and, therefore, the optimization problem (66) can be reformulated as a d.c. programming problem as*

$$\begin{aligned} R_0 = \quad & \underset{\Lambda}{\text{maximize}}\,\{g(\Lambda) - f(\Lambda)\} = -\underset{\Lambda}{\text{minimize}}\,\{f(\Lambda) - g(\Lambda)\} \\ \text{subject to} \quad & \text{tr}\{\Lambda_F\Lambda_F^H\} \le T_d P_d, \end{aligned} \tag{72}$$

where $f(\Lambda)$ and $g(\Lambda)$ are convex functions of Λ given as

$$\begin{aligned} f(\Lambda) = \log\Bigg(\frac{1}{L^2}\sum_{\substack{i,j\\ j>i}}\prod_{n=1}^{M_R} & |\boldsymbol{I}_{T_d} + \frac{1}{2}(\tilde{\boldsymbol{X}}_i\Lambda\tilde{\boldsymbol{X}}_i^H + \tilde{\boldsymbol{X}}_j\Lambda\tilde{\boldsymbol{X}}_j^H)\tilde{\lambda}_R^n \\ & + \frac{1}{4}(\tilde{\boldsymbol{X}}_i - \tilde{\boldsymbol{X}}_j)\Lambda(\tilde{\boldsymbol{X}}_i - \tilde{\boldsymbol{X}}_j)^H\hat{\lambda}_R^n|^{-1}\cdot \\ & \prod_{\substack{k\neq i\\ l\neq j, l>k}}\prod_{n=1}^{M_R}|\boldsymbol{I}_{T_d} + \tilde{\boldsymbol{X}}_k\Lambda\tilde{\boldsymbol{X}}_k^H\tilde{\lambda}_R^n|^{-\frac{1}{2}}|\boldsymbol{I}_{T_d} + \tilde{\boldsymbol{X}}_l\Lambda\tilde{\boldsymbol{X}}_l^H\tilde{\lambda}_R^n|^{-\frac{1}{2}}\Bigg), \end{aligned} \tag{73}$$

and

$$g(\Lambda) = \log\left(\prod_{\substack{i,j\\ j>i}}\prod_{n=1}^{M_R}|\boldsymbol{I}_{T_d} + \tilde{\boldsymbol{X}}_i\Lambda\tilde{\boldsymbol{X}}_i^H\tilde{\lambda}_R^n|^{-\frac{1}{2}}|\boldsymbol{I}_{T_d} + \tilde{\boldsymbol{X}}_j\Lambda\tilde{\boldsymbol{X}}_j^H\tilde{\lambda}_R^n|^{-\frac{1}{2}}\right). \tag{74}$$

Proof. See Appendix 6. ∎

4.3 Numerical optimization

There are several algorithms to solve the d.c. programming problem in (72), e.g., BnB or outer approximation [154] and prismatic BnB algorithm [155]. Converting the problem into a canonical d.c. program and then using the Edge Following Algorithm [155] could be an alternative choice. More algorithms may be found in [155] and [154]. In this section, we use the prismatic BnB algorithm to obtain the optimal power loading matrix $\Lambda\Lambda^H$ due to its smaller complexity compared to the above-mentioned algorithms. The prismatic BnB algorithm requires solving the linear program (LP) at each iteration. A detailed description of the algorithm is given below.

4.3.1 Prismatic branch-and-bound (BnB) algorithm

Construction of simplex

For a given $(M_T - 1)$-simplex $S = [\mathbf{p}^1, \mathbf{p}^2, \cdots, \mathbf{p}^{M_T}]$ contains the feasible set $\mathcal{D} \in \mathbb{R}^{M_T}$ of (72), from which a prism is induced $\mathcal{T} = T(S) = \{(\mathbf{p}, t) \in \mathbb{R}^{M_T} \times \mathbb{R} : \mathbf{p} \in S\}$. The $\mathbf{p}^1, \mathbf{p}^2, \cdots, \mathbf{p}^{M_T}$ are the vertices of S. The prism $T(S)$ has M_T edges that are vertical lines (i.e., lines parallel to the t-axis) which pass through the M_T vertices of S, respectively.

The initial simplex $S \subset \mathcal{D}$ is a polytope with a small number of vertices. We construct $S \triangleq \{\mathbf{p} \in \mathbb{R}^{M_T} : \sum_{k=1}^{M_T} p_k \leq T_d P_d, \mathbf{p} \succcurlyeq \mathbf{0}\}$.

Partitioning of simplex

For a sub-division process, also called branching, of the simplices, we use an exhaustive bisection method [154] for ease of implementation. The sub-division process determines the convergence of the algorithm. A simplex is bisected at the mid-point over its longest edge into two sub-simplices. Consider the longest edge is between vertices $\mathbf{p}^i$ and $\mathbf{p}^j$ for a simplex S_1 with M_T vertices. Now using the bisection method, simplex S_1 is replaced with two new sub-simplices S_2, S_3 with a shared vertex $\mathbf{p}^w = (1/2)(\mathbf{p}^i + \mathbf{p}^j)$.

Lower bound computation

In order to compute the lower bound, we reformulate the objective function (72) into a concave minimization optimization problem which is relaxed to an affine set constraint and a linear objective function. The d.c. program (72) can be reformulated into a global concave minimization problem by adding an additional variable t as:

$$\begin{array}{lll} \varphi(t^\star, \mathbf{p}^\star) = & \underset{t,\mathbf{p}}{\text{maximize}} \{t - g(\mathbf{p})\} & \\ \text{subject to} & \frac{1}{T_d}\sum_{k=1}^{M_T} p_k \leq P_d, p_k \geq 0 & \\ & f(\mathbf{p}) - t \leq 0, & \end{array} \tag{75}$$

where $\mathbf{p} = \{p_1, \cdots, p_{M_T}\}$ is a vector containing diagonal elements of $\Lambda\Lambda^H$. The objective function $\{t - g(\mathbf{p})\}$ is concave and the feasible set $\mathcal{D} = \{(\mathbf{p}, t) \in \mathbb{R} : \frac{1}{T_d}\sum_{k=1}^{M_T} p_k \leq P_d, p_k \geq 0, f(\mathbf{p}) - t \leq 0\}$ is convex. Clearly, if $(t^\star, \mathbf{p}^\star)$ is an optimal solution of (75), then $\mathbf{p}^\star$ is an optimal solution to (72) as well and $t^\star = f(\mathbf{p}^\star)$.

Now we will relax the convex constraint set $\mathcal{D}$ to a piecewise linear convex set by outer approximating the convex function $f(\mathbf{p})$ as

$$f_{M_i}(\mathbf{p}) = \min_{\mathbf{p}^z \in M_i} \{(\mathbf{p} - \mathbf{p}^z)^T \partial f(\mathbf{p}^z) + f(\mathbf{p}^z)\}, \tag{76}$$

where M_i is the set of feasible vectors $\mathbf{p}$ and $\partial f(\mathbf{p}^z)$ is a sub-gradient of f at $\mathbf{p}^z$. The approximated function $f_{M_i}(\mathbf{p})$ is piecewise linear approximation of $f(\mathbf{p})$. Let $\mathcal{P}_i = \{(\mathbf{p}, t) : \mathbf{p} \in \mathcal{D}, f_{M_i}(\mathbf{p}) - t \leq 0\}$ and $\mathcal{F} = \{(\mathbf{p}, t) : \mathbf{p} \in \mathcal{D}, f(\mathbf{p}) - t \leq 0\}$. For all $\mathbf{p}$, $f_{M_i}(\mathbf{p}) \leq f(\mathbf{p})$, implies $\mathcal{F} \subseteq \mathcal{P}_i$, and $\mathcal{P}_i$ is a linear piecewise approximation of the feasible set $\mathcal{F}$ at ith iteration index. Furthermore, $\max\{f_{M_i}(\mathbf{p}) - g(\mathbf{p})\} \leq \max\{f(\mathbf{p}) - g(\mathbf{p})\}$ and is a lower bound of the cutoff rate found using (72). Moreover, by adding points to set M_i, the polyhedron outer approximation $\mathcal{P}$ of $\mathcal{F}$ can be successively improved because $f_{M_{i-1}}(\mathbf{p}) \leq f_{M_i}(\mathbf{p})$ if $M_{i-1} \subseteq M_i$, with $M_i = M_{i-1} \cup \{\mathbf{p}_{\max,i-1}\}$ and $M_1 = V(F_1)$, where $\mathbf{p}_{\max,i-1}$ is a feasible vector found at $(i-1)$th iteration index.

Now we write the approximate polyhedron $\mathcal{P}$ in matrix polyhedron form [156] as

$$\mathcal{P}_i \quad = \quad \{(\mathbf{p}, t) : \mathbf{A}_i\mathbf{p} - \mathbf{a}_i t \leq \mathbf{b}_i\}, \tag{77}$$

where

$$\mathbf{A}_i = \begin{bmatrix} \mathbf{1}_{1\times M_T} \\ -\mathbf{I}_{M_T} \\ \partial f(\mathbf{p}_1)^T \\ \vdots \\ \partial f(\mathbf{p}_{|M_i|})^T \end{bmatrix} \tag{78a}$$

$$\mathbf{a}_i = \begin{bmatrix} \mathbf{0}_{(M_T+1)\times 1} \\ \mathbf{1}_{(|M_i|+1)\times 1} \end{bmatrix} \tag{78b}$$

$$\mathbf{b}_i = \begin{bmatrix} P_d \\ \mathbf{0}_{M_T\times 1} \\ (\mathbf{p}_1)^T\partial f(\mathbf{p}_1) - f(\mathbf{p}_1) \\ \vdots \\ (\mathbf{p}_{|M_i|})^T\partial f(\mathbf{p}_{|M_i|}) - f(\mathbf{p}_{|M_i|}) \end{bmatrix}. \tag{78c}$$

The sub-gradient of $f(\mathbf{p})$ is $\nabla_{\mathbf{p}} f(\mathbf{p}) = [\frac{\partial f(\mathbf{p})}{\partial p_1}, \cdots, \frac{\partial f(\mathbf{p})}{\partial p_{M_T}}]^T$, where

$$\begin{aligned} \frac{\partial f(\mathbf{p})}{\partial p_m} = \frac{-1}{\log(2)\ q_{ij}} \Bigg[\sum_{i,j} \Bigg(q_{ij} \Big[\sum_{n}^{M_R} \frac{\partial \log(|\mathbf{B}|)}{\partial \mathbf{p}} \\ + \frac{1}{2} \sum_{\substack{k\neq i \\ l\neq j, l>k}} \sum_{n=1}^{M_R} \frac{\partial \log(|\mathbf{C}_k|)}{\partial \mathbf{p}} + \frac{\partial \log(|\mathbf{C}_l|)}{\partial \mathbf{p}} \Big] \Bigg) \Bigg]_{m,m}, \end{aligned} \tag{79a}$$

$$\begin{aligned} \frac{\partial \log(|\mathbf{B}|)}{\partial \mathbf{p}} = \frac{1}{2}(\Lambda_T \tilde{\mathbf{X}}_i^H \mathbf{B}^{-1} \tilde{\mathbf{X}}_i + \Lambda_T \tilde{\mathbf{X}}_j^H \mathbf{B}^{-1} \tilde{\mathbf{X}}_j)^T \tilde{\lambda}_R^n \\ + \frac{1}{4}(\Lambda_T(\tilde{\mathbf{X}}_i - \tilde{\mathbf{X}}_j)^H \mathbf{B}^{-1}(\tilde{\mathbf{X}}_i - \tilde{\mathbf{X}}_j))^T \hat{\lambda}_R^n \end{aligned} \tag{79b}$$

$$\frac{\partial \log(|\mathbf{C}_k|)}{\partial \mathbf{p}} = (\Lambda_T \tilde{\mathbf{X}}_k^H \mathbf{C}_k^{-1} \tilde{\mathbf{X}}_k)^T \tilde{\lambda}_R^n \tag{79c}$$

$$q_{ij} = \prod_{n}^{M_R} |\mathbf{B}|^{-1} \prod_{\substack{k\neq i \\ l\neq j, l>k}} \prod_{n=1}^{M_R} |\mathbf{C}_k|^{-\frac{1}{2}} |\mathbf{C}_l|^{-\frac{1}{2}}. \tag{79d}$$

In order to compute the lower bound of the objective function $t - g(\mathbf{p})$ over $\mathcal{T} \cap \mathcal{P}$, consider the points $(\mathbf{p}, t)$ which satisfy the total power constraint and lead to constant values $t - g(\mathbf{p}) = \alpha_i$, where

$$\alpha_i = \min\{f_{M_i}(\mathbf{p}) - g(\mathbf{p})\} \tag{80}$$

is a local upper bound at the ith iteration. Let $\mathbf{V}$ denote the matrix with columns $\mathbf{p}^1, \ldots, \mathbf{p}^{M_T}$. The lower bound of $t - g(\mathbf{p})$ can be calculated by solving the LP in (Γ_i, t) [156] as

$$\begin{array}{ll} \underset{\Lambda_i, t}{\text{maximize}} & t - \sum_{k=1}^{M_T} \gamma_i^k t^k \\ \text{subject to} & \mathbf{a}_i t - \mathbf{A}_i \mathbf{V}_i \Gamma_i \leq \mathbf{b}_i, \end{array} \tag{81}$$

where Γ_i is a vector with elements $\gamma_1, \ldots, \gamma_{M_T}$, $t_i = \alpha_i + g(\mathbf{p})$, and $\mathbf{A}, \mathbf{a}, \mathbf{b}$ are given in (78).

If the above LP has a feasible solution, $(\Gamma_i^\star, t_i^\star)$ is an optimal solution and $c^\star$ its optimal value, the lower bound is given as

$$\beta_i = \begin{cases} +\infty, & \text{if LP has no feasible solution} \\ \alpha_i, & \text{if } c^\star \leq 0 \\ \alpha_i - c^\star, & \text{if } c^\star > 0, \end{cases} \tag{82}$$

and the feasible point available for updating the upper bound is $\mathbf{p}_{\min,i} = \mathbf{V}_i \Gamma_i^\star$.

Upper bound computation

The upper bound computation is rather simple and straightforward. Any feasible vector $\mathbf{p}$ represents a valid upper bound. Starting with an initial upper bound $\alpha_1 = \min\{f_{M_1}(\mathbf{p}) - g(\mathbf{p})\}$, at the ith iterations, the upper bound can be computed as:

$$\alpha_i = \min\{f_{M_i}(\mathbf{p}) - g(\mathbf{p})\}, \tag{83}$$

and the corresponding power vector given by $\mathbf{p}_{\text{UB},i} = \operatorname{argmin}_{\mathbf{p}}\{f_{M_i}(\mathbf{p}) - g(\mathbf{p})\}$, where $\mathbf{p} \in \{M_i, \mathbf{p}_{\min,i}\}$.

Algorithm 2, which is presented below, finds the optimal power loading vector to the transmit antennae.

Algorithm 2 PRISMATIC BnB ALGORITHM.

Input: Input constellation set $\mathcal{S} \in \{\mathbf{S}_i : 0 \leq i \leq L-1\}$, matrix $\mathbf{V}_F$, P_d, M_T, and tolerance ϵ.

Output: Value of a cutoff rate (CR) and optimal power loading vector $\mathbf{p}^\star$ across the transmitting antennae.

1: Initialization: Given tolerance $\epsilon > 0$. Set $i = 1$, $\mathcal{R} \in \{T(S_1)\}$.
2: Stopping criterion: if $\alpha - \beta_i > \epsilon|\alpha|$ go to Step 3, otherwise STOP.
3: **while** $\mathcal{R} \neq \phi$ **do**
4: $\quad \mathbf{V}_i = T(S_i)$
5: $\quad$ Set $\mathcal{R}(i) = \phi$
6: $\quad$ Solve LP to compute lower bound β_i using (82),
7: $\quad$ If LP solution is feasible then $\mathbf{p}_{\min,i} = \mathbf{V}_i \Lambda_i^\star$ and update $M_i \in \{M_i, \mathbf{p}_{\min,i}\}$.
8: $\quad$ Compute upper bound $\alpha_i = \min_{\mathbf{p}\in M_i}\{f_{M_i}(\mathbf{p}) - g(\mathbf{p})\}$, $\mathbf{p}_{\mathrm{UB},i} = \arg\min_{\mathbf{p}\in M_i}\{f_{M_i}(\mathbf{p}) - g(\mathbf{p})\}$.
9: $\quad$ Update $\alpha = \min\{\alpha, \alpha_i\}$
10: $\quad$ **if** $\alpha == \alpha_i$ **then**
11: $\quad\quad \mathbf{p}^\star = \mathbf{p}_{\mathrm{UB},i}$
12: $\quad$ **if** $\alpha - \beta_i > \epsilon|\alpha|$ **then**
13: $\quad\quad$ Split $T(S_i)$ along one of its longest edge into $T(S_i^1)$ and $T(S_i^2)$.
14: $\quad\quad$ Update $\mathcal{R} \in \{T(S_i^1), T(S_i^2)\}$.
CR $= \alpha$.

4.3.2 Optimization under unitary matrix constraint

Once we obtain the optimal matrix Λ_F, the maximization of the CR with respect to the $\mathbf{V}_F$, can be reformulated as

$$\begin{aligned} \underset{\mathbf{V}_F}{\text{maximize}} \quad & \varrho \\ \text{subject to} \quad & \mathbf{V}_F\mathbf{V}_F^H = \mathbf{V}_F^H\mathbf{V}_F = \mathbf{I}. \end{aligned} \tag{84}$$

This is a nonconvex optimization problem with a nonlinear constraint. To solve this problem, we use the self-tuning Riemannian SD Algorithm 3 given in [157, Table-II]. We need to calculate the complex conjugate derivative of the CR with respect to $\mathbf{V}_F$:

$$\Gamma = \frac{\partial \varrho}{\partial \mathbf{V}_F^*} = \frac{-\sum_{i,j}\left(w_{ij}\Big[\sum_{n}^{M_R}\frac{1}{2}\big(\frac{\partial \log(|\mathbf{C}_i|)}{\partial \mathbf{V}_F^*} + \frac{\partial \log(|\mathbf{C}_j|)}{\partial \mathbf{V}_F^*}\big) - \frac{\partial \log(|\mathbf{B}|)}{\partial \mathbf{V}_F^*}\Big]\right)}{\log(2)\ w_{ij}}, \tag{85a}$$

$$\frac{\partial \log(|\mathbf{B}|)}{\partial \mathbf{V}_F^*} = \frac{1}{2}(\tilde{\lambda}_R^n(\mathbf{X}_i^H \mathbf{B}^{-1}\mathbf{X}_i + \mathbf{X}_j^H \mathbf{B}^{-1}\mathbf{X}_j) + \frac{1}{4}\hat{\lambda}_R^n(\mathbf{X}_i - \mathbf{X}_j)^H \mathbf{B}^{-1}(\mathbf{X}_i - \mathbf{X}_j))\mathbf{V}_F\Lambda, \tag{85b}$$

$$\frac{\partial \log(|\mathbf{C}_i|)}{\partial \mathbf{V}_F^*} = \mathbf{X}_i^H \mathbf{C}_i^{-1}\mathbf{X}_i\mathbf{V}_F\Lambda\tilde{\lambda}_R^n, \tag{85c}$$

$$w_{ij} = \prod_n^{M_R} |\mathbf{B}||\mathbf{C}_i|^{-\frac{1}{2}}|\mathbf{C}_j|^{-\frac{1}{2}}. \tag{85d}$$

The gradient direction in Riemannian space is defined as [157]

$$\mathbf{G} = \Gamma\mathbf{V}_F^H - \mathbf{V}_F\Gamma^H. \tag{86}$$

Algorithm 3 Self-Tuning Riemannian SD Algorithm 3 [157, Table II].

Input: Unitary matrix $\mathbf{V}_F$.

Output: Optimized unitary matrix $\mathbf{V}_F = \mathbf{W}_{k+1}$.

1: Initialization: k= 0, $\mathbf{W}_k = \mathbf{V}_F$ and $\mu = 1$.
2: Compute the gradient of the cost function on the Euclidean space: $\Gamma = \frac{\partial \varrho}{\partial \mathbf{V}_F^*}$.
3: Compute the gradient direction on the Riemannian space: $\mathbf{G}_k = \Gamma\mathbf{V}_F^H - \mathbf{V}_F\Gamma^H$.
4: **if** $\langle \mathbf{G}_k, \mathbf{G}_k\rangle_{\mathrm{I}} = \frac{1}{2}\Re\{\mathrm{tr}\{\mathbf{G}_k\mathbf{G}_k^H\}\} \lll 0$ **then**
5: STOP.
6: Determine the rotation matrices: $\mathbf{P}_k := \exp(-\mu\mathbf{G}_k)$, $\mathbf{Q}_k = \mathbf{P}_k\mathbf{P}_k$.
7: **while** $\varrho(\mathbf{W}_k) - \varrho(\mathbf{Q}_k\mathbf{W}_k) \geq \mu\langle \mathbf{G}_k, \mathbf{G}_k\rangle_{\mathrm{I}}$ **do**
8: $\mathbf{P}_k := \mathbf{Q}_k$, $\mathbf{Q}_k = \mathbf{P}_k\mathbf{P}_k$, $\mu := 2\mu$
9: **while** $\varrho(\mathbf{W}_k) - \varrho(\mathbf{P}_k\mathbf{W}_k)(\mu/2)\langle \mathbf{G}_k, \mathbf{G}_k\rangle_{\mathrm{I}}$ **do**
10: $\mathbf{P}_k := \exp(-\mu\mathbf{G}_k)$, $\mu := \mu/2$
11: Update: $\mathbf{W}_{k+1} = \mathbf{P}_k\mathbf{W}_k$, $k = k + 1$, and go to Step 2.

By combining Algorithm 2 and Algorithm 3, we now present an iterative two-step Algorithm 4 to find the linear precoder matrix $\mathbf{F}$.

Algorithm 4 TWO-STEP ITERATIVE ALGORITHM TO FIND LINEAR PRECODER.

Input: Input constellation set $\mathcal{S} \in \{\mathbf{S}_i : 0 \leq i \leq L-1\}$, matrices $\mathbf{V}_F^{\text{init}}$, $\mathbf{U}_F$ P_d, and M_T.

Output: R_0 value and close-to-optimal linear precoder matrix $\mathbf{F}$.

1: Initialization: Set $k = 1$, $\mathbf{V}_F^{(0)} = \mathbf{V}_F^{\text{init}}$.
2: Stopping criterion: Convergence STOP otherwise go to step 3.
3: Solve (72) using Algorithm 2 for $\Lambda_F^{(k)}$ for a given $\mathbf{V}_F^{(k-1)}$.
4: Solve (84) using Algorithm 3 for $\mathbf{V}_F^{(k)}$ using $\Lambda_F^{(k)}$ from previous step.
5: Set $k := k + 1$.

4.4 Numerical results and discussion

Coded FER and MI are used as performance metrics to compare the performance of the CR-optimized precoders with the conventional methods (no precoding) and the PCCs in various MIMO transmission schemes. In all the presented examples, the precoder matrices are optimized for the true SNR_d value, unless otherwise stated. For the computer simulation, we considered the turbo-coded system with frames of length equal to 512 symbols. The exponentially correlated fading model is considered on both the transmit and the receive sides. The transmit and receive correlation matrix is given by: $(\mathbf{R}_{\{T,R\}})_{i,j} = \rho_{\{T,R\}}^{|i-j|}$ for $i, j \in \{1, \cdots, M_{\{T,R\}}\}$, where $\rho_{\{T,R\}}$ denotes normalized correlation coefficient of the channel and satisfies $0 \leq \rho_{\{T,R\}} < 1$. The values used for ρ_T and ρ_R in the simulations are 0.45 and 0.90, respectively.

At the receiver, the knowledge of the channel estimation covariance matrix $\tilde{\Sigma}$ is also considered to be available to the decoding metric as in [143]. The decoder estimates the LLRs of the coded bit for soft decision decoding from the modulated symbols. Let us denote the transmitted bits of each signal $\mathbf{b} = \{b_1, \ldots, b_N\}$. The LLR for the l^{th} bit in $\mathbf{b}$ is given by (58).

Since our design criterion is a lower bound to the mutual information, we consider the mutual information as one of our performance metrics. The Monte Carlo computer simulations have been used to obtain the mutual information of the conventional constellations with/without precoder and CR PCCs in the SM and STBC transmission schemes. The mutual information with a discrete-input and continuous-output channel with imperfect CSIR is given by (31).

4.4.1 Spatial multiplexing

First, we compare the coded FER performances and the MIs of the CR-optimized precoder with the no precoder case, and CR-PCCs in the SM transmission mode. In the case with/without precoders, the spatial multiplexed codeword $\mathbf{s}$ draws its symbols from the conventional constellations, e.g., M-QAM, independently for each M_T transmit antenna. On the other hand, with the PCCs, the spatial multiplexed codewords are designed simultaneously across the M_T transmit antennae and their bit-mapping performed using the modified binary switching algorithm (MBSA)[117].

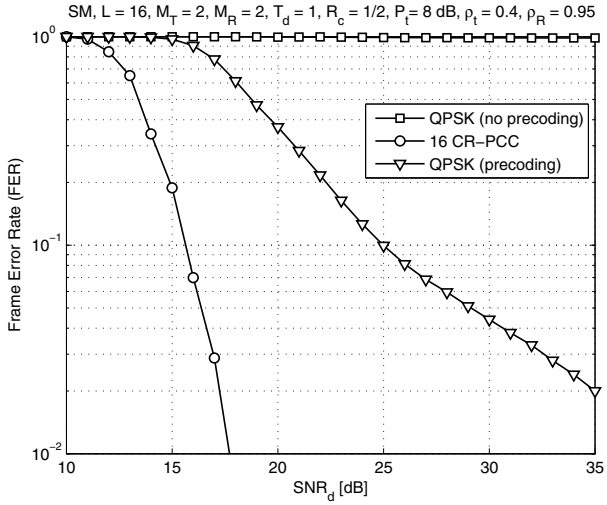

Fig. 28. Coded FER of 2×2 MIMO system versus $\mathrm{SNR_d}$ for fixed $\mathrm{SNR_t} = 8$ dB with $L = 16$, $M_T = 2$, $M_R = 2$, $T_d = 1$, $\rho_T = 0.45$ and $\rho_R = 0.9$.

The coded FER versus $\mathrm{SNR_d}$ performances for the SM transmission with precoding, no precoding and PCCs, for 2×2 MIMO systems, are plotted in Fig. 28. In this example, the codeword vector $\mathbf{s}$ draws its symbols from the QPSK and 16-CR PCC constellation for the precoding/no precoding and PCC cases, respectively. We further set the value of the training power or $\mathrm{SNR_t}$ to be fixed and equal to 8 dB and turbo code rate $(R_c) = 1/2$.

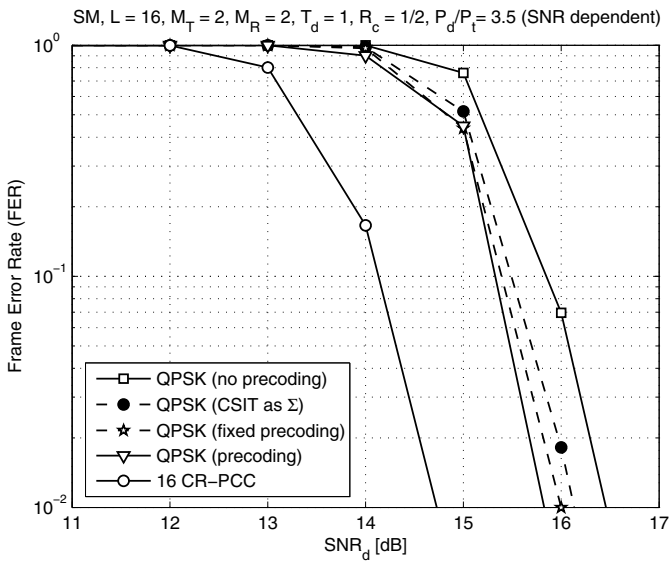

Fig. 29. Coded FER of 2×2 MIMO system versus $\mathrm{SNR_d}$ with varying $\mathrm{SNR_t}$ and $L = 16$, $M_T = 2$, $M_R = 2$, $T_d = 1$, $\rho_T = 0.45$ and $\rho_R = 0.9$.

In the previous example, we used a fixed training power. However, usually the training power increases with the data power and their ratio remains the same. In all subsequent numerical examples, we allow the training power to vary with the data power with data-to-training power ratio (i.e., P_d/P_t) of 3.5. In Fig. 29, we compare the coded FER versus $\mathrm{SNR_d}$ performances of the SM transmission with the CR precoding, conventional precoding, fixed CR precoding, no precoding and CR PCCs. In the conventional precoding, the correlation of the actual channel is used as CSIT. In the fixed CR precoding, a precoder designed for some fixed value of $\mathrm{SNR_d}$ is used for all other $\mathrm{SNR_d}$ values; this is to illustrate the more practical performance. In Fig. 30, we compare the coded FER versus $\mathrm{SNR_d}$ performances of the SM transmission with the precoding, no precoding and PCCs. In these two examples, we kept the simulation parameters similar to those in the previous example, except for the number of transmit antennae, which is $M_T = 2$ in Fig. 29 and $M_T = 4$ in Fig. 30. In the next example, we evaluate and compare the MI versus $\mathrm{SNR_d}$ performance of the precoded, no

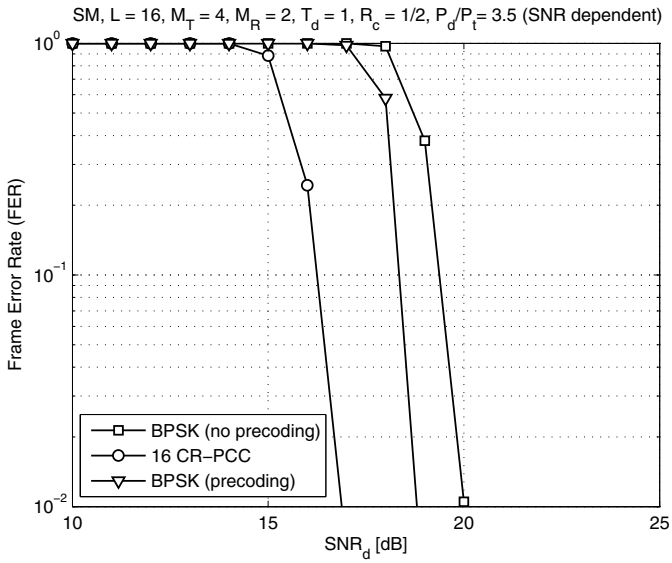

Fig. 30. Coded FER of 4×2 MIMO system versus $\mathbf{SNR_d}$ with varying $\mathbf{SNR_t}$ and $L = 16$, $M_T = 4$, $M_R = 2$, $T_d = 1$, $\rho_T = 0.45$ and $\rho_R = 0.9$.

precoded and CR-PCCs. The results are illustrated in Fig. 31. The simulation parameters in this example are kept the same as those in Fig. 29.

It can be observed form Figs. 28-31 that the spatially multiplexed CR-PCCs have significantly higher FER and MI performance gains compared to those of conventional constellations (e.g., QAM, BPSK, etc.) combined with the CR-optimized precoder and no precoder cases. In the SM mode of transmission, designing the codewords[11] adapted to the imperfect CSIR not only gives a good minimum distance between the codewords, which is essential to combat imperfect CSIR, but also the beamforming gains. On the other hand, the precoder combined with the conventional constellations provides beamforming gains. Thus, utilizing the available CSIT in designing the codebook is beneficial as compared to using it to design precoders. Given the simplicity and backward compatibility of the precoding approach, its performance can be very competitive in realistic applications.

[11]The PPC are constructed simultaneously across the M_T transmit antennae and codewords lie inside an $2M_T$ dimensional real sphere [114].

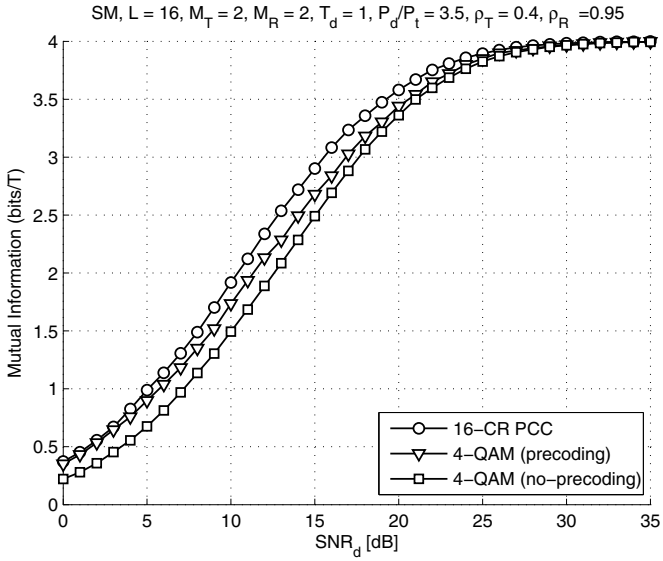

Fig. 31. Mutual information of 2×2 MIMO system versus SNR_d with varying SNR_t and $L = 16$, $M_T = 2$, $M_R = 2$, $T_d = 1$, $\rho_T = 0.45$ and $\rho_R = 0.9$.

.

Conventionally, precoders are designed to adapt to the channel correlation matrix knowledge as partial CSIT. The conventional precoder used in this example is numerically obtained by solving (69) with an assumption that Σ of the actual channel is available as CSIT. With this assumption, designing the conventional precoder using the CR criterion is fairly equivalent to criteria proposed by others, such as maximizing capacity in [62, 158], etc. As expected, it can be observed that the CR-optimized precoder, designed to adapt to the estimated channel error covariance matrix $\tilde{\Sigma}$, gives better performance as compared to the conventional precoders.

4.4.2 Space-time codes

Now we will evaluate and compare the performances of the CR-optimized precoder combined with the ST codes for $M_T = 2$, $M_R = 2$, and $T_d \geq 2$. The training power also varies with the data power as $P_d/P_t = 3.5$. We present two examples, one for $T_d = 2$ and another for $T_d = 4$. In the first example, we use the

Alamouti codes as the OSTBC, and in the second example, a USTC obtained by Giese and Skoglund [94].

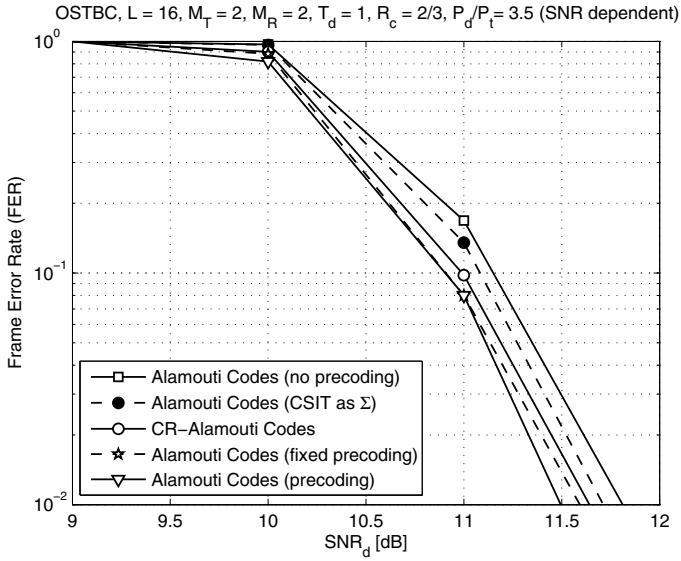

Fig. 32. Coded FER of 2×2 MIMO system versus $\mathrm{SNR_d}$ for the Alamouti codes with varying $\mathrm{SNR_t}$ and $L = 16$, $M_T = 2$, $M_R = 2$, $T_d = 2$, $\rho_T = 0.45$ and $\rho_R = 0.9$, [123] (©2013 VDE VERLAG GMBH).

Fig. 32 compares the coded FER versus $\mathrm{SNR_d}$ performances of the Alamouti code in conjunction with the CR-optimized precoder, fixed CR-optimized precoder (designed for fixed $\mathrm{SNR_d} = 11$ dB), conventional (no precoder), conventional precoder[12], and the CR-optimized Alamouti code [117]. For a fair comparison, the Alamouti code chooses its elements from the conventional 4-QAM constellation, and, on the other hand, the CR-optimized Alamouti code chooses its elements from the CR-optimized 16-CR partially coherent constellations (PCCs) such that the data rate is the same in all five cases shown. The turbo code rate $R_c = \frac{2}{3}$ and training power varies as $P_d/P_t = 3.5$. In Fig. 33, we present the MI versus $\mathrm{SNR_d}$ plots of the CR-optimized Alamouti code [117] and the conventional Alamouti codes combined with the CR-optimized precoder and

[12]Conventional precoders are designed with an assumption that covariance Σ of the actual channel is available as CSIT [149].

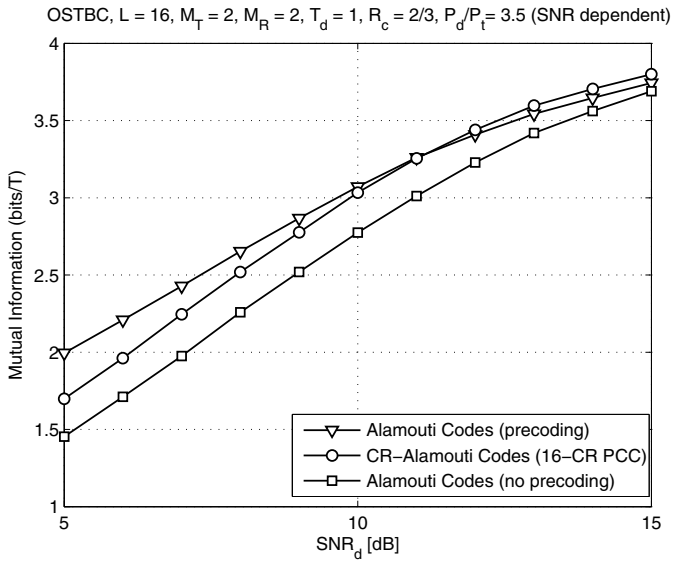

Fig. 33. Mutual information of 2×2 MIMO system versus $\mathrm{SNR_d}$ for the Alamouti codes with varying $\mathrm{SNR_t}$ and $L = 16$, $M_T = 2$, $M_R = 2$, $T_d = 2$, $\rho_T = 0.45$ and $\rho_R = 0.9$.

no precoder. Simulation parameters used in this example are kept the same as those in Fig. 32. In the STBC transmission mode, the MI of the CR-optimized precoders is higher than that of the CR-optimized constellations and conventional constellations with no precoders.

Next, we evaluate the performance of the linear precoder, combined with the unitary ST codes, obtained by solving (69). Another unitary matrix designed for the partially coherent channels proposed in [93] could also be used in this example. The unitary matrices [94] are obtained by combining non-coherent [75] and coherent codes. The idea of adaptively determining the number of coherent and non-coherent component codes goes according to the weighting factor (estimation covariance or $\mathrm{SNR_t}$) between their intra-subspace and inter-subspace distances [94]. For the non-coherent case ($\mathrm{SNR_t} = 0$), the inter-subspace distance between two signals $\Phi_i$and Φ_j depends on the principal angles between the subspaces spanned by Φ_i and Φ_j. For the coherent case (high $\mathrm{SNR_t}$), two signals in the same subspace have vanishing inter-subspace and non-vanishing

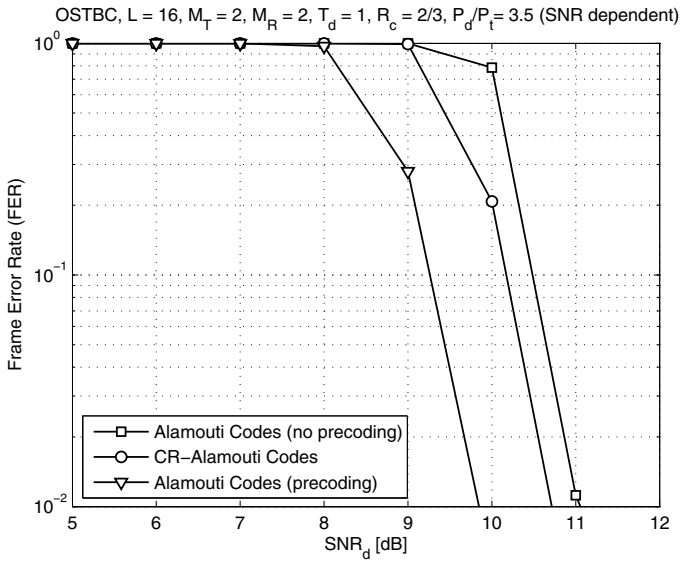

Fig. 34. Coded FER of 2×2 MIMO system versus $\mathbf{SNR_d}$ for the Alamouti codes with varying $\mathbf{SNR_t}$ and $L = 16$, $M_T = 2$, $M_R = 2$, $T_d = 2$, and i.i.d. channel.

intra-subspace distances since they depend on the singular values of the difference matrix $\Phi_i - \Phi_j$. In other words, a higher estimation variance will involve more non-coherent components to achieve a large inter-subspace distance and less coherent component codes, and vice versa.

In the example above, we could have compared the performances of a purely non-coherent code (16 unitary code) to those of a signal set based on combining eight non-coherent codes with two coherent codes, and a constellation combining four non-coherent codes with four coherent codes. However, for the clarity of the plots in Fig. 35, we only evaluate the performance of the USTC obtained combining four non-coherent codes with four coherent codes. The coded FER and BER versus $\mathrm{SNR_t}$ performances of the USTC combined with precoding, no precoding and CR-optimized USTC, designed at $\mathrm{SNR_d}$ per block of 3 dB, are compared in Fig. 35 with $R_c = \frac{2}{3}$. In the next example, we evaluate and compare the MI of the CR-optimized precoder to the CR-optimized unitary constellations and conventional unitary constellations in the STBC transmission

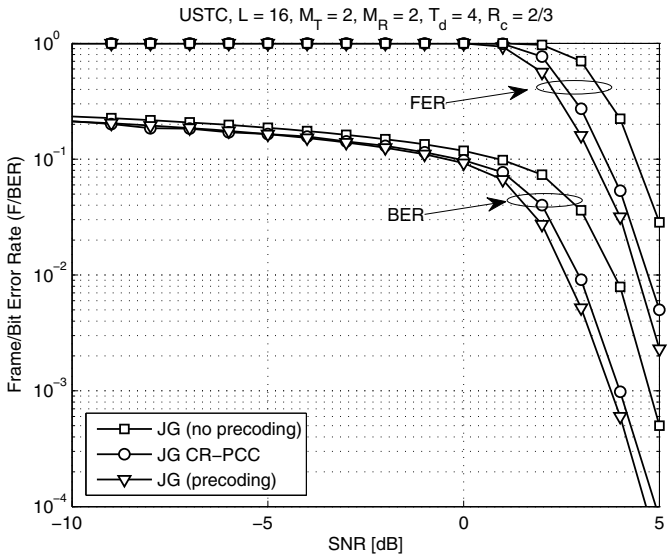

Fig. 35. Coded FER of 2×2 MIMO system versus $\mathrm{SNR_t}$ for the USTC with varying $\mathrm{SNR_t}$ and $L = 16$, $M_T = 2$, $M_R = 2$, $T_d = 4$, $\rho_T = 0.3$ and $\rho_R = 0.45$, [123] (©2013 VDE VERLAG GMBH).

mode in Fig. 36. The simulation parameters in this example are kept the same as those in Fig. 35.

In the case of STBCs, which provide diversity gains, we can observe from Figs. 32, 33, 35, and 36 that the CR-optimized precoders show significant FER and MI gains as compared to the CR-optimized and the conventional Alamouti codes and USTCs. The reason for this is that the CR-optimized Alamouti codes and USTCs, designed to combat imperfect CSIR, are sub-optimal. Moreover, they transmit energy in an isotropic manner similar to their conventional counterparts. Whereas the conventional Alamouti codes and USTCs combined with CR-optimized precoder generate beamforming gains along with the diversity gains. Thus, utilizing CSIT in designing the precoders is beneficial, especially in the low-to-medium $\mathrm{SNR_d}$ ratio regime, as compared to using it to design the codewords as done in [117]. However, in the high $\mathrm{SNR_d}$ regime, the MI of the CR-optimized Alamouti codes shows better gains. At high $\mathrm{SNR_d}$, the impact of

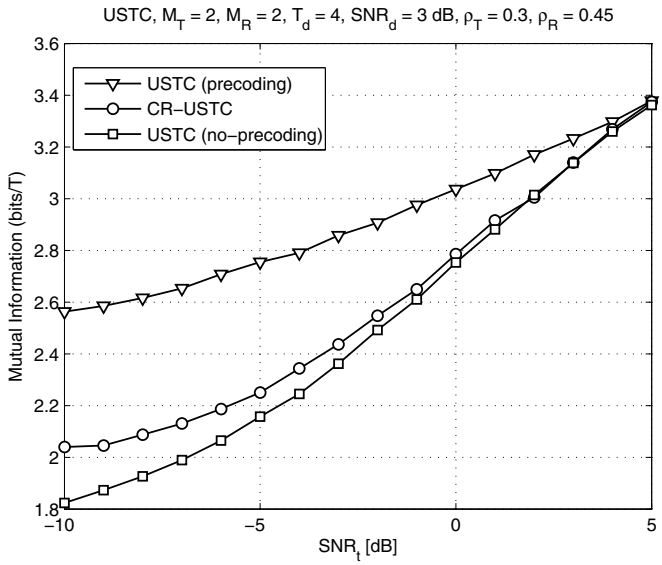

Fig. 36. Mutual information of 2×2 MIMO system versus $\mathbf{SNR_t}$ for the USTC designed for a $\mathbf{SNR_d}$ value of 3 dB and $M_T = 2$, $M_R = 2$, $T_d = 4$, $\rho_T = 0.30$ and $\rho_R = 0.45$.

transmit correlation is negligible on the performance [159]. Therefore, the power allocation approaches uniform directions resulting in no beamforming gain.

Furthermore, the performance for the CR-optimized precoders with the conventional precoders is also plotted in Fig. 32. The conventional precoders used in this example are numerically obtained by solving (69) with the assumption that covariance Σ of the actual channel is available as CSIT. As mentioned before, with the above CSIT assumption, designing the precoders with the CR criterion is fairly equivalent to other criteria such as minimizing SER in [149], PEP in [160], etc. As expected, the performance of the CR-optimized precoder is higher as compared to the conventional precoders.

Finally, we compare the performances of the Alamouti codes combined with CR-optimized prcoders with the CR PCC and no precoding in Fig. 34. We assumed that the transmitter and the receiver antennae are uncorrelated and channel estimation error variance is available as CSIT. All other simulation parameters in this example are the same as those in Fig. 32. It can be observed

that the CR-optimized precoders show higher performance gains compared to the CR PCCs and no precoding cases. Generally, for the uncorrelated antenna case, the CR optimized precoders should transmit in an isotropic manner (i.e., equal power allocation to the transmit antennae). However, in a low $\mathrm{SNR_d}$ regime, where channel estimation error is high, the CR-optimized precoder allocates full power to one of the transmit antenna in order to reduce the cross terms (due to channel estimation errors) appearing while decoding. In the Alamouti case, the higher the channel estimation error is, the worse would be the performance. However, in a high $\mathrm{SNR_d}$ regime, the performances of the CR-optimized precoder and CR PCC are the same (not shown here).

4.5 Conclusion

We have studied the single-user MIMO precoder design problem for the doubly spatially correlated, partially coherent Rayleigh-fading channels with discrete inputs. We assumed that the channel is estimated at the receiver using the LMMSE estimator while the transmitter has the perfect knowledge of the estimated channel covariance matrix. The precoder matrix is designed to adapt to the degradation caused by the imperfect channel estimation at the receiver and the presence of the spatial correlation. The cutoff rate, a lower bound on the MI, has been proposed to be used as the design criterion. A closed and tractable form of the cutoff rate expression has been derived. The suitability of the cutoff rate expression for the discrete inputs makes it possible to design close-to-optimal precoders which can be used with the conventional constellations such as M-QAM or M-PSK. A prismatic BnB and self-tuning Riemannian SD algorithms are proposed to be used in an iterative manner to numerically search a close-to-optimal linear precoder with a given average power constraint at the transmitter. The proposed CR-optimized precoders are used with the SM and ST block transmission modes. Numerical examples are presented to compare the performances of the CR-optimized precoders with the conventional no precoder case and CR-optimized PCCs in terms of the FER and MI. In the SM transmission mode, it is demonstrated through numerical examples that the use of available CSIT in designing the PCCs is useful over the precoder design. However, in the ST block transmission case, CSIT can be useful in designing the precoders over the PCCs.

5 Conclusion and future directions

The problem of single-user MIMO ST codes and linear precoder matrix design for a partially coherent channel was considered. We assumed a Rayleigh flat-fading channel and its coefficients had been estimated at the receiver using the LMMSE estimator while the transmitter had a perfect knowledge of the estimated channel covariance matrix. The aim was to design the ST codes and linear precoder matrices, to adapt to the degradation caused by the imperfect channel estimation at the receiver and the presence of the spatial correlation, in order to extract the diversity and multiplexing gain offered by the MIMO systems with partial (imperfect) CSIR. The first chapter included motivation and a literature review related to the topic under consideration.

The ST code design for a partially coherent i.i.d. channel was considered in Chapter 2. A design criterion for ST codes in this scenario based on the CR maximization was derived. Close-to-optimal PCCs were obtained for both single and multiple transmit antennae. The continuous optimization problem was solved numerically using the SQP algorithm. Through single transmit antenna PCCs, we demonstrated the dependency of shape and structure of the resulting constellations on the channel estimation errors. The MI and SER performance of the PCCs were compared to KLD-optimized PCCs and conventional constellations. Numerical results demonstrated that the CR-PCCs have higher mutual information in a low or medium SNR regime compared to that of the KLD-based PCCs, USTCs and conventional QAM constellations. The SER performance of the CR-PCCs is similar to that of the KLD-based PCCs and have better performance compared to USTCs. The resulting single transmit antenna constellations are also shown to have lower PAPR values compared to those of KLD based PCCs. In addition, the signal set construction method was presented which provides control over the constellation's PAPR values and takes care that no signal points have a zero amplitude.

In Chapter 3, the ST code design for a doubly correlated partially coherent channel and its performance evaluation with FEC codes were considered. We considered two criteria: first one was the UB-ABEP for a single transmit antenna and the second one was the CR for multiple transmit antennae. Both UB-ABEP

and CR expressions were derived to take the spatial correlation into account along with the channel estimation error covariance matrix. Efficient bit mapping schemes were presented for the resulting PCCs in order to use them with FEC codes. The single transmit antenna PCC optimized using the UB-ABEP was able to maintain the Gray mapping. For multiple transmit antennae, a two-step methodology was proposed. In the first step, the CR was maximized to obtain the codebook, and, in the second step, a MBSA was used to find the corresponding efficient bit mapping. The numerical results demonstrated the effectiveness of the optimized constellations and bit mappings. The resulting constellations were shown to have significantly better FER gains and improved power efficiencies compared to those of the conventional constellations with turbo codes.

The problem of linear precoder matrix design for a single-user MIMO for a doubly correlated partially coherent channel was studied in Chapter 4. The precoder matrix was designed to adapt to the degradation caused by the imperfect channel estimation at the receiver and the presence of the spatial correlation. The CR expression was again used as a linear precoder matrix. Furthermore, the CR expression was modified to include the precoder matrix into the expression. The precoder matrix was decomposed using the SVD into the input shaping matrix, power loading matrix, and beamforming matrix. The beamforming matrix was found to coincide with the eigenvectors of the transmit correlation matrix. The power loading and input shaping matrices were solved numerically using the difference of convex (d.c.) programming algorithm and optimization under the unitary constraint, respectively. A two-step iterative algorithm (the first step concerned using a prismatic BnB algorithm and the second step a self-tuning Riemannian SD algorithm) was proposed to numerically search a close-to-optimal linear precoder with a given average power constraint at the transmitter. Precoders were used in conjunction with two MIMO transmission schemes: the spatial multiplexing (SM) and space-time (ST) block transmission modes. Numerical examples were presented to compare the performances of the CR optimized precoders with a conventional no precoder case and the CR-optimized PCCs in terms of the FER and MI. In the SM transmission mode, it was demonstrated through numerical examples that the use of available CSIT in designing the PCCs was useful over the precoder design. However, in the ST

block transmission case, CSIT was found to be useful in designing the precoders over the PCCs.

The designs and methodologies presented in this thesis unfold several interesting research avenues. Below, we list some possible topics for further studies:

- Code design for multiple-access channels and broadcast channels seems largely unexplored with respect to the imperfect CSIR case. Impact of imperfect channel estimates on the performance of the multi-user systems is as inevitable as in the single-user case. An extension from a single-user partially coherent constellation design to a multi-user scenario is a promising direction for future work.
- Cooperative communication through distributed single antenna nodes has been extensively studied for improved signal quality and better coverage [161–163]. Therein the source node broadcasts information to the relay and the destination. The destination node detects the received data assuming that perfect CSI of source-to-relay, source-to-destination, and relay-to-destination links is available. Again, this assumption is not always true in practice. Design of distributed PCCs when the destination node has partial CSI of all the links is another possible direction for future research.
- Spectrum and energy efficiencies are among the most important venues for technological advancement in current and emerging wireless communication networks. Coded modulation [164–166] is one way to reduce both the spectrum and the energy usage. Extending the CR expression as a criterion to design the coded modulations schemes for partially coherent channels is also a promising future direction.
- Due to the nonlinear structure of PCCs, it is expected that this feature inhibits the use of efficient suboptimal techniques like sphere detectors in the detection process. Thus, design of low-complexity receiver algorithms is an important future research topic.

References

1. Dahlman E, Parkvall S & Sköld J (2011) 4G LTE / LTE-Advanced for Mobile Broadband. Academic Press.
2. Raaf B, Zirwas W, Friederichs KJ, Tiirola E, Laitila M, Marsch P & Wichman R (2011) Vision for beyond 4G broadband radio systems. In: Proceedings of the IEEE International Symposium on Personal, Indoor, and Mobile Radio Communications, pp. 2369–2373.
3. Rappaport T, Sun S, Mayzus R, Zhao H, Azar Y, Wang K, Wong G, Schulz J, Samimi M & Gutierrez F (2013) Millimeter wave mobile communications for 5G cellular: It will work! IEEE Access 1: 335–349.
4. Foschini GJ & Gans MJ (1998) On limits of wireless communications in a fading environment when using multiple antennas. Wireless Personal Communications, Kluwer Academic Publishers 6: 311–335.
5. Paulraj A, Nabar RD & Gore D (2003) Introduction to space-time wireless communications. Cambridge University Press, Cambridge, U.K.
6. Ivrlac M, Utschick W & Nossek J (2003) Fading correlations in wireless MIMO communication systems. IEEE Journal on Selected Areas in Communications 21(5): 819–828.
7. Kang M & Alouini MS (2003) Impact of correlation on the capacity of MIMO channels. In: Proceedings of the IEEE International Conference on Communications, volume 4, pp. 2623–2627. Anchorage, Alaska, USA.
8. Chiani M, Win M & Zanella A (2003) On the capacity of spatially correlated MIMO Rayleigh-fading channels. IEEE Transactions on Information Theory 49(10): 2363–2371.
9. Shiu D, Foshini GJ, Gans MJ & Kahn JM (2000) Fading correlation and its effect on the capacity of multi-element antenna systems. IEEE Transactions on Communications 48(3): 25–29.
10. Zanella A, Chiani M & Win M (2005) Performance of MIMO MRC in correlated Rayleigh fading environments. In: Proceedings of the IEEE Vehicular Technology Conference, volume 3, pp. 1633–1637. Stockholm, Sweden.
11. Cho J, Ahn KS, Baik HK, Kim YI & Ahn JH (2006) Symbol error probability for space-time block codes over spatially correlated Rayleigh fading channels. In: Proceedings of the IEEE Vehicular Technology Conference, volume 2, pp. 1–5. Montréal, Canada.
12. Maaref A & Aïssa S (2006) Performance analysis of orthogonal space-time block codes in spatially correlated MIMO Nakagami fading channels. IEEE Transactions on Wireless Communications 5(4): 807–817.
13. McKay M, Grant A & Collings I (2007) Performance analysis of MIMO-MRC in double-correlated Rayleigh environments. IEEE Transactions on Communications 55(3): 497–507.
14. Firag A, Smith P, Suraweera H & Nallanathan A (2011) Performance of beamforming in correlated MISO systems with estimation error and feedback delay. IEEE Transactions on Wireless Communications 10(8): 2592–2602.

15. Dall'Anese E, Assalini A & Pupolin S (2009) On the effect of imperfect channel estimation upon the capacity of correlated MIMO fading channels. In: Proceedings of the IEEE Vehicular Technology Conference, pp. 1–5. Barcelona, Spain.
16. Musavian L, Nakhai M, Dohler M & Aghvami A (2007) Effect of channel uncertainty on the mutual information of MIMO fading channels. IEEE Transactions on Vehicular Technology 56(5): 2798–2806.
17. Yoo T, Yoon E & Goldsmith A (2004) MIMO capacity with channel uncertainty: Does feedback help? In: Proceedings of the IEEE Global Telecommunication Conference, volume 1, pp. 96–100. Dallas, TX, USA.
18. Stüber G (2007) Principles of Mobile Communications. Kulwer Academic Publisher Group, Norwell, MA.
19. Sklar B (2001) Digital communications: fundamentals and applications. Prentice-Hall, Englewood Cliffs, NJ, USA.
20. Rappaport TS (1996) Wireless Communications, Principles and Practice. Prentice-Hall, New Jersey.
21. Braun W & Dersch U (1991) Physical mobile radio channel model. IEEE Transactions on Vehicular Technology 40(3): 472 – 482.
22. Winters JH, Salz J & Gitlin RD (1994) The impact of antenna diversity on the capacity of wireless communication systems. IEEE Transactions on Communications 42(2/3/4).
23. Telatar E (1999) Capacity of multi-antenna Gaussian channels. European Transactions on Telecommunications 10(6): 585–595.
24. Tarokh V, Seshadri N & Calderbank AR (1998) Space-time codes for high data rate wireless communication: Performance criterion and code construction. IEEE Transactions on Information Theory 44(2): 744–765.
25. Tarokh V, Jafarkhani H & Calderbank AR (1999) Space-time block coding for wireless communications: Performance results. IEEE Journal on Selected Areas in Communications 17(3): 451–460.
26. Zheng L & Tse DNC (2003) Diversity and multiplexing: A fundamental tradeoff in multiple-antenna channels. IEEE Transactions on Information Theory 49(5): 1073–1096.
27. Barabarossa S (2005) Multiantenna Wireless Communication Systems. Artech House, Boston, USA.
28. Cover TM & Thomas JA (2006) Elements of Information Theory. John Wiley, New York, USA, second edition.
29. Cover TM & Thomas JA (1991) Elements of Information Theory. John Wiley, New York, USA.
30. Palomar D & Fonollosa J (2005) Practical algorithms for a family of waterfilling solutions. IEEE Transactions on Signal Processing 53(2): 686–395.
31. Goldsmith A, Jafar S, Jindal N & Vishwanath S (2003) Capacity limits of MIMO channels. IEEE Journal on Selected Areas in Communications 21(5): 684–702.
32. Hassibi B & Hochwald BM (2002) High-rate codes that are linear in space and time. IEEE Transactions on Information Theory 48(7): 1804–1824.
33. Foschini G (1996) Layered space–time architecture for wireless communication in a fading environment when using multi-element antennas. Bell Labs Technical Journal 1(2): 41–59.

34. Marzetta T & Hochwald B (1999) Capacity of a mobile multiple-antenna communication link in Rayleigh flat fading. IEEE Transactions on Information Theory 45(1): 139–157.
35. Telatar IE (1995) Capacity of multi-antenna Gaussian channels. Technical report, Bell Laboratories. Internal Tech.Memo, pp. 1–28.
36. Raleigh GG & Cioffi JM (1998) Spatio-temporal coding for wireless communication. IEEE Transactions on Communications 46(3): 357–366.
37. Raleigh GG & Jones VK (1999) Multivariate modulation and coding for wireless communication. IEEE Journal on Selected Areas in Communications 17(5): 851–866.
38. Chizhik D, Foschini G, Gans M & Valenzuela R (2002) Keyholes, correlations, and capacities of multielement transmit and receive antennas. IEEE Transactions on Wireless Communications 1(2): 361–368.
39. Chuah CN, Tse D, Kahn JM & Valenzuela-02 RA (2002) Capacity scaling in MIMO wireless systems under correlated fading. IEEE Transactions on Information Theory 48(3): 637–650.
40. Tulino AM, Lozano A & Verdú S (2005) Impact of antenna correlation on the capacity of multiantenna channels. IEEE Transactions on Information Theory 51(7): 2491–2509.
41. Biglieri E, Claderbank R, Constatinides A, Goldsmith A, Paulraj A & Poor VH (2007) MIMO Wireless Communications. Cambridge University Press, Cambridge.
42. Paulraj AJ, Gore DA, Nabar RU & Bolcskei H (2004) An overview of MIMO communications — A key to gigabit wireless. Proceedings of the IEEE 92(2): 198–218.
43. Stuber GL, Barry JR, Li YG, Ingram MA & Pratt TG (2004) Broadband MIMO-OFDM wireless communication. Proceedings of the IEEE 92(2): 271–294.
44. Gesbert D, Shafi M, Shiu D, Smith PJ & Naguib A (2003) From theory to practice: An overview of MIMO space-time coded wireless systems. IEEE Journal on Selected Areas in Communications 21(3): 281–302.
45. Seshadri N & Winters JH (1993) Two signaling schemes for improving the error performance of frequency-division-duplex (FDD) transmission systems using transmitter antenna diversity. In: Proceedings of the IEEE Vehicular Technology Conference, pp. 508–511. Secaucus, USA.
46. Guey JC, Fitz MP, Bell MR & Kuo WY (1999) Signal design for transmitter diversity wireless communication systems over Rayleigh fading channels. IEEE Transactions on Communications 47(4): 527–537.
47. Tarokh V, Naguib A, Seshadri N & Calderbank AR (1999) Space-time codes for high data rate wireless communication: Performance criteria in the presence of channel estimation errors, mobility and multiple paths. IEEE Transactions on Communications 47(2): 199–207.
48. Tarokh V, Naguib A, Seshadri N & Calderbank AR (1999) Combined array processing and space-time coding. IEEE Transactions on Information Theory 45(4)(4): 1121–1128.
49. Alamouti S (1998) A simple transmit diversity technique for wireless communications. IEEE Journal on Selected Areas in Communications 16(8): 1451–1458.

50. Ganesan G & Stoica P (2001) Space-time block codes: A maximum SNR approach. IEEE Transactions on Information Theory 47(4): 1650–1656.
51. Ganesan G (2002) Designing space-time codes using orthogonal designs. Ph.D. thesis, Uppsala University, Sweden.
52. Tarokh V, Jafarkhani H & Calderbank A (1999) Space-time block codes from orthogonal designs. IEEE Transactions on Information Theory 45(5): 1456–1467.
53. Jafarkhani H (2001) A quasi-orthogonal space-time block code. IEEE Transactions on Communications 49(1): 1–3.
54. Tirkkonen O, Boariu A & Hottinen A (2000) Minimal non-orthogonality rate 1 space-time block code for 3+ Tx antennas. In: Proceedings of the IEEE International Symposium on Spread Spectrum Techniques and Applications, pp. 429–432. Parsippany, NJ, USA.
55. Papadias C & Foschini G (2003) Capacity-approaching space-time codes for systems employing four transmitter antennas. IEEE Transactions on Information Theory 49(3): 726–732.
56. Su W & Xia X (2004) Signal constellations for quasi-orthogonal space-time block codes with full diversity. IEEE Transactions on Information Theory 50(10): 2331–2347.
57. Stoica P & Ganesan G (2002) Maximum-SNR spatial-temporal formatting designs for MIMO channels. IEEE Transactions on Signal Processing 50(12): 3036–3042.
58. Lozano A & Papadias C (2002) Layered space-time receivers for frequency-selective wireless channels. IEEE Transactions on Communications 50(1): 65–73.
59. Cover TM (1998) Comments on broadcast channels. IEEE Transactions on Information Theory 44(6): 2524–2530.
60. Scaglione A, Stoica P, Barbarossa S, Giannakis G & Sampath H (2002) Optimal designs for space-time linear precoders and decoders. IEEE Transactions on Signal Processing 50(5): 1051–1064.
61. Xiao C, Zheng Y & Ding Z (2011) Globally optimal linear precoders for finite alphabet signals over complex vector Gaussian channels. IEEE Transactions on Signal Processing 59(7): 3301–3314.
62. Zeng W, Xiao C, Wang M & Lu J (2012) Linear precoding for finite-alphabet inputs over MIMO fading channels with statistical CSI. IEEE Transactions on Signal Processing 60(6): 3134–3148.
63. Rong Y, Vorobyov S & Gershman A (2005) Linear block precoding for OFDM systems based on maximization of mean cutoff rate. IEEE Transactions on Signal Processing 53(12): 4691–4696.
64. Rey F, Lamarca M & Vazquez G (2010) Linear precoder design through cut-off rate maximization in MIMO-OFDM coded systems with imperfect CSIT. IEEE Transactions on Signal Processing 58(3): 1741–1755.
65. Sampath H, Stoica P & Paulraj A (2001) Generalized linear precoder and decoder design for MIMO channels using the weighted MMSE criterion. IEEE Transactions on Communications 49(12): 2198–2206.
66. Yan Z, Wong K & Luo ZQ (2005) Optimal diagonal precoder for multiantenna communication systems. IEEE Transactions on Signal Processing 53(6): 2089–2100.

67. Collin L, Berder O, Rostaing P & Burel G (2004) Optimal minimum distance-based precoder for MIMO spatial multiplexing systems. IEEE Transactions on Signal Processing 52(3): 617–627.
68. Ngo Q, Berder O & Scalart P (2012) Minimum Euclidean distance based precoders for MIMO systems using rectangular QAM modulations. IEEE Transactions on Signal Processing 60(3): 1527 – 1533.
69. Lozano A, Tulino AM & Verdú S (2006) Optimum power allocation for parallel Gaussian channels with arbitrary input distributions. IEEE Transactions on Information Theory 52(7): 3033–3051.
70. Xiao C & Zheng Y (2008) On the mutual information and power allocation for vector Gaussian channels with finite discrete inputs. In: Proceedings of the IEEE Global Telecommunication Conference, pp. 1–5. New Orleans, Louisiana, USA.
71. Pérez-Cruz F, Rodrigues M & Verdú S (2010) MIMO Gaussian channels with arbitrary inputs: Optimal precoding and power allocation. IEEE Transactions on Information Theory 56(3): 1070–1084.
72. Payaró M & Palomar D (2009) On optimal precoding in linear vector Gaussian channels with arbitrary input distribution. In: Proceedings of the IEEE International Symposium on Information Theory, pp. 1085–1089. Seoul, Korea.
73. Lamarca M (2009) Linear precoding for mutual information maximization in MIMO systems. In: Proceedings of the VDE International Symposium on Wireless Communication Systems, pp. 26–30. Tuscany, Italy.
74. Hochwald BM & Marzetta TL (2000) Unitary space-time modulation for multiple-antenna communications in Rayleigh flat fading. IEEE Transactions on Information Theory 46(2): 543–563.
75. Hochwald B, Marzetta T, Richardson T, Sweldens W & Urbanke R (2000) Systematic design of unitary space-time constellations. IEEE Transactions on Information Theory 46(6): 1962–1973.
76. Wu X & Srikant R (2007) MIMO channels in the low-SNR regime: Communication rate, error exponent, and signal peakiness. IEEE Transactions on Information Theory 53(4): 1290–1309.
77. Rao C & Hassibi B (2004) Analysis of multiple-antenna wireless links at low SNR. IEEE Transactions on Information Theory 50(9).
78. Srinivasan S & Varanasi M (2009) Optimal constellations for the low-SNR noncoherent MIMO block Rayleigh-fading channel. IEEE Transactions on Information Theory 55(2): 776–796.
79. Hochwald B & Sweldens W (2000) Differential unitary space-time modulations. IEEE Transactions on Communications 48(12): 2041–2052.
80. Tarokh V & Jafarkhani H (2000) A differential detection scheme for transit diversity. IEEE Journal on Selected Areas in Communications 18(7): 1043–1047.
81. Hughes BL (2000) Differential space-time modulations. IEEE Transactions on Information Theory 46(7): 2567–2578.
82. Ganesan G & Stoica P (2002) Differential modulation using space-time block codes. IEEE Signal Processing Letters 9(2): 57–60.
83. Hassibi B & Hochwald BM (2002) Cayley differential unitary space-time codes. IEEE Transactions on Information Theory 48(6): 1485–1503.

84. Hero I AO & Marzetta T (2001) Cutoff rate and signal design for the quasi-static Rayleigh-fading space-time channel. IEEE Transactions on Information Theory 47(6): 2400–2416.
85. McCloud M, Brehler M & Varanasi M (2002) Signal design and convolutional coding for noncoherent space-time communication on the block-Rayleigh-fading channel. IEEE Transactions on Information Theory 48(5): 1186–1194.
86. Borran MJ, Sabharwal A & Aazhang B (2003) On design criteria and construction of noncoherent space-time constellations. IEEE Transactions on Information Theory 49(10): 2332–2351.
87. Srinivasan S & Varanasi M (2007) Constellation design for the noncoherent MIMO Rayleigh fading channel at general SNR. IEEE Transactions on Information Theory 53(4): 1572–1584.
88. Wu Y, Ruotsalainen K & Juntti M (2008) Unitary space-time constellation design based on the Chernoff bound of the pairwise error probability. IEEE Transactions on Information Theory 54(8): 3842–3850.
89. Medard M (2000) The effect upon channel capacity in wireless communications of perfect and imperfect knowledge of the channel. IEEE Transactions on Information Theory 46(3): 933–946.
90. Lapidoth A & Shamai S (2002) Fading channels: how perfect need "perfect side information" be? IEEE Transactions on Information Theory 48(5): 1118–1134.
91. Ray S, Medard M, Zheng L & Abounadi J (2004) On the sublinear behavior of MIMO channel capacity at low SNR. In: Proceedings of the IEEE International Symposium on Information Theory and its Applications, pp. 1031–1034. Parma, Italy.
92. Yoo T & Goldsmith A (2006) Capacity and power allocation for fading MIMO channels with channel estimation error. IEEE Transactions on Information Theory 52(5): 2203 – 2214.
93. Baccarelli E & Biagi M (2004) Performance and optimized design of space-time codes for MIMO wireless systems with imperfect channel estimates. IEEE Transactions on Signal Processing 52(10): 2911–2923.
94. Giese J & Skoglund M (2007) Space-time constellation design for partial CSI at the receiver. IEEE Transactions on Information Theory 53(8): 2715–2731.
95. Wu Y & Pätzold M (2007) Asymptotic symbol error probability analysis for orthogonal space-time block codes with channel estimation error. In: Proceedings of the International Symposium on Wireless Personal Multimedia Communications, pp. 68–72. Jaipur, India.
96. Borran MJ, Sabharwal A & Aazhang B (2009) Design criterion and construction methods for partially coherent multiple antenna constellations. IEEE Transactions on Wireless Communications 8(8): 4122–4133.
97. Tarokh V, Jafarkhani H & Calderbank AR (1999) Space-time block codes from orthogonal designs. IEEE Transactions on Information Theory 45(5): 1456–1467.
98. Palomar DP (2003) A unified framework for communications through MIMO channels. Ph.D. thesis, Department of Signal Theory and Communications, Technical University of Catalonia, Barcelona, Spain.
99. Zhang X, Palomar DP & Ottersten B (2008) Statistically robust design of linear MIMO transceivers. IEEE Transactions on Signal Processing 56(8): 3678–3689.

100. Serbetli S & Yener A (2006) MMSE transmitter design for correlated MIMO systems with imperfect channel estimates: power allocation trade-offs. IEEE Transactions on Wireless Communications 5(8): 2295–2304.
101. Ding M & Blostein S (2009) MIMO minimum total MSE transceiver design with imperfect CSI at both ends. IEEE Transactions on Signal Processing 57(3).
102. Ding M & Blostein S (2010) Maximum mutual information design for MIMO systems with imperfect channel knowledge. IEEE Transactions on Information Theory 56(10): 4793–4801.
103. Gallager R (1965) A simple derivation of the coding theorem and some applications. IEEE Transactions on Information Theory 11(1): 3–18.
104. Wozencraft J & Kennedy R (1966) Modulation and demodulation for probabilistic coding. IEEE Transactions on Information Theory 12(3): 291–297.
105. Massey JL (1974) Coding and modulation in digital communications. In: Proceedings of the International Zurich Seminar on Digital Communications, volume 1, pp. E2.1 – E2.4. Zurich, Switzerland.
106. Berrou C, Glavieux A & Thitimajshima P (1993) Near Shannon limit error correcting coding and decoding: Turbo codes. In: Proceedings of the IEEE International Conference on Communications, volume 2, pp. 1064–1070. Geneva, Switzerland.
107. Biglieri E, Proakis J & Shamai S (1998) Fading channels: Information-theoretic and communications aspects. IEEE Transactions on Information Theory 44(6): 2619–2692.
108. Davidson J & Kalet I (1997) Bhattacharyya bound, cutoff rate, and constellation design for the companding channel. IEEE Transactions on Communications 45(7): 779–787.
109. Misra S, Swami A & Tong L (2006) Cutoff rate optimal binary inputs with imperfect CSI. IEEE Transactions on Wireless Communications 5(10): 2903–2913.
110. Mehta NB, Digham F, Molisch A & Zhang J (2004) Rate of MIMO systems with CSI at transmitter and receiver from pilot-aided estimation. In: Proceedings of the IEEE Vehicular Technology Conference, volume 3, pp. 1575–1579. Los Angeles, CA, USA.
111. Kailath T (1967) The Divergence and Bhattacharyya distance measures in signal selection. IEEE Transactions on Communication Technology 15(1): 52–60.
112. Dogandzic A (2003) Chernoff bounds on pairwise error probabilities of space-time codes. IEEE Transactions on Information Theory 49(5): 1327–1336.
113. Yadav A, Juntti M & Lilleberg J (2010) Rate-adaptive space-time constellation design for partially coherent Rayleigh fading channels. In: Proceedings of the European Wireless Conference, pp. 738–743. LUCCA, Italy.
114. Yadav A, Juntti M & Lilleberg J (2012) Cutoff rate optimized space-time signal design for partially coherent channel. IEEE Transactions on Communications 60(6): 1563–1574.
115. Yadav A, Juntti M & Lilleberg J (2013) Multiple antenna constellation design for partially coherent Rayleigh fading channels. In: Proceedings of the ITG Conference on Systems Communication and Coding, pp. 1–6. Munich, Germany.
116. Yadav A, Juntti M & Lilleberg J (2012) Constellation design and mapping for partially coherent correlated channel with coding. In: Proceedings of the IEEE International Conference on Communications, pp. 6206–6211. Ottawa, Canada.

117. Yadav A, Juntti M & Lilleberg J (2013) Partially coherent constellation design and bit-mapping with coding for correlated fading channels. IEEE Transactions on Communications, to appear.
118. Zeger K & Gersho A (1990) Pseudo-Gray coding. IEEE Transactions on Communications 38(12): 2147–2158.
119. Bahceci I & Duman T (2002) Combined turbo coding and unitary space-time modulation. IEEE Transactions on Communications 50(8): 1244–1249.
120. Li Y & Xia XG (2005) Constellation mapping for space-time matrix modulation with iterative demodulation/decoding. IEEE Transactions on Communications 53(5): 764–768.
121. Tran N, Nguyen H & Le-Ngoc T (2007) Coded unitary space-time modulation with iterative decoding: Error performance and mapping design. IEEE Transactions on Communications 55(4): 703–716.
122. Yadav A, Juntti M & Lilleberg J (2013) Linear precoder design for doubly correlated partially coherent fading MIMO channels. IEEE Transactions on Wireless Communications, submitted Mar. 2013, revised Oct. 2013.
123. Yadav A, Juntti M & Lilleberg J (2013) Linear precoder design for correlated partially coherent channels with discrete inputs. In: Proceedings of the VDE International Symposium on Wireless Communication Systems, pp. 351–355. Ilmenau, Germany.
124. Hassibi B & Hochwald BM (2003) How much training is needed in multiple–antenna wireless links? IEEE Transactions on Information Theory 49(4): 951–963.
125. Viterbi A & Omura J (1979) Principles of Digital Communication and Coding. McGraw-Hill, New York.
126. Babu CC (1972) On the probability of error and the expected Bhattacharyya distance in multiclass pattern recognition. Proceedings of the IEEE 60(11): 1451–1452.
127. MATLAB (2010) 7.10.0 (R2010a). The MathWorks Inc., Natick, Massachusetts.
128. Nocedal J & Wright SJ (1999) Numerical Optimization. New York: Springer.
129. Zhou Z & Vucetic B (2004) Design of adaptive modulation using imperfect CSI in MIMO systems. IEE Electronics Letters 40(17): 1073–1075.
130. Abou-Faycal IC, Trott MD & Shamai S (2001) The capacity of discrete-time memoryless Rayleigh-fading channels. IEEE Transactions on Information Theory 47(4): 1290 –1301.
131. Gursoy M (2009) Error rate analysis for peaky signaling over fading channels. IEEE Transactions on Communications 57(9): 2546–2550.
132. Siwamogsatham S & Fitz MP (2002) Robust space-time codes for correlated Rayleigh fading channels. IEEE Transactions on Signal Processing 50(10): 2408–2416.
133. Pedersen KI, Andersen JB, Kermoal JP & Mogensen P (2000) A stohastic multiple-input-mobile-output radio channel model for evaluation of space-time coding algorithms. In: Proceedings of the IEEE Vehicular Technology Conference, pp. 893–897. Boston, USA.
134. Kermoal JP, Schumacher L, Pedersen K, Mogensen PE & Frederiksen F (2002) A stochastic MIMO radio channel model with experimental validation. IEEE

Journal on Selected Areas in Communications 20(6): 1211–1226.
135. Czink N, Matz G, Seethaler D & Hlawatsch F (2005) Improved MMSE estimation of correlated MIMO channels using a structured correlation estimator pp. 595–599.
136. Li L & Wang Z (2006) A novel spatial correlation estimation technique for MIMO communication system. In: Proceedings of the IEEE Vehicular Technology Conference, pp. 987–990. Montréal, Canada.
137. Liu Y, Wong T & Hager WW (2007) Training signal design for estimation of correlated MIMO channels with colored interference. IEEE Journal on Selected Areas in Communications 55(4): 1486 – 1497.
138. Kay SM (1993) Fundamentals of Statistical Signal Processing: Estimation Theory. Prentice-Hall, Englewood Cliffs, NJ, USA.
139. Lassing J, Strom E, Agrell E & Ottosson T (2003) Computation of the exact bit-error rate of coherent M-ary PSK with Gray code bit mapping. IEEE Transactions on Communications 51(11): 1758–1760.
140. Kadota T & Shepp L (1967) On the best finite set of linear observables for discriminating two Gaussian signals. IEEE Transactions on Information Theory 13(2): 278–284.
141. Belfiore JC, Rekaya G & Viterbo E (2005) The golden code: A 2×2 full-rate space-time code with nonvanishing determinants. IEEE Transactions on Information Theory 51(4): 1432–1436.
142. Schreckenbach F, Gortz N, Hagenauer J & Bauch G (2003) Optimization of symbol mappings for bit-interleaved coded modulation with iterative decoding. IEEE Communications Letters 7(12): 593–595.
143. Wang M, Xiao W & Brown T (2002) Soft decision metric generation for QAM with channel estimation error. IEEE Transactions on Communications 50(7): 1058–1061.
144. Kim TT, Jöngren G & Skoglund M (2004) Weighted space-time bit-interleaved coded modulation. In: Proceedings of the IEEE Information Theory Workshop, pp. 375–380. San Antonio, TX, USA.
145. Xiao C, Zheng Y & Ding Z (2011) Globally optimal linear precoders for finite alphabet signals over complex vector Gaussian channels. IEEE Transactions on Signal Processing 59(7): 3301–3314.
146. Sampath H & Paulraj A (2002) Linear precoding for space-time coded systems with known fading correlations. IEEE Communications Letters 6(6): 239–241.
147. Hjørungnes A & Gesbert D (2007) Precoding of orthogonal space-time block codes in arbitrarily correlated MIMO channels: Iterative and closed-form solutions. IEEE Transactions on Wireless Communications 6(3): 1072–1082.
148. Huang J, Au E & Lau V (2008) Precoder design for space-time coded MIMO systems with imperfect channel state information detection. IEEE Transactions on Wireless Communications 7(6): 1977–1981.
149. Phan K, Vorobyov S & Tellambura C (2009) Precoder design for space-time coded systems over correlated Rayleigh fading channels using convex optimization. IEEE Transactions on Signal Processing 57(2): 814–819.
150. Zhou S & Giannakis GB (2003) Optimal transmitter eigen-beamforming and space-time block coding based on channel correlation. IEEE Transactions on

Information Theory 49(7): 1673–1690.
151. Liu L & Jafarkhani H (2005) Application of quasi-orthogonal space-time block codes in beamforming. IEEE Transactions on Signal Processing 53(1): 54–63.
152. Nguyen VK & Xiang Y (2005) MMSE precoder for unitary space-time codes in correlated time-varying channels. IEEE Signal Processing Letters 12(8): 569Ű572.
153. Guo Y, Zhu S & Liang Z (2007) Linear precoding of unitary space-time code for GLRT decoder. IEICE Transactions on Fundamentals of Electronics, Communications and Computer Sciences E91-A(2): 695–699.
154. Horst R & Tuy H (1995) Global Optimization: Deterministic Approaches. Springer, New York, third edition.
155. Horst R, Pardolos P & Thoai N (2000) Introduction to Global Optimization. Kluwer Academic Publishers, Dordrecht, Boston, London, second edition.
156. Horst R, Phong TQ, Thoai NV & Vries J (1991) On solving a D.C. programming problem by a sequence of linear programs 1: 183–203.
157. Abrudan T, Eriksson J & Koivunen V (2009) Conjugate gradient algorithm for optimization under unitary matrix constraint. IEEE Transactions on Signal Processing 89(9): 1704–1714.
158. Jorswieck EA & Boche H (2004) Channel capacity and capacity-range of beamforming in MIMO wireless systems under correlated fading with covariance feedback. IEEE Transactions on Wireless Communications 3(5): 1543–1553.
159. Björnson E, Jorswieck E & Ottersten B (2010) Impact of spatial correlation and precoding design in OSTBC MIMO systems. IEEE Transactions on Wireless Communications 9(11): 3578–3589.
160. Jöngren G, Skoglund M & Ottersten B (2002) Combining beamforming and orthogonal space-time block coding. IEEE Transactions on Information Theory 48(3): 611–627.
161. Sendonaris A, Erkip E & Aazhang B (2003) User cooperation diversity–part I: System description. IEEE Transactions on Communications 51(11): 1927–1938.
162. Sendonaris A, Erkip E & Aazhang B (2003) User cooperation diversity–part II: Implementation aspects and performance analysis. IEEE Transactions on Communications 51(11): 1939–1948.
163. Murphy P, Sabharwal A & Aazhang B (2007) Building a cooperative communications system. Computing Research Repository abs/0707.2998.
164. Ungerboeck G (1982) Channel coding with multilevel/phase signals. IEEE Transactions on Information Theory 28(1): 55–67.
165. Zehavi E (1992) 8-PSK trellis codes for a Rayleigh channel. IEEE Transactions on Communications 40(5): 873–884.
166. Caire G, Taricco G & Biglieri E (1998) Bit-interleaved coded modulation. IEEE Transactions on Information Theory 44: 927–946.
167. Horn R & Johnson C (1985) Matrix Analysis. Cambridge University Press, Cambridge, United Kingdom.
168. Brookes M (2011) The Matrix Reference Manual. http://www.ee.imperial.ac.uk/hp/staff/dmb/matrix/intro.html, [online].
169. Lütkepohl H (1996) Handbook of Matrices. John Wiley and Sons, New York.

Appendix 1 Some standard results

The following results are used throughout these appendices.

Lemma 2 *[167–169] Let for any M-by-N matrix $\boldsymbol{A}$, N-by-M matrix $\boldsymbol{B}$, and M-by-M matrix $\boldsymbol{X}$, the following identities hold*

$$|\boldsymbol{I}_M + \boldsymbol{AB}| = |\boldsymbol{I}_N + \boldsymbol{BA}|, \tag{87}$$

$$|\boldsymbol{I}_M \otimes \boldsymbol{A}| = |\boldsymbol{A}|^M, \tag{88}$$

$$(\boldsymbol{A} \otimes \boldsymbol{B})(\boldsymbol{C} \otimes \boldsymbol{D}) = \boldsymbol{AC} \otimes \boldsymbol{BD} \tag{89}$$

$$|\boldsymbol{X} + \boldsymbol{AB}| = |\boldsymbol{X}||\boldsymbol{I}_M + \boldsymbol{BX}^{-1}\boldsymbol{A}|, \tag{90}$$

$$|\boldsymbol{I} + \epsilon\boldsymbol{X}| = 1 + \mathrm{tr}(\boldsymbol{X})\epsilon + \mathcal{O}(\epsilon^2), \tag{91}$$

$$|\boldsymbol{I} - \alpha\boldsymbol{X}| = \prod_{i=1}^{M}(1 - \alpha\lambda_i), \tag{92}$$

where ϵ is a very small positive number, λ_i are eigenvalues of $\boldsymbol{X}$ and α is some constant.

Appendix 2 Proof of Proposition 1: Cutoff rate expression for i.i.d. channel

For notational convenience, we rewrite (1) by stacking the columns of $\mathbf{Y}$, $\mathbf{H}$, and $\mathbf{W}$ into their respective vector counterparts, and we obtain

$$\mathbf{y} \quad = \quad \mathbf{Z}\mathbf{h} + \mathbf{w}, \tag{93}$$

where $\mathbf{Z} = \mathbf{I}_{M_R} \otimes \mathbf{S}$.

The received vector $(\mathbf{y}|\mathbf{Z}_i, \hat{\mathbf{h}}) \sim \mathcal{CN}(\mathbf{Z}_i\hat{\mathbf{h}}, \mathbf{R}_i)$, where $\mathbf{R}_i = (\mathbf{I} + \sigma_E^2 \mathbf{Z}_i \mathbf{Z}_i^H)$, is the variance of the received vector when $\mathbf{Z}_i$ is transmitted. The cutoff rate (6) for the discrete input and continuous output channel with partial channel information at the receiver can be rewritten as

$$R_0 = \max_{\{\pi_i\}_{i=1}^{L}} -\log \left\{ \sum_i \sum_j \mathbb{E}_{\hat{\mathbf{h}}} \left[\int \sqrt{p(\mathbf{y}|\mathbf{Z}_i, \hat{\mathbf{h}}) p(\mathbf{y}|\mathbf{Z}_j, \hat{\mathbf{h}})} d\mathbf{y} \right] \right\}, \tag{94}$$

since $p(\mathbf{y}, \hat{\mathbf{h}}|\mathbf{Z}_i) = p(\mathbf{y}|\mathbf{Z}_i, \hat{\mathbf{h}}) p(\hat{\mathbf{h}})$ and interchanging the order of summation and integration.

The inner integral

$$\mathcal{I} = \int \sqrt{p(\mathbf{y}|\mathbf{Z}_i, \hat{\mathbf{h}}) p(\mathbf{y}|\mathbf{Z}_j, \hat{\mathbf{h}})} d\mathbf{y} \tag{95}$$

is computed in the following lemma.

Lemma 3 *[112, Appendix-I] Let $\boldsymbol{B}$ represent a positive-definite Hermitian $n \times n$ matrix and $\boldsymbol{A}$ a Hermitian $n \times n$ matrix; let $\boldsymbol{a}$ and $\boldsymbol{b}$ represent $n \times 1$ vectors of complex constant; let a_0 and b_0 represent complex scalars. Then*

$$\begin{aligned} &\int \frac{1}{2}(\boldsymbol{x}^H \boldsymbol{A}\boldsymbol{x} + \boldsymbol{x}^H \boldsymbol{a} + \boldsymbol{a}^H \boldsymbol{x} + a_0 + a_0^*) \exp\{-\frac{1}{2}(\boldsymbol{x}^H \boldsymbol{B}\boldsymbol{x} + \boldsymbol{x}^H \boldsymbol{b} + \boldsymbol{b}^H \boldsymbol{x} + b_0 + b_0^*)\} d\boldsymbol{x} \\ &= \frac{1}{2}\pi^n |\tfrac{1}{2}\boldsymbol{B}|^{-1} \cdot [2\mathrm{tr}(\boldsymbol{A}\boldsymbol{B}^{-1}) - \boldsymbol{b}^H \boldsymbol{B}^{-1}\boldsymbol{a} - \boldsymbol{a}^H \boldsymbol{B}^{-1}\boldsymbol{b} + \boldsymbol{b}^H \boldsymbol{B}^{-1}\boldsymbol{A}\boldsymbol{B}^{-1}\boldsymbol{b} \\ &+ 2Re\{a_0\}] \exp\left[\tfrac{1}{2}\boldsymbol{b}^H \boldsymbol{B}^{-1}\boldsymbol{b} - Re\{b_0\}\right]. \end{aligned} \tag{96}$$

Apply Lemma 3 with $\mathbf{x} = \mathbf{y} - \mathbf{Z}_i\hat{\mathbf{h}}$, $\mathbf{B} = [\mathbf{R}_i^{-1} + \mathbf{R}_j^{-1}]$, $\mathbf{A} = \mathbf{0}$, $\mathbf{a}$=$\mathbf{0}$, $\mathbf{b} = \mathbf{R}_i^{-1}(\mathbf{Z}_i - \mathbf{Z}_j)\hat{\mathbf{h}}$, $a_0 = 1/(|\pi\mathbf{R}_i|^{\frac{1}{2}}|\pi\mathbf{R}_j|^{\frac{1}{2}})$, and $b_0 = \frac{1}{2}\hat{\mathbf{h}}^H(\mathbf{Z}_i - \mathbf{Z}_j)^H \mathbf{R}_i^{-1}(\mathbf{Z}_i - \mathbf{Z}_j)\hat{\mathbf{h}}$

on (95), we get

$$\mathcal{I} = \underbrace{\frac{|\mathbf{R}_i|^{1/2} \cdot |\mathbf{R}_j|^{1/2}}{|\frac{1}{2}\mathbf{R}_i + \frac{1}{2}\mathbf{R}_j|}}_{\mathbf{K}} \exp\{-\tfrac{1}{4}\hat{\mathbf{h}}^H \underbrace{(\mathbf{Z}_i - \mathbf{Z}_j)^H (\frac{1}{2}\mathbf{R}_i + \frac{1}{2}\mathbf{R}_j)^{-1}(\mathbf{Z}_i - \mathbf{Z}_j)}_{\mathbf{Q}} \hat{\mathbf{h}}\}. \tag{97}$$

Now using the Rayleigh-fading model for the channel coefficients, we average (97) over $\hat{\mathbf{h}}$

$$\bar{\mathcal{I}} = \int \mathcal{I} \cdot \frac{1}{|\pi(1-\sigma_E^2)|} \cdot \exp\left[-\hat{\mathbf{h}}^H (1-\sigma_E^2)^{-1} \hat{\mathbf{h}}\right] d\hat{\mathbf{h}}, \tag{98}$$

which can be computed again by applying Lemma 3 with $\mathbf{x} = \hat{\mathbf{h}}$, $\mathbf{B} = 2(1-\sigma_E^2)^{-1} + \frac{1}{2}\mathbf{Q}$, $\mathbf{A} = \mathbf{0}$, $\mathbf{a} = \mathbf{0}$, $\mathbf{b} = \mathbf{0}$, $a_0 = \frac{\mathbf{K}}{2|\pi(1-\sigma_E^2)|}$, and $b_0 = 0$, yielding

$$\bar{\mathcal{I}} \quad = \quad \frac{|\mathbf{K}|}{|\mathbf{I}_{M_T M_R} + \frac{1}{4}\mathbf{Q}(1-\sigma_E^2)|}. \tag{99}$$

Using (88), (90) and (99) results in (7).

Appendix 3 Derivation of (27): Cutoff rate with unitary constellations

Starting from (7) and using (87), [84, Lemma 6] and Fischer's inequality [167, Theorem 7.8.3], we can write (7) in the following form

$$R_0 \geq \max_{\{\mathbf{s}_i\}_{i=1}^{L}} -\log\left\{\frac{1}{L^2}\sum_i\sum_j \frac{|\mathbf{I}_{M_T}+\sigma_E^2\mathbf{S}_i^H\mathbf{S}_i|^{1/2}|\mathbf{I}_{M_T}+\sigma_E^2\mathbf{S}_j^H\mathbf{S}_j|^{1/2}}{|\mathbf{I}_{M_T}+\frac{1}{2}\sigma_E^2\mathbf{S}_i^H\mathbf{S}_i||\mathbf{I}_{M_T}+\frac{1}{2}\sigma_E^2\mathbf{S}_j^H\mathbf{S}_j||I_{M_T}-\mathcal{K}_{ij}^H\mathcal{K}_{ij}|} \right.$$
$$\left. \frac{1}{|\mathbf{I}_{T_d}+\frac{1}{4}(1-\sigma_E^2)(\mathbf{S}_i-\mathbf{S}_j)(\mathbf{S}_i-\mathbf{S}_j)^H|}\right\}, \tag{100}$$

where $\mathcal{K}_{ij}=\tilde{\mathbf{S}}_j^H\tilde{\mathbf{S}}_i$, $\tilde{\mathbf{S}}_i=\mathbf{S}_i[\mathbf{I}+\frac{1}{2}\mathbf{S}_i^H\mathbf{S}_i]^{-1/2}$ and $\tilde{\mathbf{S}}_j=\mathbf{S}_j[\mathbf{I}+\frac{1}{2}\mathbf{S}_j^H\mathbf{S}_j]^{-1/2}$.

Now replacing matrix $\mathbf{S}_i$ with $\Phi_i\mathbf{D}_i$, where $\mathbf{D}_i=\sqrt{d_i}\mathbf{I}_{M_T}$, assuming $\frac{1}{4}(1-\sigma_E^2)$ is small and using (91) and (92), we get (27).

Appendix 4 Derivation of (35)

Starting with (33) and performing a vectorization operation followed by the linear MMSE estimate of vec($\mathbf{G}_w$), we get $\hat{\mathbf{h}}_w$. Now the channel estimation error covariance matrix is given by [138]

$$\begin{aligned}
\tilde{\Sigma} &= \mathbb{E}[\text{vec}(\tilde{\mathbf{H}})\text{vec}(\tilde{\mathbf{H}})^H] && \text{(101a)}\\
&= \mathbb{E}[\{\text{vec}(\mathbf{H}_w) - \text{vec}(\hat{\mathbf{H}}_w)\}\{\text{vec}(\mathbf{H}_w) - \text{vec}(\hat{\mathbf{H}})_w\}^H] && \text{(101b)}\\
&= \mathbf{I}_{M_R M_T} - [\mathbf{I}_{M_R M_T} + \sigma_{ce}^2 \mathbf{R}_R^{-1} \otimes \mathbf{I}_{M_T}]^{-1} && \text{(101c)}\\
&= (\mathbf{I}_{M_R} - [\mathbf{I}_{M_R} + \sigma_{ce}^2 \mathbf{R}_R^{-1}]^{-1}) \otimes \mathbf{I}_{M_T}. && \text{(101d)}
\end{aligned}$$

Using the matrix inversion lemma [138]

$$(\mathbf{A} + \mathbf{BCD})^{-1} \quad = \quad \mathbf{A}^{-1} - \mathbf{A}^{-1}\mathbf{B}(\mathbf{C}^{-1} + \mathbf{DA}^{-1}\mathbf{B})^{-1}\mathbf{DA}^{-1} \qquad (102)$$

we can write

$$\mathbf{I}_{M_R} - [\mathbf{I}_{M_R} + \sigma_{ce}^2 \mathbf{R}_R^{-1}]^{-1} \quad = \quad [\mathbf{I}_{M_R} + \sigma_{ce}^{-2} \mathbf{R}_R]^{-1}. \qquad (103)$$

Now substituting (103) into (101d) and the estimation error vector can be written as $[\mathbf{I}_{M_R} + \sigma_{ce}^{-2}\mathbf{R}_R]^{-1/2} \otimes \mathbf{I}_{M_T}\text{vec}(\mathbf{E}_w)$, where $\mathbf{E}_w$ is a random matrix which has a zero mean and identity covariance matrix, which is the same as (35). The matrix version of the channel estimation vector is given by $\mathbf{E}_w[\mathbf{I}_{M_R} + \sigma_{ce}^{-2}\mathbf{R}_R]^{-1/2}$ which is the same as (36).

Appendix 5 Proof of Proposition 4: Cutoff rate expression for correlated channel

Starting from (40), the received vector $(\mathbf{y}|\mathbf{Z}_i, \hat{\tilde{\mathbf{h}}}) \sim \mathcal{CN}(\mathbf{Z}_i\hat{\tilde{\mathbf{h}}}, \mathbf{R}_i)$, where $\mathbf{R}_i = (\mathbf{I}+\mathbf{Z}_i\tilde{\Lambda}\mathbf{Z}_i^H)$ is the covariance of the received vector when $\mathbf{Z}_i$ is transmitted. $\tilde{\Lambda}$ is a covariance matrix of $\tilde{\tilde{\mathbf{h}}}$ and is equal to $\mathbb{E}[\tilde{\tilde{\mathbf{h}}}\tilde{\tilde{\mathbf{h}}}^H] = \tilde{\Lambda}_R \otimes \Lambda_T$. The Bhattacharyya coefficient $\rho_{cor}(i,j)$ between $\mathbf{Z}_i$ and $\mathbf{Z}_j$ averaged over $\hat{\tilde{\mathbf{h}}}$ is given by

$$\rho_{cor}(i,j) \quad = \quad \mathbb{E}\left[\int_{\mathcal{Y}} \sqrt{p(\mathbf{y}|\mathbf{Z}_i, \hat{\tilde{\mathbf{h}}})p(\mathbf{y}|\mathbf{Z}_j, \hat{\tilde{\mathbf{h}}})}d\mathbf{y}\right]. \tag{104}$$

The expectation and integral can be evaluated in the same manner as in Appendix 2 to get

$$\frac{|\mathbf{I}_{T_dM_R} + \mathbf{Z}_i\tilde{\Lambda}\mathbf{Z}_i^H|^{\frac{1}{2}}|\mathbf{I}_{T_dM_R} + \mathbf{Z}_j\tilde{\Lambda}\mathbf{Z}_j^H|^{\frac{1}{2}}}{|\mathbf{I}_{T_dM_R} + \frac{1}{2}(\mathbf{Z}_i\tilde{\Lambda}\mathbf{Z}_i^H + \mathbf{Z}_j\tilde{\Lambda}\mathbf{Z}_j^H)||\mathbf{I}_{M_TM_R} + \frac{1}{4}\frac{\hat{\Lambda}(\mathbf{Z}_i-\mathbf{Z}_j)^H(\mathbf{Z}_i-\mathbf{Z}_j)}{\mathbf{I}_{TM_R}+\frac{1}{2}(\mathbf{Z}_i\tilde{\Lambda}\mathbf{Z}_i^H+\mathbf{Z}_j\tilde{\Lambda}\mathbf{Z}_j^H)}|} \tag{105}$$

which can be further simplified by using an identity (90) to

$$\frac{|\mathbf{I}_{T_dM_R} + \mathbf{Z}_i\tilde{\Lambda}\mathbf{Z}_i^H|^{\frac{1}{2}}|\mathbf{I}_{T_dM_R} + \mathbf{Z}_j\tilde{\Lambda}\mathbf{Z}_j^H|^{\frac{1}{2}}}{|\mathbf{I}_{T_dM_R} + \frac{1}{2}(\mathbf{Z}_i\tilde{\Lambda}\mathbf{Z}_i^H + \mathbf{Z}_j\tilde{\Lambda}\mathbf{Z}_j^H) + \frac{1}{4}(\mathbf{Z}_i-\mathbf{Z}_j)\hat{\Lambda}(\mathbf{Z}_i-\mathbf{Z}_j)^H|}. \tag{106}$$

We can simplify further (106) by using an identity (89), rewriting $\mathbf{I}_{T_dM_R} + \mathbf{Z}_i\tilde{\Lambda}\mathbf{Z}_i^H$ as

$$\begin{aligned}
&\mathbf{I}_{M_R} \otimes \mathbf{I}_{T_d} + (\mathbf{I}_{M_R} \otimes \mathbf{X}_i)(\tilde{\Lambda}_R \otimes \Lambda_T)(\mathbf{I}_{M_R} \otimes \mathbf{X}_i)^H \\
&\quad = \mathbf{I}_{M_R} \otimes \mathbf{I}_{T_d} + (\mathbf{I}_{M_R}\tilde{\Lambda}_R\mathbf{I}_{M_R} \otimes \mathbf{X}_i\Lambda_T\mathbf{X}_i^H) && \text{(107a)} \\
&\quad = \mathbf{I}_{M_R} \otimes \mathbf{I}_{T_d} + (\mathbf{I}_{M_R} \otimes \tilde{\lambda}_R^n\mathbf{X}_i\Lambda_T\mathbf{X}_i^H) && \text{(107b)} \\
&\quad = \mathbf{I}_{M_R} \otimes (\mathbf{I}_T + \tilde{\lambda}_R^n\mathbf{X}_i\Lambda_T\mathbf{X}_i^H), && \text{(107c)}
\end{aligned}$$

and $\mathbf{I}_{T_dM_R} + \frac{1}{2}(\mathbf{Z}_i\tilde{\Lambda}\mathbf{Z}_i^H + \mathbf{Z}_j\tilde{\Lambda}\mathbf{Z}_j^H) + \frac{1}{4}(\mathbf{Z}_i-\mathbf{Z}_j)\hat{\Lambda}(\mathbf{Z}_i-\mathbf{Z}_j)^H$ as

$$\mathbf{I}_{M_R} \otimes \left(\mathbf{I}_{T_d} + \tfrac{1}{2}\tilde{\lambda}_R^n(\mathbf{X}_i\Lambda_T\mathbf{X}_i^H + \mathbf{X}_j\Lambda_T\mathbf{X}_j^H) + \tfrac{1}{4}\hat{\lambda}_R^n(\mathbf{X}_i-\mathbf{X}_j)\Lambda_T(\mathbf{X}_i-\mathbf{X}_j)^H\right). \tag{108}$$

Substituting (107c) and (108) in (106) and using an identity (88) results in (45).

Appendix 6 Proof of Theorem 1

In order to proof Theorem 1, we use the following two lemmas:

Lemma 4 *[87, Lemma 1] Function* $f(\mu, \mathbf{D}_1, \mathbf{D}_2) = |(\mathbf{I}+\mu(\mathbf{A}\mathbf{D}_1\mathbf{A}^H+\mathbf{B}\mathbf{D}_2\mathbf{B}^H))|^{-1}$ *defined over positive semidefinite diagonal matrices* $\mathbf{D}_1, \mathbf{D}_2$ *and positive number* μ *is a jointly log-convex function of* $\mathbf{D}_1$ *and* $\mathbf{D}_2$ *for fixed* μ.

Lemma 5 *[87, Lemma 2] Let* $h_i(\mathbf{x})$ *and* $g_i(\mathbf{x})$ *be log-convex functions* $\forall i = 1, \cdots, L$ *over* $\mathbb{R}^n$ *and* c_i *be nonnegative constants. Then* $f(\mathbf{x}) = \log(\sum_i c_i \frac{h_i(\mathbf{x})}{g_i(\mathbf{x})})$ *is d.c. and has a d.c. decomposition*

$$\log\left(\sum_i c_i g_i(\mathbf{x}) \prod_{j\neq i} h_j(\mathbf{x})\right) - \sum_i \log h_i(\mathbf{x}) \tag{109}$$

Now, without loss of generality, we can write the (71) as

$$R_0 = -\log\left(\frac{1}{L^2}\sum_i\sum_j \prod_{n=1}^{M_R} \frac{|\mathbf{I}_{T_d} + \frac{1}{2}(\tilde{\mathbf{X}}_i\Lambda\tilde{\mathbf{X}_i}^H + \tilde{\mathbf{X}}_j\Lambda\tilde{\mathbf{X}_j}^H)\tilde{\lambda}_R^n + \frac{1}{4}(\tilde{\mathbf{X}}_i - \tilde{\mathbf{X}}_j)\Lambda(\tilde{\mathbf{X}}_i - \tilde{\mathbf{X}}_j)^H\hat{\lambda}_R^n|^{-1}}{|\mathbf{I}_{T_d} + \tilde{\mathbf{X}}_i\Lambda\tilde{\mathbf{X}}_i^H\tilde{\lambda}_R^n|^{-\frac{1}{2}}|\mathbf{I}_{T_d} + \tilde{\mathbf{X}_j}\Lambda\tilde{\mathbf{X}_j}^H\tilde{\lambda}_R^n|^{-\frac{1}{2}}}\right). \tag{110}$$

Using Lemma 5, the argument of $\log(\cdot)$ in (110) may be expressed as

$$\frac{1}{L^2}\sum_{\substack{i,j\\j>i}}\left(\prod_{n=1}^{M_R}|\mathbf{I}_{T_d} + \frac{1}{2}(\tilde{\mathbf{X}}_k\Lambda\tilde{\mathbf{X}}_k^H + \tilde{\mathbf{X}}_l\Lambda\tilde{\mathbf{X}}_l^H)\tilde{\lambda}_R^n + \frac{1}{4}(\tilde{\mathbf{X}}_k - \tilde{\mathbf{X}}_l)\Lambda(\tilde{\mathbf{X}}_k - \tilde{\mathbf{X}}_l)^H\hat{\lambda}_R^n|^{-1}\cdot \prod_{\substack{k\neq i\\ l\neq j, l>k}}\prod_{n=1}^{M_R}|\mathbf{I}_{T_d} + \tilde{\mathbf{X}}_i\Lambda\tilde{\mathbf{X}}_i^H\tilde{\lambda}_R^n|^{-\frac{1}{2}}|\mathbf{I}_{T_d} + \tilde{\mathbf{X}_j}\Lambda\tilde{\mathbf{X}_j}^H\tilde{\lambda}_R^n|^{-\frac{1}{2}}\right) \Big/ \prod_{\substack{i,j\\j>i}}\prod_{n=1}^{M_R}|\mathbf{I}_{T_d} + \tilde{\mathbf{X}}_i\Lambda\tilde{\mathbf{X}}_i^H\tilde{\lambda}_R^n|^{-\frac{1}{2}}|\mathbf{I}_{T_d} + \tilde{\mathbf{X}_j}\Lambda\tilde{\mathbf{X}_j}^H\tilde{\lambda}_R^n|^{-\frac{1}{2}}. \tag{111}$$

By Lemma 4, $|\mathbf{I}_{T_d} + \frac{1}{2}(\tilde{\mathbf{X}}_k\Lambda\tilde{\mathbf{X}}_k^H + \tilde{\mathbf{X}}_l\Lambda\tilde{\mathbf{X}}_l^H)\tilde{\lambda}_R^n + \frac{1}{4}(\tilde{\mathbf{X}}_k - \tilde{\mathbf{X}}_l)\Lambda(\tilde{\mathbf{X}}_k - \tilde{\mathbf{X}}_l)^H\hat{\lambda}_R^n|^{-1}$, $|\mathbf{I}_{T_d} + \tilde{\mathbf{X}}_i\Lambda\tilde{\mathbf{X}}_i^H\tilde{\lambda}_R^n|^{-1}$ and $|\mathbf{I}_{T_d} + \tilde{\mathbf{X}}_j\Lambda\tilde{\mathbf{X}}_j^H\tilde{\lambda}_R^n|^{-1}$ are log-convex functions of Λ. Operations like raised to a positive index, times positive constant, sum, and product of log-convex functions preserve log-convexity. Thus, (111) is the ratio

of two log-convex functions. Taking $\log(\cdot)$ therefore gives d.c. decomposition for CR expression as $f(\Lambda) - g(\Lambda)$, where $f(\Lambda)$ and $g(\Lambda)$ are defined in (73) and (74), respectively. Maximizing the negative CR expression can be written as its minimization, which is (72).

449. Pirinen, Rauno (2013) Towards regional development by Higher Education Institutions : an empirical study of a University of Applied Sciences

450. Mäkinen, Liisa (2013) Improvement of resource efficiency in deinked pulp mill

451. Guo, Yimo (2013) Image and video analysis by local descriptors and deformable image registration

452. Pantisano, Francesco (2013) Cooperative interference and radio resource management in self-organizing small cell networks

453. Ojanperä, Tiia (2013) Cross-layer optimized video streaming in heterogeneous wireless networks

454. Pietikäinen, Martti (2013) Metalli- ja elektroniikkateollisuus Oulun eteläisen alueella : kehitys koulutuksen ja teknologian näkökulmasta

455. Pitkääho, Satu (2013) Catalytic oxidation of chlorinated volatile organic compounds, dichloromethane and perchloroethylene : new knowledge for the industrial CVOC emission abatement

456. Morais de Lima, Carlos Héracles (2013) Opportunistic resource and network management in autonomous packet access systems

457. Nardelli, Pedro Henrique Juliano (2013) Analysis of the spatial throughput in interference networks

458. Ferreira, Denzil (2013) AWARE: A mobile context instrumentation middleware to collaboratively understand human behavior

459. Ruusunen, Mika (2013) Signal correlations in biomass combustion – an information theoretic analysis

460. Kotelba, Adrian (2013) Theory of rational decision-making and its applications to adaptive transmission

461. Lauri, Janne (2013) Doppler optical coherence tomography in determination of suspension viscosity

462. Kukkola, Jarmo (2013) Gas sensors based on nanostructured tungsten oxides

463. Reiman, Arto (2013) Holistic work system design and management : a participatory development approach to delivery truck drivers' work outside the cab

464. Tammela, Simo (2013) Enhancing migration and reproduction of salmonid fishes : method development and research using physical and numerical modelling

Book orders:
Granum: Virtual book store
http://granum.uta.fi/granum/

UNIVERSITY OF OULU P.O. Box 8000 FI-90014 UNIVERSITY OF OULU FINLAND

ACTA UNIVERSITATIS OULUENSIS

ISBN 978-952-62-0213-6 (Paperback)
ISBN 978-952-62-0214-3 (PDF)
ISSN 0355-3213 (Print)
ISSN 1796-2226 (Online)

UNIVERSITY of OULU
OULUN YLIOPISTO